IS-T--1487

DE90 016415

Monomolecular and Thin Polymer Films: Fabrication, Characterization, Applications, and Models of Wetting

by

Chau, Lai Kwan

PHD Thesis submitted to Iowa State University

Ames Laboratory, U.S. DOE

Iowa State University

Ames, Iowa 50011

Date Transmitted: August 24, 1990

PREPARED FOR THE U.S. DEPARTMENT OF ENERGY

UNDER CONTRACT NO. W-7405-Eng-82.

DISCLAIMER

Monomolecular and thin polymer films:

Fabrication, characterization, applications, and models of wetting

Lai Kwan Chau

In charge of major work: Marc D. Porter and Dennis C. Johnson
From the Department of Chemistry
Iowa State University

A variety of chemically modified surfaces were synthesized and their molecular structures and reactivities were characterized. These interfaces include: (i) Monomolecular films of n-alkanoic acids ($CH_3(CH_2)_nCOOH$) and n-perfluorocarboxylic acids ($CF_3(CF_2)_nCOOH$) on silver; and (ii) calcichrome immobilized at an anion exchange polymer film. The monomolecular films were fabricated by the self-assembly method and characterized by optical ellipsometry, infrared reflection spectroscopy, and contact angle measurements. A comparison is given of the properties of these films with regard to composition, defectiveness, intermolecular environment, molecular orientation, wettability, and formation thermodynamics. As it is relevant to monolayer formation thermodynamics, the isoelectric point of the surface of evaporated silver films was determined by contact angle titration. Potential applications of these films are discussed.

Monomolecular films as models of wetting are also examined in terms of van der Waals interactions at the macroscopic interfaces. Theoretical considerations of the effects of intermolecular forces on depth sensitivity of wetting and limiting contact angles of various systems are assessed.

One of the synthesized interfaces has been applied as a Ca(II) optical sensor. The sensor was fabricated by electrostatic immobilization of calcichrome at an anion exchange polymer film. The structure and reactivity of this interface was characterized by ultraviolet-visible diffuse reflectance spectroscopy and infrared photoacoustic spectroscopy. Equations to determine the metal complex formation constant and acid dissociation constants of the immobilized reagent from diffuse reflectance spectra are developed. Possible causes affecting the reactivity of an immobilized indicator are discussed.

Monomolecular and thin polymer films:
Fabrication, characterization, applications, and models of wetting

by

Lai Kwan Chau

A Dissertation Submitted to the

Graduate Faculty in Partial Fulfillment of the

Requirements for the Degree of

DOCTOR OF PHILOSOPHY

Department: Chemistry

Major: Analytical Chemistry

Approved:

Marc D. Porter

In Charge of Major Work

For the Major Department

For the Graduate College

Iowa State University
Ames, Iowa

1990

TABLE OF CONTENTS

GENERAL INTRODUCTION

Molecular films, ordered thin organic films in a thickness range from a few nanometer (a monolayer) to several hundred nanometers, show considerable technological promise. In particular, a number of potential applications have been identified. These include nonlinear and active optical devices [1,2], chemical, biochemical, and physical sensors [3-11], packaging and insulating layers for integrated circuits [12-14], patternable materials both for resists [15] and for information storage [16], surface modification (e.g., wetting [17] and electrode properties [18]), and synthetic biomembranes [19]. In addition, structurally well defined organic monolayers on solid surfaces also provide a rational approach to simplify and model a large variety of interfacial phenomena such as adhesion [20,21], lubrication [22,23], corrosion inhibition [24] and wetting [17]. Scientific studies of molecular interactions in thin-film structures would lead to an understanding of the collective properties of ordered arrays. This has only recently been possible with organic films, which were characterized in more detail by a number of the newer surface science techniques. For these reasons, the physical, chemical, biological, and theoretical aspects of thin molecular films should be studied and their potential as models assessed.

Organized molecular films can be produced by both Langmuir-Blodgett (LB) [25] and self-assembly (SA) [26] techniques. The LB films are appealing for study because of the facile manner in which a single monolayer or multilayers can be deposited. Such a capability brings to desire application as organic superlattices created by the successive deposition of alternating layers of different molecules. Whether these materials could even find use is highly speculative at the present time, but they do serve as good model systems. Unfortunately, these LB assemblies are often metastable [27] and, in addition, the requirement of a compressed film at the air-water interface in the LB process severely limits the molecular structures that can be used to form monolayers [25]. In contrast, SA, which

takes place in homogeneous solution under equilibrium conditions, offers possibilities for avoiding some of these difficulties. Interest in SA monolayers has focussed on a number of systems, including organosilanes on silicon/silicon dioxide [28-33], carboxylic acids on metal oxides [34-38], and organosulfur compounds on gold [39-53] and other metals [54,55].

Intermolecular ordering in mono- and multilayer assemblies on solid surfaces is being probed in an effort to answer long-standing questions regarding the relationship between intermolecular ordering and the macroscopic properties of the film. Structural information will make it possible to separate the various free energy contributions driving these structures, such as head/surface binding, head/head interactions, entropies and energies of trans/gauche isomerization, and van der Waals interactions between neighboring tails. A framework can thus be provided for design of the individual moieties in molecules as well as the substrate to enhance particular cooperative properties of the assembly.

Attempts to fabricate new and complex molecular films with novel properties cannot be done efficiently without significant advances in the present analytical capabilities. The detailed structural characterization of subtle molecular features of thin organic films presents new and challenging problems for the field of materials characterization. Because these are organic materials, the methods must not involve any damaging interactions and yet must be capable of determining subtle features such as conformation and orientation of functional groups. The ability to analyze at different depths in the film is also desirable. In contrast, many of the very useful and sensitive tools for analysis of inorganic surfaces and thin films are largely damaging, insensitive to the subtleties of organic structures, and involve high-vacuum techniques. Development of in situ analytical techniques is greatly needed for film-vapor and film-solution systems. Excellent examples can be found in biological systems where measurements should be made directly in biological media (in vivo) rather than the

standard ultrahigh-vacuum conditions required by many surface analysis techniques. In some cases, such as integrated microcircuit devices, it is also desirable to perform analyses over very small surface regions having submicron dimensions. Few techniques are capable of accomplishing this.

X-ray photoelectron spectroscopy (XPS) and infrared reflection spectroscopy (IRS) are two spectroscopic techniques that have become standard methods for characterizing organic films and surfaces. While XPS analysis is restricted to vacuum conditions, it has the advantage of seeing the outermost regions (top 1-100 Å) of most solid surfaces for a number of elements and in a variety of chemical bonding situations [56]. On the other hand, IRS offers the potential for analysis of planar thin films on metal surfaces [57,58] and overlayers under liquids [59], and recent experiments have shown the feasibility of monolayer studies on non-metallic substrates such as carbon [60], silicon [61], and water [62]. An adjunct technique is single-wavelength optical ellipsometry, which has been useful for measuring the thickness of a thin film [63]. Other useful spectroscopic and diffraction techniques include Raman spectroscopy [64,65], secondary ion mass spectrometry [66], extended X-ray absorption fine structure [67], and second-harmonic generation at a surface [68]. In general, all spectroscopic and diffraction analyses give information which is averaged over regions large compared to atomic scales. In contrast, scanning tunneling microscopy [69] and atomic force microscopy [70] are techniques capable of atomic resolution at a specific sites. The tunneling technique is limited to dielectric films with thickness in the 1.0-4.0 nm range because anything much thicker than that would prevent tunneling.

One classic technique, contact angle measurement, has received considerable attention in recent years [17]. Although the technique is only capable of yielding little detailed information about surfaces, the high sensitivity of wetting to the microscopic composition and structure of solid surfaces has proved invaluable for probing the character of solid-liquid

and solid-solid interfaces involving organic solids. The range of information obtained by contact angle measurements can be increased by measuring contact angle as a function of the pH of aqueous drops [71], by using probe liquids other than water [72], and by examining both advancing and receding contact angles [73,74]. Measurement of contact angles relies heavily on comparisons of measurements in similar systems rather than on interpretation of absolute values obtained from only one system. Due to the lack of understanding of the influence of the depth of functional groups beneath the surface to different probe liquids on wetting, it is invaluable to understand the intermolecular forces acting at these interfaces.

SECTION I. SURFACE ISOELECTRIC POINT OF EVAPORATED SILVER FILMS: DETERMINATION BY CONTACT ANGLE TITRATION

Surface Isoelectric Point of Evaporated Silver Films: Determination by Contact Angle Titration

Lai-Kwan Chau and Marc D. Porter

Department of Chemistry and Ames Laboratory - USDOE

Iowa State University

Ames, Iowa 50011

ABSTRACT

The dependence of the contact angle on the pH of the probe liquid has been used to examine the acid-base reactivity of the native oxide of evaporated silver films. The results indicate that these films have a surface isoelectric point of ~10.4, which corresponds to a basic oxide. Thermodynamic formulas are also derived to relate the change in contact angle with the charge density of the surface.

INTRODUCTION

The acid-base properties of metal surfaces are important to a variety of technologically significant processes, including heterogeneous catalysis [1], adhesion [2], ore floatation [2,3], and corrosion inhibition [4]. Recently, the oxides at Al [5,6] and Ag [7,8] have been used as reactive sites for the formation of organic monolayer films via the dissociative chemisorption of carboxylic acid-functionalized compounds to form the carboxylate salts. These monolayers are part of a class of unique surface phases which exhibit a well-defined structure in contrast to the compositional and morphological heterogeneity of functionalized polymeric materials, a characteristic that has led to their application as models for examining the fundamental details of interfacial structure-reactivity relationships. Although the bonding between the head group and substrate is recognized as playing an important role in the formation of these structures, defining its significance relative to other factors (e.g., cohesive interactions between neighboring tail groups) remains a complex and as yet unresolved issue. Furthermore, delineating the significance of each factor will become increasingly important as approaches to create novel interfacial properties via the formation of multi-component monolayers by co-adsorption from solution are developed.

We recently became interested in detailing the differences in the bond strengths of monolayer formed from n-alkanoic acid and n-perfluorocarboxylic acids at evaporated silver films [7,8]. Following the relationships of Bolger [2], such strengths can be predicted from the differences in the isoelectric point of the surfaces (IEPS) and the pK_a (viz. $-\log K_a$, where K_a is the acid dissociation constant) of the adsorbate precursor. To the best of our knowledge, however, measurements of the IEPS of silver have not appeared. In view of the importance of this information to ongoing efforts in this area, this paper reports on the determination of the IEPS at silver by contact angle titration. To accompany these results, a thermodynamic analysis is developed that relates the change in contact angle to the charge

density at the oxide surface. We also briefly comment on the general utility of this method, which has been used extensively for determining the acidity of organic surfaces [9,10], through comparisons with the more commonly used electrokinetic [3], potentiometric [11], and indicator adsorption [12,13] methods.

EXPERIMENTAL

Silver films were prepared by resistive evaporation of a thin (10-20 nm) chromium film followed by a thicker (250-350 nm) silver film onto polished 2 in. diameter single crystal silicon wafers in a cryopumped E360A Edwards Coating System. The evaporation rates were 0.2 and 3.0-4.0 nm/s for chromium and silver, respectively. The surfaces were composed of about a monolayer of oxygen and small amounts of chlorine, sulfur, and carbon, as indicated by Auger electron spectroscopy. Micrographs, which were obtained in the laboratory ambient with a scanning tunneling microscope (Nanoscope II, Digital Instruments Inc.), indicate that the silver surface consisted of "hills" approximately 10 nm high, which were separated by about 60 nm. Such a topography corresponds to a roughness factor of ~1.4

Contact angles were measured in the laboratory ambient using a goniometer (Rame-Hart, Inc.). A drop of a fixed volume (~2μL) was formed on the end of a syringe needle and lowered into contact with the surface. As the needle was raised, the drop detached from the tip and advanced across the surface. The contact angles were then measured within 30 seconds of detachment. Exposure of the silver films to the laboratory ambient was minimized by performing the contact angle measurements immediately upon removal of the samples from the evaporator. Adsorption of laboratory contaminents at this surface presents only a minimal problem, provided that care is taken with cleanliness and that the measurements are made as soon as possible after preparation of the surface. Contact angle measurements of the oxides at more reactive metal surfaces such as copper, however, will likely necessitate the use of a controlled environment chamber. Deionized water was used as the probe liquid and its pH was adjusted with sodium hydroxide.

RESULTS AND DISCUSSION

Most metal surfaces are composed of metal oxides. In the laboratory ambient, the oxides at the surfaces hydrate to form a high density [2,14] of hydroxyl groups (1-5 hydroxyl group per 100 $Å^2$ of surface area). Empirically, such a surface can be represented as $MO_m(OH)_n$, where M is a metal. The surface hydroxyl groups adsorb water molecules via hydrogen bonding interactions wherein the surface acts either as the acid or base. An acidic surface site shows a tendency to donate a proton or a cation or to accept electrons or an anion, whereas a basic surface site shows a tendency to accept a proton or a cation or to donate electrons [15]. Upon contact with an electrolyte, the oxide surface may acquire an ionic charge by the following reactions:

$$\overline{M\text{-}OH} + OH^- \leftrightarrow \overline{M\text{-}O^-} + H_2O \qquad (1)$$

$$\overline{M\text{-}OH} + H_3O^+ \leftrightarrow \overline{M\text{-}OH_2^+} + H_2O \qquad (2)$$

where equations 1 and 2 are representative of the acidic and basic reactivities of the oxide, respectively. By definition, the pH at which the number of positive charges equals the number of negative charges is the isoelectric point of the surface (IEPS) or the point of zero charge (PZC). A low IEPS indicates an acidic surface, whereas a high IEPS indicates a basic surface.

Colloidal silver hydroxide shows amphoteric properties comparable to those in equations 1 and 2 [16]. On the basis of the amphoteric dissociation model [17,18], the deprotonation reactions that are involved in the establishment of a surface charge in the electrical double layer at silver hydroxide can be represented as:

$$\overline{AgOH_2^+} + H_2O \leftrightarrow \overline{AgOH} + H_3O^+ \qquad (3)$$

$$\overline{AgOH} + H_2O \leftrightarrow \overline{AgO^-} + H_3O^+ \qquad (4)$$

Reaction 4 has a K_a of 7.9×10^{-13} at 25°C [16]. Adding reactions 3 and 4 yields

$$\overline{AgOH_2^+} \leftrightarrow \overline{AgO^-} + 2H^+ \quad (5)$$

for which the equilibrium constant, K_T, is given as

$$K_T = a_{H^+}{}^2[\overline{AgO^-}]\gamma_-/[\overline{AgOH_2^+}]\gamma_+ \quad (6)$$

As written, K_T is a measure of the strength with which the silver oxide surface binds protons. If the activity coefficients (γ_-,γ_+) of the two surface sites are comparable, it then follows from equation 6 that K_T can be calculated via the pH of the PZC.

The changes in composition in reactions 3 and 4 will also be reflected by a change in interfacial tension, which is a direct measurement of intermolecular forces between a solid and a contacting liquid. At equilibrium, the interfacial tension between a solid and liquid, γ_{SL}, is defined by reference to a liquid drop resting on a solid surface and is quantitatively expressed by the Young relation [19]:

$$\gamma_{SV}^\circ - \gamma_{SL} = \gamma_{LV}^\circ \cos\theta \quad (7)$$

where γ_{SV}° and γ_{LV}° are the respective solid and liquid surface tensions in equilibrium with the saturated liquid vapor, and θ is the contact angle between liquid and solid. Assuming that changes in both γ_{SV}° and γ_{LV}° with pH are negligibly small (assumptions that have previously been validated by contact angle titrations at polyethylene and carboxylic acid functionalized polyethylene films [9]), decreases in θ will reflect an increase in the number of ionized surface groups through an increase in γ_{SL}. Thus, by variation of the pH of the contacting liquid, the ionization of the oxide surface can be followed as a "contact angle titration". This approach has been used successfully to determine the IEPS at silver iodide surfaces [20] as well as to follow the ionization of carboxylic acid sites at functionalized organic films [9,10].

In addition, contact angle titration data can be used to determine the IEPS of oxide surfaces such as silver hydroxide through considerations of surface excesses at the solid-liquid interfaces. For a silver hydroxide surface in equilibrium with sodium hydroxide at

constant temperature and pressure, the change in surface energy at the solid-liquid interface, $d\gamma_{SL}$, is related to the change in chemical potential of sodium hydroxide, $d\mu_{NaOH}$, by

$$-d\gamma_{SL} = \Gamma_{NaOH} d\mu_{NaOH} \quad (8)$$

where Γ_{NaOH} is the surface excess of sodium hydroxide. The surface charge density of the silver hydroxide-solution interface, σ, is related to Γ_{NaOH} by

$$\sigma = \Gamma_{NaOH} F \quad (9)$$

where F is the Faraday constant. Hence, substituting equation 9 into equation 8 yields:

$$-d\gamma_{SL} = \sigma d\mu_{NaOH}/F \quad (10)$$

Since OH^- is a potential-determining ion for the silver hydroxide-solution interface, then

$$d\mu_{NaOH} = 2.303RTd(pH) \quad (11)$$

where R and T are the gas constant and absolute temperature, respectively, and d(pH) is the change in pH. Differentiating equation 7 gives

$$d\gamma_{SV}^{\circ} - d\gamma_{SL} = \cos\theta d\gamma_{LV}^{\circ} + \gamma_{LV}^{\circ} d(\cos\theta) \quad (12)$$

Since, as noted previously, γ_{SV}° and γ_{LV}° are effectively independent of pH, equation 12 becomes

$$-d\gamma_{SL} = \gamma_{LV}^{\circ} d(\cos\theta) \quad (13)$$

Combining equations 10, 11 and 13 yields

$$\sigma/F = \gamma_{LV}^{\circ} d(\cos\theta)/2.303\ RTd(pH) \quad (14)$$

which indicates that the change in θ is controlled by σ. Since at the PZC, $\sigma = 0$, then

$$d(\cos\theta)/d(pH) = 0 \quad (15)$$

Therefore, in the absence of specifically adsorbed ions [3,11, 21], a maximum in θ or minimum in $\cos\theta$ will occur at the PZC as the pH of the probe liquid is changed.

A plot of θ versus pH of the contacting liquid at the surface of our evaporated silver films is shown in Figure 1. Starting at low pH, θ increases with increasing pH and reaches a

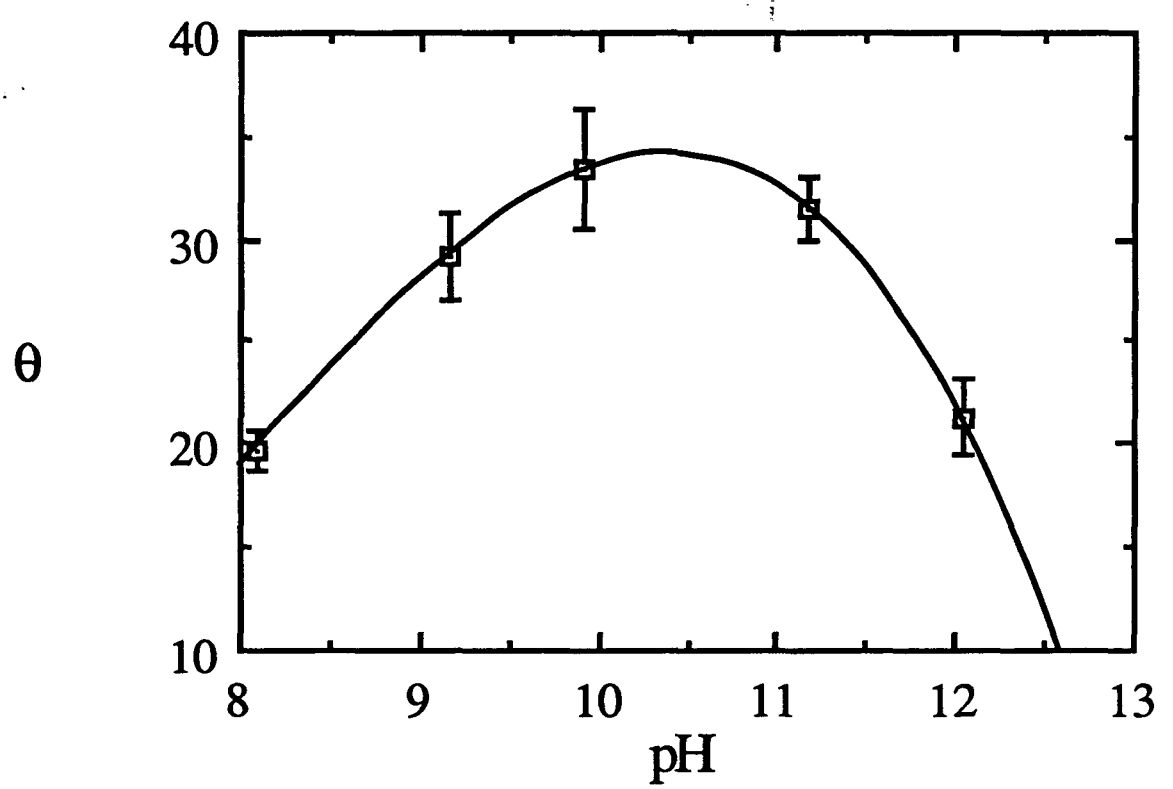

Figure 1. Dependence of contact angle (θ) of water on evaporated silver films as a function of pH. A polynomial curve fit of the data yields the third order equation: $\theta = 178.0 - 81.8(pH) + 11.8(pH)^2 - 0.5(pH)^3$. The data are reported as the mean of several locations on three replica samples, and the uncertainties are given as the standard deviation.

maximum at pH ~10.4. The change in θ reflects a decrease in γ_{SL} via reaction 3. Past this maximum, θ decreases as a result of an increase in γ_{SL} through reaction 4. From equation 15, the maximum at pH ~10.4 corresponds to the IEPS of our evaporated silver films, the value of which is in indicative of a basic basic oxide. Thus, K_T in equation 6 is equal to 1.6×10^{-21}, which further shows that protons are strongly held at the surface. Since K_T is equal to the products of the K_a's of reactions 3 and 4, the K_a of reaction 3 can be estimated assuming that the K_a for colloidal silver hydroxide in reaction 4 can be accurately translated to our silver oxides surfaces. This analysis yields a K_a for reaction 3 of $\sim 2.0 \times 10^{-9}$, the magnitude of which is consistent with the successive deprotonation of $AgOH_2^+$ and AgOH (i.e., K_a for reaction 3 > K_a for reaction 4 [16]).

In summary, the high IEPS of ~10.4 indicates that our evaporated silver films react as a basic oxide surface. Based on this result, we plan to examine the bonding strength between an adsorbed carboxylic acid and the oxide surface of silver, as predicted by the relationship of Bolger [2], through competitive adsorption experiments with carboxylic acid-functionalized adsorbate precursors which exhibit a range of acid strengths and structures. The variables affecting the IEPS include: (1) the charge of the metal ion, (2) the hydration state, (3) the coordination number, and (4) the structural or adsorbed impurities [22]. We also note that of the available methods for determination of surface acidity, the indicator method is limited to white or light-colored surfaces, although the use of fluorescent indicators may provide a means to overcome this limitation. Additionally, electrokinetic and potentiometric methods require powdered samples. In contrast, the method of contact angle titration provides a facile approach for the determination of the acidity of smooth solid surfaces.

REFERENCES

1. Benesi, H. A.; Winquist, B. H. C. Adv. Catal. 1978, 27, 97-182.
2. Bolger, J. C. in Adhesion Aspects of Polymeric Coatings; Mittal, K. L., Ed.; Plenum: New York, 1983; pp 3-18.
3. Yoon, R. H.; Salman, T. Can. Met. Quart. **1971**, 10, 171-177.
4. Hackerman, N.; Makrides, A. C. Ind. Eng. Chem. **1954**, 46, 523-527.
5. Allara, D. L.; Nuzzo, R. G. Langmuir **1985**, 1, 45-52.
6. Allara, D. L.; Nuzzo, R. G. Langmuir **1985**, 1, 52-66.
7. Schlotter, N. E.; Porter, M. D.; Bright, T. B.; Allara, D. L. Chem. Phys. Lett. **1986**, 132, 93-98.
8. Chau, L. K.; Porter, M. D. Chem. Phys. Lett., 1990, 167, 198-204.
9. Holmes-Farley, S. R.; Reamey, R. H.; McCarthy, T. J.; Deutch, J.; Whitesides, G. M. Langmuir **1985**, 1, 725-740.
10. Bain, C. D.; Whitesides, G. M. Langmuir **1989**, 5, 1370-1378.
11. Parks, G. A.; Bruyn, P. L. J. Phys. Chem. **1962**, 66, 967-973.
12. Atkinson, D.; Curthoys, G. Chem. Soc. Rev. **1979**, 8, 475-497.
13. Tanabe, K. Solid Acids and Bases; Academic: Tokyo, 1970; Chapter 2-3.
14. Boehm, H.-P. Angew. Chem., Int. Ed. Engl. **1966**, 5, 533-544.
15. Yamanaka, T.; Tanabe, K. J. Phys. Chem. **1976**, 80, 1723.
16. Johnston, H. L.; Cuta, F.; Garrett, A. B. J. Am. Chem. Soc. **1933**, 55, 2311-2325.
17. Davis, J. A.; James, R. O.; Leckie, J. O. J. Colloid Interface Sci. **1978**, 63, 480-499.
18. Chan, D.; Perram, J. W.; White, L. R.; Healy, T. W. J. Chem. Soc. Faraday Trans I **1975**, 71, 1046-1057.
19. Adamson, A. W. Physical Chemistry of Surfaces, 4th Ed.; Wiley: New York, 1982; pp 338-340.

20. Billett, D. F.; Hough, D. B.; Ottewill, R. H. J Electroanal. Chem. **1976**, 74, 107-120.

21. Moriwaki, H.; Yoshikawa, Y.; Morimoto, T. Langmuir **1990**, 6, 847-850.

22. Parks, G. A. Chem. Rev. **1965**, 65, 177-198.

SECTION II. COMPOSITION AND STRUCTURE OF SPONTANEOUSLY ADSORBED MONOLAYERS OF n-PERFLUOROCARBOXYLIC ACIDS ON SILVER

Composition and Structure of Spontaneously Adsorbed Monolayers of n-perfluorocarboxylic Acids on Silver

Lai-Kwan Chau and Marc D. Porter

Department of Chemistry and Ames Laboratory - USDOE

Iowa State University

Ames, Iowa 50011

ABSTRACT

Monolayer films of n-perfluorocarboxylic acids ($CF_3(CF_2)_nCOOH$ where n=0-2, 5-8) have been formed by spontaneous adsorption at silver. Infrared reflection spectroscopy, optical ellipsometry, and contact angle measurements indicate that these films exhibit low surface free energies, that the carboxylic acid group is symmetrically bound at the silver substrate as a carboxylate bridging ligand, and that the structure is composed of tilted (~40° from the surface normal) perfluorocarbon chains and small structural defects.

INTRODUCTION

Thin polymeric and monomolecular films of organofluorine compounds possess a variety of unique chemical and physical properties [1-4]. Many of these properties result from the low cohesive interactions between neighboring fluorocarbon chains, which lead to low surface free energies and low coefficients of friction. These and other properties (e.g., low dielectric constants, high dielectric strengths, and effective heat dissipation) have led to the use of such films for the construction of interfaces with applications to adhesion, lubrication, and microelectronics devices. Hence, molecular level descriptions of the interactions that control the formation, structure, and chemical properties of these films are of fundamental importance.

One approach for examining the molecular level details of organofluorine and other organic thin films is the use of monolayers that exhibit a high degree of structural order. Such monolayers can be prepared by Langmuir-Blodgett [5-7] or spontaneous adsorption [8-13] techniques to provide interfaces that are structurally and compositionally more defined than those of polymeric films. To date, studies of the molecular level details of ordered monolayers have been confined primarily to those composed of long alkyl chains [5-12]. Comparatively little is known concerning the composition and structure of monolayers containing fluorocarbon moieties [14].

This study examines the composition, structure, and wetting properties of spontaneously adsorbed monolayer films of perfluorinated carboxylic acids ($CF_3(CF_2)_nCOOH$, n=0-2, 5-8) at silver, as probed by infrared reflection spectroscopy (IRS), optical ellipsometry, and contact angle measurements. The composition and spatial arrangement of these monolayers were examined by IRS; the packing densities and wetting properties were probed by optical ellipsometry and contact angle measurements. Particular interest is given to the dependence of the packing density and wettability of the surface

structure on the length of the perfluorocarbon chain. Insights from this study are also relevant to the perfluorocarbon monolayers extensively examined with contact angle measurements by others [4,15-19].

EXPERIMENTAL

Monolayer films were formed by immersing evaporated silver films for 10-30 minutes into 1.0 mM solutions of perfluorinated carboxylic acids in absolute ethanol. The intermediate chain lengths (n=3, 4) are commercially unavailable at this time. Upon removal from solution, the films were rinsed with absolute ethanol and hexane. The evolution of the structure and wettability of the monolayers was monitored as a function of immersion time by IRS, optical ellipsometry and contact angle measurements.

The substrates were prepared by resistive evaporation of a thin (10-20 nm) chromium film followed by a thicker (250-350 nm) silver film onto polished 2 in. diameter single crystal silicon wafers. The roughness of the silver films was characterized by scanning tunneling microscopy. Micrographs indicate a surface that consists of "hills" approximately 10 nm high, which are separated by about 60 nm. Such topography corresponds to a roughness factor of ~1.4. The surfaces were covered by approximately a monolayer of oxygen and small amounts of chlorine, sulfur, and carbon as indicated by Auger electron spectroscopy.

For IRS, p-polarized light was incident at 78° from the surface normal. For the transmission IR measurements, the n-perfluorocarboxylic acids or their analogous silver salts were dispersed in a KBr matrix. Spectra were collected with a Nicolet 740 spectrometer at 2 cm^{-1} resolution with a bare gold film as a reference substrate. The procedure for cleaning the gold reference films has been previously described [10]. The monolayer thicknesses were determined by assuming a refractive index of 1.28 [20] from ellipsometric data that were obtained with a Gaertner L116B ellipsometer. Wetting properties were measured with a goniometer (Rame-Hart, Inc.), and are reported as advancing contact angles [11]. Micrographs of the silver surface were obtained in the ambient laboratory environment with a Nanoscope II scanning tunneling microscope (Digital Instruments Inc.).

Table I. Mode assignments and peak positions for perfluorooctanoic acid in KBr matrix and as monolayer adsorbed at silver[a]

Peak position (cm^{-1})			Vibrational mode[b]
acid in KBr	silver salt in KBr	as monolayer	
1771	---	---	ν(C=O)
---	1613	---	$\nu_a(COO^-)$
---	1420	1404	$\nu_s(COO^-)$
1366	1365	1365	$\nu_s(CF_2,A_1)$
1330	1324	1321	$\nu_s(CF_2,E_2)$
1295	1297	1293	$\nu(CC,E_1)$
1237	1238	1251	$\nu_a(CF_2,E_1)$
1204	1204	1216	$\nu_a(CF_2,A_2)+\nu(CF_3)$
1146	1145	1151	$\nu_s(CF_2,E_1)$

[a] Band assignments and labeling scheme from references 21-28.

[b] Key: ν=stretch; ν_s=symmetric stretch; ν_a=asymmetric stretch.

RESULTS AND DISCUSSION

Characterization with infrared spectroscopy

The molecular composition and orientation of the perfluorinated carboxylic acid monolayers were probed with IR spectroscopy. Figure 1A is an IRS spectrum for a monolayer of perfluorooctanoic acid at silver. Transmission IR spectra of the bulk perfluorooctanoic acid and its silver salt are given in Figures 1B and 1C, respectively. Peak positions and tentative vibrational mode assignments are shown in Table I. The IR spectrum of bulk perfluorooctanoic acid (Figure 1B) has an absorption near 1771 cm^{-1} for ν(C=O) of the carboxylic acid group, whereas the corresponding silver salt has bands at 1613 and 1420 cm^{-1} for $\nu_a(COO^-)$ and $\nu_s(COO^-)$, respectively. The ν(C=O) is absent in the monolayer spectrum (Figure 1A). This absence, together with the presence of $\nu s(COO^-)$ at 1404 cm^{-1}, indicate that the chemisorption process results in the formation of a carboxylate salt. Further, the lack of a detectable $\nu_a(COO^-)$ near 1613 cm^{-1} suggests that the carboxylate head group is symmetrically bound at the silver substrate as a bridging or bidentate ligand [29]. This conclusion is based on the "IR surface selection rule" which gives rise to a preferential excitation of vibrational modes with dipoles normal to highly reflecting metallic surfaces [30,31]. X-ray crystallographic studies of bulk silver perfluorocarboxylate support a bridging structure [32,33].

Several related studies provide further insights into the nature of the reaction between carboxylic acids and the silver surface. In ultra high vacuum [29], formic acid adsorbs in its undissociated molecular form at an atomically clean Ag surface. However, the reaction of atomically clean silver with oxygen results in a surface that produces adsorbed water and formate ion upon exposure to formic acid. Silver surfaces exposed to the ambient laboratory environment form oxides (AgO, AgO_2, AgO_3), with AgO being the predominant

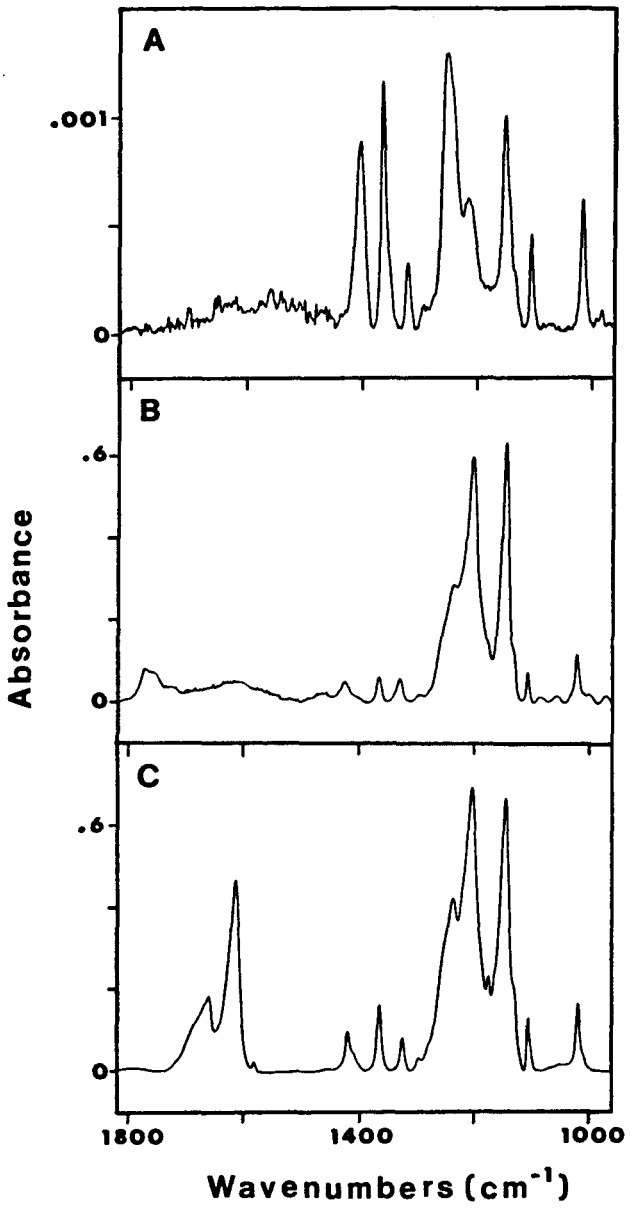

Figure 1. (A) Infrared external reflection spectrum of perfluorooctanoic acid as a monolayer on silver; (B) Infrared spectrum of perfluorooctanoic acid dispersed in KBr; (C) Infrared spectrum of silver perfluorooctanoate dispersed in KBr.

species [34]. The highly basic nature of AgO results in its extensive conversion to a AgOH species in the presence of water vapor [35]. The isoelectric point of the predominately AgOH surface, which we have measured by contact angle titrations [36], is ~10.4. This value is in reasonable agreement with that predicted by considerations of the effective ionic charge to size ratio of Ag [37]. Thus, as has been observed for arachidic acid ($CH_3(CH_2)_{20}COOH$) monolayers [12], the dissociative chemisorption of n-perfluorocarboxylic acids is consistent with the acid-base interfacial chemistry at the silver surface.

In addition to probing molecular composition, IRS was also used to determine the average orientation of these monolayers. Orientation was determined by a comparison of the measured absorbances with those calculated for an isotropic monolayer with classical electromagnetic theory and included considerations of the "IR surface selection rule" [30,31,38,39]. Perfluorocarbon chains have a 15/7 helical conformation above 19°C [40]. For a long perfluorocarbon chain (e.g., those in polytetrafluoroethylene (PTFE)), the transition dipole moment of the CF_2 stretch with A_2 symmetry is parallel to the chain axis, whereas those with E_1 symmetry are perpendicular to the chain axis [22]. However, the finite length of short perfluorocarbon chains results in a small deviation (<3°) in the spatial orientation of the transition dipole moments that are associated with $\nu_a(CF_2)$ mode with E_1 symmetry. The transition dipole moment that is associated with A_2 symmetry deviates by 21-24°. Quantitatively, a chain axis which is oriented exactly normal to a smooth metallic surface will lead to a small ($<1x10^{-5}$ absorbance units) signal for both the $\nu_a(CF_2)$ and $\nu_s(CF_2)$ modes with E_1 symmetry. The results of the calculations with the $\nu_a(CF_2)$ and $\nu_s(CF_2)$ indicate an average tilt of the molecular axis of the long perfluorocarbon chains (n=6-8) of ≈40°. Such tilts are in reasonable agreement with the symmetric binding of the carboxylate group at silver and the 116° C-C-C bond angle of fluorocarbon chain [41], which would yield a tilt of ~38°. Although an exact determination of uncertainty of the 40°

chain tilt has not yet been completed, the difference between the chain tilts may arise from the presence of defects in the monolayer. Defects would give rise to disordered chain packing, and hence, larger chain tilts. The structures of the monolayers for shorter perfluorocarbon are comparable to the longer chains, and exhibit a small decrease in coverage and a small increase in disorder, as evident from IRS data. The decrease in coverage is inferred from a small decrease in the absorbances of the $\nu_s(COO^-)$ for the shorter chains. A detailed discussion of the results of the structural examination of these monolayers will be reported elsewhere.

Characterization with optical ellipsometry

Optical ellipsometry is a convenient means of determining an average thickness of a monolayer film [9]. The ellipsometric data in Figure 2 indicate that the thicknesses of the n-perfluorocarboxylic acid monolayers increase linearly with an increase in n. Linear regression analysis of the data yields a slope of 0.8 Å per CF_2 group and an intercept of 4.6 Å. To compare these data to a simple structural model, thicknesses were calculated for two idealized n-perfluorocarboxylate monolayers with a 15/7 helical conformation for the perfluorocarbon chain. For one, the chain axis was oriented perpendicular to the surface. For the other, the chain axis was tilted 40° from the surface normal. The thicknesses of these model structures were estimated from tabulations of covalent and van der Waals radii [42] and x-ray crystallographic data for silver perfluorocarboxylate [32]. The theoretical slopes and intercepts for the perpendicular and tilted orientations are 1.29 Å/CF_2 and 4.64 Å, and 0.99 Å/CF_2 and 4.64 Å, respectively.

Comparisons of the observed slopes with those for the model films in Figure 2 indicate a large average tilt for the perfluorocarbon chains. Further, the observed thicknesses

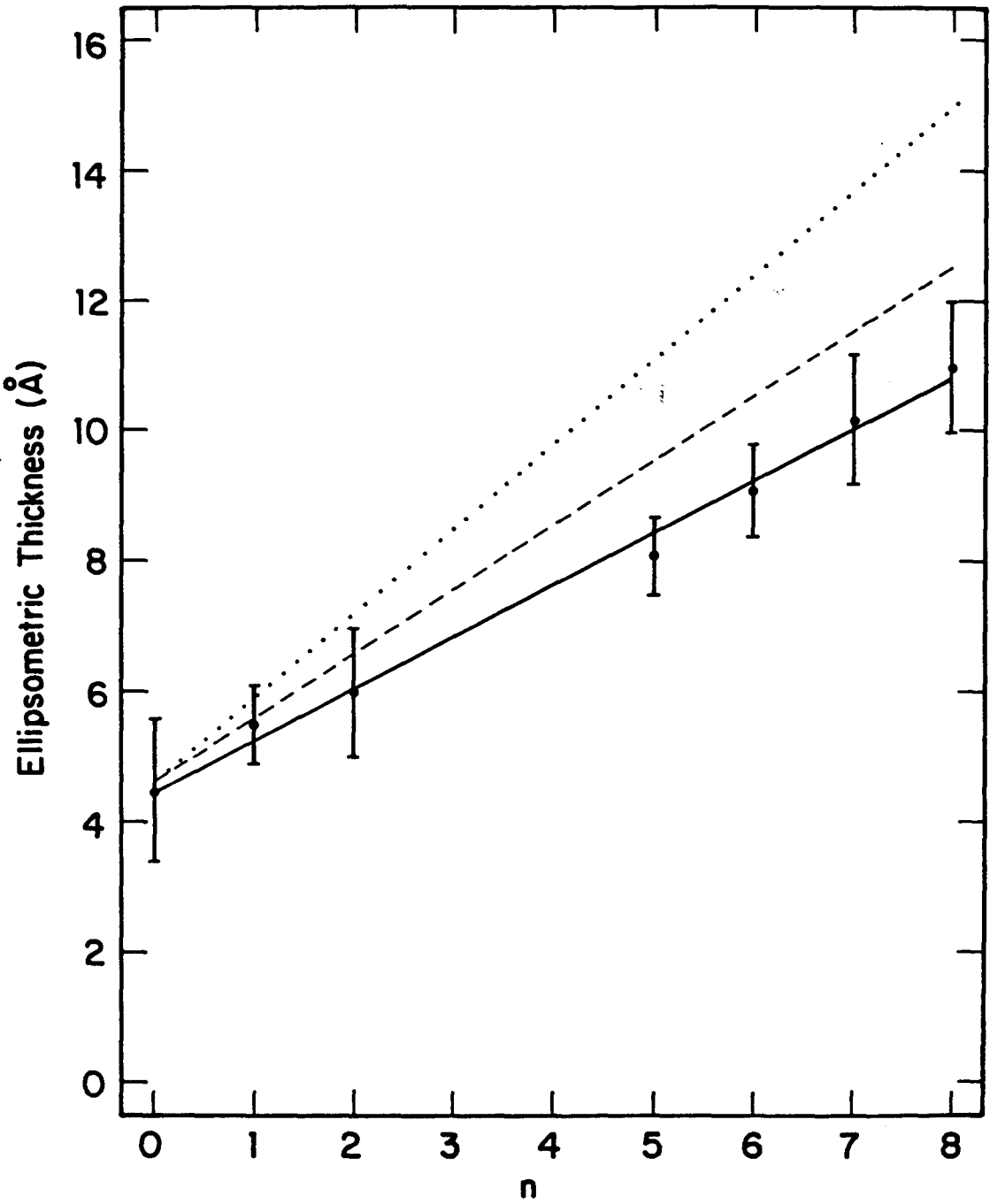

Figure 2. Film thickness for monolayers of $CF_3(CF_2)_nCOOH$ adsorbed at silver; the ellipsometrically determined thickness (—), estimated thickness for a fully extended chain normal to the surface (···) and tilted 40° from the surface normal (---), are plotted against the number of CF_2 groups in the chain, n.

are slightly less than those calculated for a chain tilt of 40°; this suggests either an average chain tilt of greater than 40° or the presence of defects in the monolayer structure. The incorporation of defects into a monolayer structure with a 40° chain tilt yields thicknesses for a fractional coverage of ~0.9 that are comparable to those observed. Thicknesses for the monolayers with fractional coverages were calculated with Maxwell-Garnett effective medium theory [43]. Considerations of contact angle hysteresis (see next section) also point to a fractional coverage of ~0.9. Although not fully understood, defects in these monolayers probably arise from both the presence of grain boundaries and other irregularities in the underlying silver substrate, as well as from the adsorption of trace amounts of strongly bound contaminants from the ambient laboratory environment. Low levels of hydrocarbon contamination were apparent from the presence of weak bands in the CH stretching regions in a few of the IR spectra of the monolayers. In summary, the trends in these ellipsometric data closely correlate with those from IRS and from contact angle measurements in the following section, pointing to a tilted chain structure and the presence of small structural defects.

Characterization with contact angle measurements

The wetting properties of the perfluorocarboxylic acid monolayers were examined with contact angle measurements. The results are given as a function of chain length in Figure 3 for the nonpolar liquid hexadecane and the polar liquids glycerol and water. Wetting properties for PTFE and a CF_3-terminated interface (perfluorooctylethanethiol monolayer at gold [44]) are included for comparison purposes. The probe liquids were selected based on their differing depth sensitivities to the underlying surface structure [45]. Two observations from the data in Figure 3 are immediately apparent. First, advancing contact angles (θ_a) for each liquid increase as the chain length increases, reaching values that are comparable to the low free energy surface of PTFE. For all three liquids, however, the limiting θ_a's are less

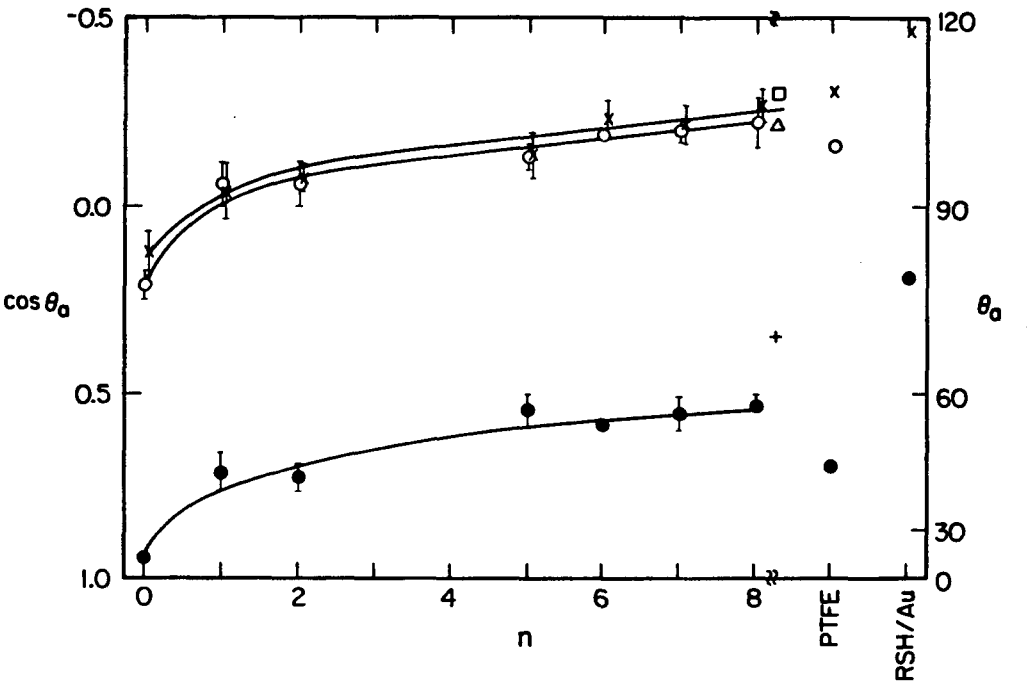

Figure 3. Advancing contact angles for monolayers of $CF_3(CF_2)_nCOOH$ adsorbed at silver (hexadecane (•), glycerol (o), and water (x)). Contact angles for the three liquids for a monolayer of $CF_3(CF_2)_8COOH$ adsorbed at silver with minimal exposure to the laboratory ambient are given by the symbols, (hexadecane (+), glycerol (Δ), and water (□)).
PTFE = polytetrafluoroethylene, R = $CF_3(CF_2)_7(CH_2)_2$.

than those for an interface terminated with a $-CF_3$ group [44]. This suggests that the perfluorocarbon chains are not closest-packed. Fractional coverages of ~0.9 monolayers were estimated by considerations of the hysteresis between the advancing and receding contact angles [46,47]. Second, the similarity in the shapes of the curves for all three liquids illustrates the ability of a single $-CF_2-$ group to screen extensively each of the probe liquids from the underlying substrate. In contrast, only hexadecane is extensively screened from the underlying structure by a single $-CH_2-$ at monolayers of ω-mercapto ethers [45]; water exhibits a depth sensitivity of ~5 Å. We attribute a large part of the difference between the perfluorocarbon and hydrocarbon monolayers to the inability of the liquids to penetrate into the bulkier and more rigid perfluorocarbon chains.

Although less than that observed for hydrocarbon chains, differences in the depth sensitivity of the probe liquids at the perfluorocarboxylic acid monolayers are apparent. For hexadecane, θ_a at the perfluorodecanoic acid monolayer is greater than that at PTFE. By comparison, θ_a for water at the perfluorodecanoic acid monolayer only approach that of PTFE. The differences between the two liquids may be explained by steric effects. Because of its smaller size, water may be accommodated into the space between neighboring $-CF_3$ groups. This allows interactions between water molecules and ω-CF_2 groups, leading to θ_a which is comparable to that at PTFE. Hexadecane, however, is sterically excluded from interacting with the ω-CF_2 groups and is therefore sensitive primarily to the terminal $-CF_3$ groups.

Effect of exposure to the laboratory ambient

As noted earlier, the IRS spectra suggested the possible influence of adsorbed contaminants on the uncoated metal surface. To test for this influence, samples were immersed into a perfluorodecanoic acid solution immediately upon removal from the vacuum

evaporation chamber. The wetting properties of monolayers prepared in this fashion are superimposed on the data in Figure 3 (θ_a(hexadecane) = 70°, θ_a(water) = 108°, and θ_a(glycerol) = 103°). These θ_a's are all greater than those measured for samples exposed to the laboratory ambient for ~15 min during an ellipsometric measurement of the uncoated substrate optical properties. The increase in θ_a's indicates an increase in the packing density of the perfluorocarbon chains. Fractional coverages of near unity are found from contact angle hysteresis considerations, pointing to the need to minimize exposure to the ambient laboratory environment to assure the formation of a more densely-packed surface structure. In comparison to other interesting monolayers, those derived from perfluocarboxylic acid monolayers are more susceptible to contamination than those from n-alkanethiols [11]. This suggests the strength of immobilization interactions at the perfluorinated acid-silver interface is qualitatively less than that at the alkanethiol-gold interface.

CONCLUSION

Infrared reflection spectroscopy, optical ellipsometry, and contact angle measurements indicate that n-perfluorocarboxylic acids adsorb at evaporated polycrystalline silver substrates to form monolayer films. The IR data indicate that the formation of monolayer results in the transformation of the carboxylic acid to a symmetrically bound carboxylate salt. Contact angle data also suggest that monomolecular films composed of n-perfluorocarboxylic acids are less penetrable by probe liquids relative to monomolecular films of alkyl chains. Extensive studies concerning the packing, surface coverage, and dynamics of film formation are currently in progress. Comparisons of formation and structure of n-perfluorocarboxylic and n-alkanoic acids are also planned.

REFERENCES

1. Brice, T. P.; Bryce, H. G.; Scholbery, H. M. Chem. Eng. News **1953**, 31, 510.
2. Mukerjee, P.; Handa, T. J. Phys. Chem. **1981**, 85, 2298.
3. Patrick, C. R. Chem. Britain **1971**, 7, 154.
4. Hare, E. F.; Shafrin, E. G.; Zisman, W. A. J. Phys. Chem. **1954**, 58, 236.
5. Chollet, P.-A. Thin Solid Films **1978**, 52, 343.
6. Allara, D. L.; Swalen, J. J. Phys. Chem. **1982**, 86, 2700.
7. Rabolt, J. F.; Burns, F. C.; Schlotter, N. E.; Swalen, J. D. J. Chem. Phys. **1983**, 78, 946.
8. Nuzzo, R. G.; Allara, D. L. J. Am. Chem. Soc. **1983**, 105, 4481.
9. Allara, D. L.; Nuzzo, R. G. Langmuir, **1985**, 1, 52.
10. Porter, M. D.; Bright, D. L.; Allara, D. L.; Chidsey, C. E. D. J. Am. Chem. Soc. **1987**, 109, 3559.
11. Bain, C. D.; Troughton, E. B.; Tao, Y. T.; Evall, J.; Whitesides, G. M.; Nuzzo, R. G. J. Am. Chem. Soc. **1989**, 111, 321.
12. Schlotter, N. E.; Porter, M. D.; Bright, T. B.; Allara, D. L. Chem. Phys. Lett. **1986**, 132, 93.
13. Zisman, W. A. In Friction and Wear; Davies, R., Ed.; Elsevier: Amsterdam, 1959.
14. Naselli, C.; Swalen, J. D.; Rabolt, J. F. J. Chem. Phys. in press.
15. Schulman, F.; Zisman, W. A. J. Colloid Sci. **1952**, 7, 465.
16. Ellison, A. H.; Fox, H. W.; Zisman, W. A. J. Phys. Chem. **1953**, 57, 622.
17. Shafrin, E. G.; Zisman, W. A. J. Phys. Chem. **1957**, 61, 1046.
18. Shafrin, E. G.; Zisman, W. A. J. Phys. Chem. **1962**, 66, 740.
19. Shafrin, E. G.; Zisman, W. A. J. Phys. Chem. **1960**, 64, 519.
20. Hudlicky, M. Organic Fluorine Chemistry; Plenum Press: New York, 1971; p 64.

21. Liang, C. Y.; Krimm, S. J. Chem. Phys. **1956**, 25, 563.
22. Moyniham, R. E. J. Am. Chem. Soc. **1959**, 81, 1045.
23. Koenig, J. L.; Boerio, F. J. J. Chem. Phys. **1969**, 50, 2823.
24. Hannon, M. J.; Boerio, F. J.; Koenig, J. L. J. Chem. Phys. **1969**, 50, 2829.
25. Boerio, F. J.; Koenig, J. L. J. Chem. Phys. **1970**, 52, 4826.
26. Zerbi, G.; Sacchi, M. Macromolecules **1973**, 6, 692.
27. Masetti, G.; Cabassi, F.; Morelli, G.; Zerbi, G. Macromolecules, **1973**, 6, 700.
28. Faniran, J. A.; Patel, K. S. Spectrochim. Acta **1976**, 32A, 1351.
29. Canning, N. D. S.; Madix, R. J. J. Phys. Chem. **1984**, 88, 2437.
30. Greenler, R. G. J. Chem. Phys. **1966**, 44, 310.
31. Pearce, H. A.; Sheppard, N. Surf. Sci. **1976**, 59, 205.
32. Blakeslee, A. E.; Hoard, J. L. J. Am. Chem. Soc. **1956**, 78, 3029.
33. Griffin, R. G.; Ellet, J. D., Jr.; Mehring, M.; Bullitt, J. G.; Waugh, J. S. J. Chem. Phys. **1972**, 57, 2147.
34. Moore, W. M.; Codella, P. J. J. Phys. Chem. **1988**, 92, 4421.
35. Bolger, J. C. In Adhesion Aspects of Polymeric Coatings; Mittal, K. L., Ed.; Plenum Press: New York, 1983.
36. Chau, L. K.; Porter, M. D. submitted for publication in J. Colloid Interface Sci.
37. Parks, G. A. Chem. Rev. **1965**, 65, 177.
38. Hansen, W. N. J. Opt. Soc. Am. **1968**, 58, 380.
39. Porter, M. D. Anal. Chem. **1988**, 60, 1143A.
40. Clark, E. S.; Muus, L. T. Z. Krist. **1962**, 117, 119.
41. Bunn, C. W.; Howells, E. R. Nature, **1954**, 174, 549.
42. Pauling, L. The Nature of the Chemical Bond; Cornell University Press: Ithaca, 1960.
43. Fenstermaker, C. A.; McCracken, F. L. Surf. Sci. **1969**, 16, 85.

44. Chidsey, C. E. D.; Loiacono, D. N. Langmuir **1990**, 6, 682-691.

45. Bain, C. D.; Whitesides, G. M. J. Am. Chem. Soc. **1988**, 110, 5897.

46. Dettre, R. H.; Johnson, R. E., Jr. J. Phys. Chem. **1965**, 69, 1507.

47. Cassie, A. B. O. Discuss. Faraday Soc. **1948**, 3, 11.

SECTION III. COMPARISON OF SELF-ASSEMBLED MONOLAYERS: FORMATION AND STRUCTURAL CHARACTERIZATION OF n-ALKANOIC ACID AND n-PERFLUOROCARBOXYLIC ACID MONOLAYERS ON SILVER

Comparison of Self-Assembled Monolayers: Formation and Structural Characterization of n-Alkanoic Acid and n-Perfluorocarboxylic Acid Monolayers on Silver

Lai-Kwan Chau, Kristy M. Wolff, and Marc D. Porter

Department of Chemistry and Ames Laboratory-USDOE

Iowa State University

Ames, Iowa 50011

ABSTRACT

Comparison has been made of monolayer assemblies of n-alkanoic acids and n-perfluorocarboxylic acids spontaneously adsorbed at silver from dilute solution. These monolayers were characterized by optical ellipsometry, contact angle measurements, and infrared spectroscopy. As the chain length decreases, these structures become less densely packed and have lower coverages. This structural change, however, is smaller for the n-perfluorocarboxylic acid monolayers. Competitive adsorption studies from mixtures of n-decanoic and n-perfluorodecanoic acid indicate that n-perfluorodecanoic acid preferentially adsorbs at silver surfaces.

INTRODUCTION

Structurally well-defined organic monolayers on solid surfaces provide a rational approach to simplify and model a large variety of interfacial phenomena such as wetting [1], adhesion [2,3], lubrication [4,5], corrosion [6], electrocatalysis [7], and surface recognition and dynamics of biomembranes [8]. These phenomena are all related to the composition and structure of the interface. For example, organofluorine compounds have the lowest recorded surface tensions [9] and therefore have been applied to modify surfaces to improve their wetting properties and to reduce wear. Furthermore, the molecular nature of the carboxylic acid monolayers, that is, a hydrophobic tail covalently bonded to a hydrophilic head group, is similar to the components of the cell wall of biological membranes. This suggests that studies of self-assembled monolayers may provide insights into structure/function relationships of these more complex system.

The reactivity between an adsorbate and a substrate depends on several parameters, including the acidity of the carboxylic acid head group, the length and composition of the tail, and the composition of the native oxide at the metal surface. The strong electronegative inductive effect of fluorine in the carbon chain increases considerably the acidity of fluorinated carboxylic acids. Thus, understanding the effect of acid strength of the head group and the length and composition of the tail will provide a basis for enhancing the design and construction of adhesive interfaces with improved performance characteristics and will impact the packaging of microelectronic devices as well as other areas of surface research.

As our goal in this area, we have been searching for approaches to study the fundamental chemical and physical interactions that control the formation and structure of chemically modified surfaces. The types of interactions which are most relevant to the structural aspects include the bonding interactions, the registry between the head group and the substrate, and the intermolecular interactions between adjacent adsorbate molecules. Most

studies of the adsorption of carboxylic acids on metals have involved surfaces exposed to air prior to adsorption and thus largely refer to adsorption on native oxide overlayers. These studies indicate that the acids chemisorbed to form silver carboxylate salts [10-12]. However, at an atomically clean silver, formic acid adsorbs only as its undissociated molecular form [10]. The dissociative chemisorption process involved in the self-assembly of a n-alkanoic acid or n-perfluorocarboxylic acid monolayer on silver is shown in equation 1:

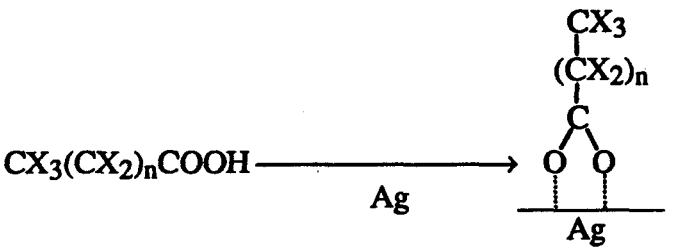

The carboxylate head group is symmetrically bound at the silver substrate as a bridging or bidentate ligand as suggested by infrared reflection spectroscopy [11,12]. X-ray crystallographic studies of bulk silver carboxylates support a bridging structure [13-15].

In this paper we compare results on the structural characterization of self-assembled monolayers of n-alkanoic acid ($CH_3(CH_2)_nCOOH$, n=0-10,12-18) and n-perfluorocarboxylic acid ($CF_3(CF_2)_nCOOH$, n=0-2,4-8) on polycrystalline silver, and present results on monolayers formed from binary mixtures of n-alkanoic and n-perfluorodecanoic acid. The importance of chain length on the packing density, intermolecular environment, geometry, and wetting properties of the monolayer assemblies are of particular interest. The preference for the adsorption of n-perfluorocarboxylic acid from binary mixtures of n-alkanoic and n-perfluorocarboxylic acid will also be addressed.

EXPERIMENTAL

Substrate preparation and characterization

The substrates were prepared by resistive evaporation of a thin (10-20 nm) chromium film followed by a thicker (250-350 nm) silver film onto polished 2 in. diameter single crystal silicon wafers in a cryopumped E360A Edwards Coating System. The evaporation rates were 0.2 and 3.0-4.0 nm/s for chromium and silver, respectively. The surfaces were covered by approximately a monolayer of oxygen and small amounts of chlorine, sulfur, and carbon as indicated by Auger spectroscopy. The roughness of the silver films was characterized by a Nanoscope II scanning tunneling microscope (Digital Instruments, Inc.) in the ambient laboratory environment. Micrographs indicate a surface that consisted of "hills" approximately 10 nm high, which were separated by about 60 nm. Such a topography corresponds to a roughness factor of ~1.4. Film crystallography was examined by comparing voltammetric stripping curves for underpotentially deposited thallium on evaporated silver films to those obtained for single crystal surfaces [16]. Cyclic voltammograms of Tl^+ underpotential deposition on evaporated silver film suggest a predominance of (100) orientation with some (111) or (110) orientation [17]. The relative amounts of these orientations was somewhat variable, which is probably a result of the variability in the deposition conditions.

Self-assembly of monolayers at silver

The n-alkanoic acid assemblies were formed by the immersion of freshly evaporated silver films for varying periods (2-24 hours) into a 1.0 mM solution of the n-alkanoic acid in hexadecane. The hexadecane was purified by column chromatography just prior to use with activity-one-α-alumina. The n-perfluorocarboxylic acid assemblies were formed by the immersion of freshly evaporated silver films for 10-30 minutes into a 1.0 mM solution of

n-perfluorocarboxylic acid in absolute ethanol. The progress of the formation of the self-assembled structures was monitored by infrared reflection spectroscopy (IRS), optical ellipsometry and contact angle measurements. Mixed monolayers of n-decanoic acid and n-perfluorodecanoic acid were formed by the immersion of freshly evaporated silver films into a binary mixture of n-alkanoic acid and n-perfluorodecanoic acid in absolute ethanol. The mole fractions of the two adsorbates were varied while the total concentration was kept constant at 1.0 mM. Upon removal from solution, the films were rinsed with absolute ethanol and hexane (HPLC grade).

Infrared spectroscopy analysis

Infrared external reflection spectra were collected with a Nicolet 740 Fourier transform spectrometer at an angle of incidence of 78° or 80° with p-polarized light. Spectra were obtained by coaddition of 1024 sample to background scans at 2 cm^{-1} resolution (zero filled) with Happ-Genzel apodization. A liquid nitrogen cooled InSb or MCT detector was used to monitor the intensity of the reflected beam. All spectra are reported as the $-\log(R/R_0)$ where R is the reflectivity of the monolayer at silver and R_0 is the reflectivity of a bare gold reference substrate. The procedure for cleaning the gold references has been previously described [18].

Ellipsometric film thickness measurements

The monolayer thicknesses were determined with a Gaertner model L116B ellipsometer at an angle of incidence of 70°. The complex refractive indexes for the substrates were measured immediately upon removal from the evaporation chamber. After monolayer formation, thicknesses of the monolayers were then measured. Real refractive

indexes of 1.45 and 1.28 were assumed for n-alkanoic acid and n-perfluorocarboxylic acid monolayers, respectively.

Contact angle measurements

Contact angles were measured using a Rame-Hart model 100 goniometer. Both advancing and receding contact angles were measured. A drop of a fixed volume (~2μL) was formed on the end of a syringe needle and lowered into contact with the surface. As the needle was raised, the drop detached from the tip and advanced across the surface. The advancing contact angles were then measured within 30 seconds. The receding angle was measured when the liquid was partially withdrawn from the drop by the syringe needle.

Atomic emission spectroscopy analysis

The silver concentration of the self-assembly solutions after immersion of silver substrates for 15 minutes to 24 hours was determined with an inductively coupled plasma atomic emission spectrometer (ICP-AES). The silver atom line at 328.068 nm was monitored. Other conditions are described previously [19], except a Cetac U-5000 ultrasonic nebulizer was used instead of a pneumatic nebulizer.

RESULTS AND DISCUSSION

Defectiveness, intermolecular environment

Optical ellipsometry is a convenient means of both determining the average thickness of a monolayer film and following the progress of film growth. Such film thickness determined could be coverage dependent, that is, the film thickness determined depends on the effective refractive index of the film. The effective complex refractive index of the film, N_e, can be calculated by assuming that the equivalent polarizability of the film is given by a simple volume average of the polarizability of the adsorbate and air [20] as:

$$(N_e^2-1)/(N_e^2+2) = q(N_s^2-1)/(N_s^2+2) \qquad (2)$$

where q is the volume fraction of the adsorbate, and N_s is the refractive index of the adsorbate. The ellipsometric data in Figure 1 show that the thicknesses of both the n-alkanoic acid and n-perfluorocarboxylic acid monolayers increase linearly with n. Linear regression analysis of the data yields a slope of 1.23 Å per CH_2 group with a corresponding intercept of 2.63 Å, and a slope of 0.79 Å per CF_2 group with a corresponding intercept of 4.49 Å. This linear dependence indicates that the change in packing density with chain length is not appreciable. Formation of multilayers was not observed for these monolayers as indicated by optical ellipsometry and IRS. In contrast, for n-alkanoic acids adsorbed at aluminum, when the chain length n is below 12, a pronounced tendency for the film to form multilayers was observed [21].

It is also important to note that the film thickness determinations are based on the difference in measured optical constants between a monolayer and a "clean" substrate prior to immersion into solution. Since the uncoated substrate has a high surface free energy, exposure to the laboratory ambient (which is necessitated for the determination of the optical functions of each uncoated substrate) leads to the rapid adsorption of a contaminant layer

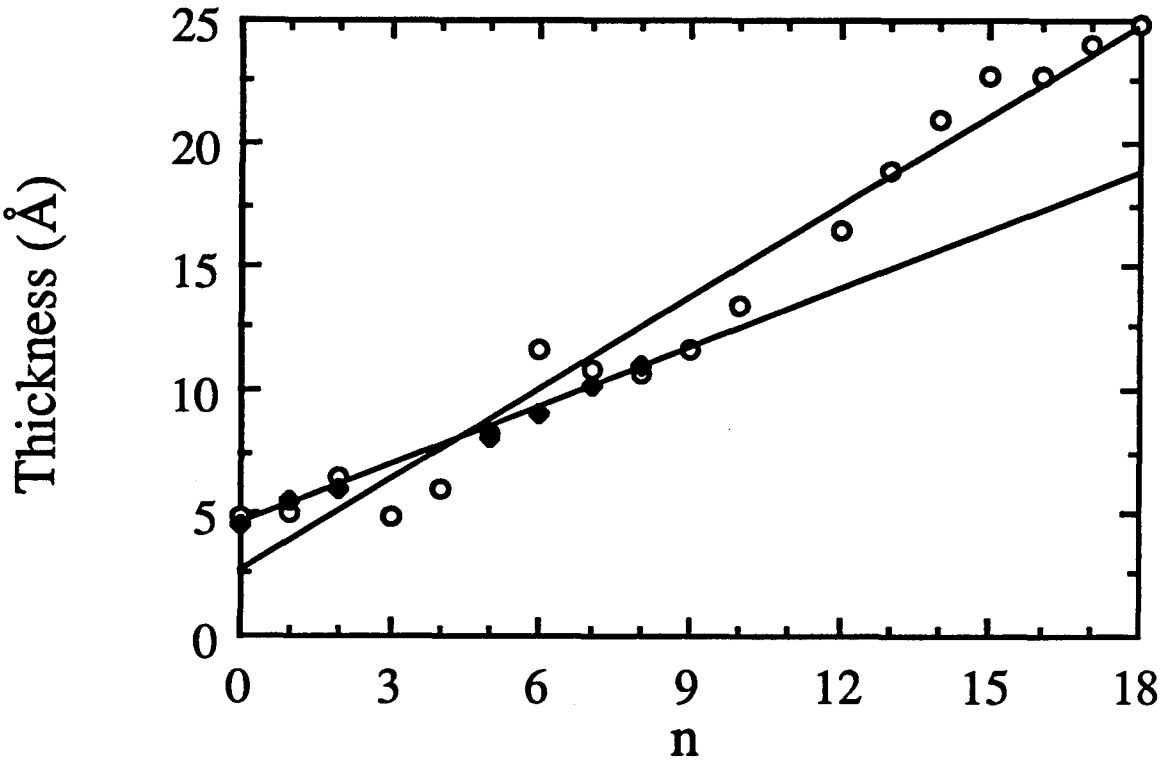

Figure 1. Ellipsometric film thicknesses for monolayers of $CH_3(CH_2)_nCOOH$ (o) and $CF_3(CF_2)_nCOOH$ (♦) at silver are plotted against n

[12]. The low surface free energies of the n-perfluorocarboxylic acid monolayers minimize the formation of a contaminant layer. Thus, the contaminant layer leads to the measurement of a thickness that is less than that of the actual monolayer. This systematic error is more severe for the long chain n-perfluorocarboxylic acid monolayers, which exhibit the lowest surface free energies. The same rationale applies to the relatively higher energy surfaces of n-alkanoic acid monolayers but to a lesser extent. Further, the observed thicknesses for long chain n-alkanoic acid monolayer are slightly larger than those calculated for a chain tilt of 27° (see next section). This may arise from our use of a constant refractive index, independent of chain length. The formation of close-packed hydrocarbon chains at large n may have a refractive index comparable to that of polyethylene (~1.5) rather than that of 1.45. Defects in these monolayers may also contribute to the discrepancy between the observed and calculated thickness. For n-perfluorocarboxylic acid monolayers, the observed thicknesses are slightly less than those calculated for a chain tilt of 40° (see next section); this suggests either an average tilt of greater than 40° or the presence of defects in the monolayer structure as indicated by equation 2. Although not fully understood, defects in these monolayers probably arise from the presence of grain boundaries and other irregularities in the underlying silver substrate and the adsorption of trace amounts of strongly bound contaminants from the laboratory ambient.

The fractional coverages of these monolayers were estimated by consideration of contact angle hysteresis. For a heterogeneous surface of two components, the observed contact angle, θ, is given by Cassie's equation [22]:

$$\cos\theta = \sigma_1\cos\theta_1 + \sigma_2\cos\theta_2 \qquad (3)$$

where σ_1 is the fraction of the surface having intrinsic contact angle θ_1, and σ_2 is the fraction having intrinsic contact angle θ_2. It was shown that advancing contact angle θ_a is relatively insensitive to coverages greater than 0.5 monolayer, while receding contact angle θ_r is

relatively sensitive to coverages greater than 0.8 monolayer [23]. If defects in a monolayer film are considered as free volume with fraction σ_2, then the free volume is filled with the probe liquid during retraction of the drop and the contact angle θ_2 equals zero. Hence, the receding contact angle can be expressed as

$$\cos\theta_r = \sigma_1\cos\theta_a + \sigma_2 \quad (4)$$

Rearranging,

$$\sigma_1 = (1-\cos\theta_r)/(1-\cos\theta_a) \quad (5)$$

Thus, the hysteresis between the advancing and receding contact angles can be used to estimate the fractional coverage of a monolayer. It should be noted that this method is based on the assumption that defects in a monolayer are free volume. However, these defect sites could also be occupied by contaminants. Therefore, comparison of hysteresis data between different monolayers can only be made if these defects have common source of origin, that is, a similar intrinsic contact angle. Figure 2 shows the fractional coverages of these monolayers as a function of n. All the samples were exposed to the laboratory ambient for ~15 minutes for the ellipsometric determination of the optical constants of the bare substrates. As is apparent, the monolayers become more densely packed and exhibit fewer defects as chain length increases. The coverage of the long chain n-alkanoic acid monolayers is nearly unity, whereas long chain n-perfluorocarboxylic acid monolayers have a fractional coverage of only ~0.9. Short chain n-alkanoic acid monolayers, however, are less densely packed relative to short chain n-perfluorocarboxylic acid monolayers.

The effects of chain conformation, orientation, coverage, and packing on the monolayer structure as a function of chain length were assessed with IR reflection spectroscopy. For n-alkanoic acid monolayers, the positions of the peak frequencies for symmetric methylene stretch $\nu_s(CH_2)$ and asymmetric methylene stretch $\nu_a(CH_2)$ indicate

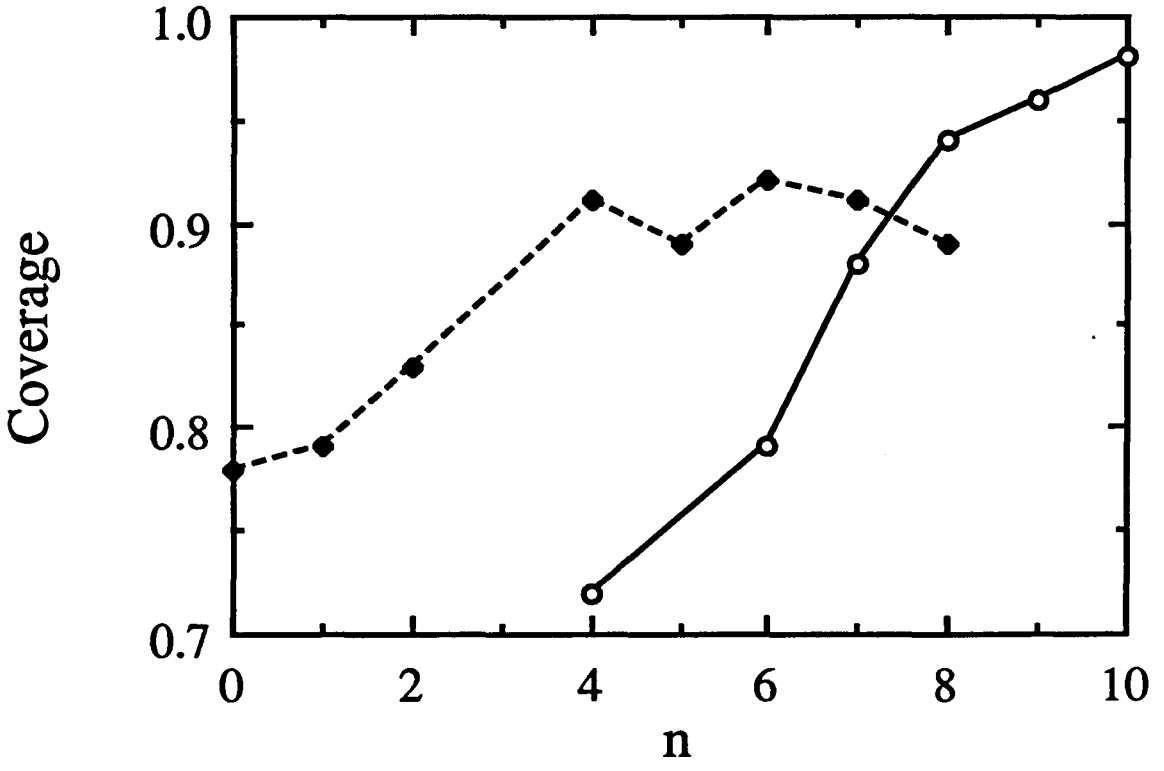

Figure 2. Fractional coverages for monolayers of $CH_3(CH_2)_nCOOH$ (o) and $CF_3(CF_2)_nCOOH$ (♦) self-assembled at silver as estimated by contact angle hysteresis are plotted against n

either a liquid-like (higher-energy) or crystalline-like (lower-energy) environment, providing insights into the intermolecular environment of the alkyl chains in the n-alkanoic acid monolayers [24]. The low absorbances of $\nu_s(CH_2)$ and $\nu_a(CH_2)$ for $n \leq 6$ precluded an accurate determination of their peak positions and peak intensities. Figure 3 shows the peak positions of $\nu_s(CH_2)$ and $\nu_a(CH_2)$ for the monolayers as a function of n. A comparison of the peak frequencies for $\nu_s(CH_2)$ in the monolayer spectra reveals that the average local environment of the alkyl chain is very similar to that existing in the bulk crystalline phase for $n \geq 8$. A similar trend is observed with $\nu_a(CH_2)$ for $n \geq 12$. In contrast, the average local chain environment for the shorter chains appears similar to that of the bulk disordered or liquid phase.

Plots of peak heights of the symmetric stretch $\nu_s(CH_2)$ as functions of n are given in Figure 4a. The broken line represents a hypothetical set of points for a linearly decreasing film thickness with constant structure. A negative deviation from linearity was observed with $n \leq 12$. Plots of peak heights of asymmetric in-plane stretch $\nu_a(CH_3,ip)$ and symmetric methyl stretch $\nu_s(CH_3,FR)$ as shown in Figure 4b exhibit an odd-even dependence on the number of methylene groups in the chain. The latter band, which is at ~2878 cm^{-1}, is in Fermi resonance with the lower frequency asymmetric CH_3 deformation mode [25]. The cause for this odd-even behavior can be revealed by examining the difference in the spatial orientation of the CH_3 stretching modes for the all-trans odd and even chains as shown in Figure 5. This conclusion is based on the the "metal-surface selection rule" which gives rise to a preferential excitation of vibrational modes with transition dipole moments normal to highly reflecting metallic surfaces [26,27]. In general, the overall trend of the intensity of the $\nu_a(CH_3,ip)$ and $\nu_s(CH_3,FR)$ modes for $n \geq 12$ is fairly insensitive to n, whereas the intensity gradually decreases for $n \leq 10$.

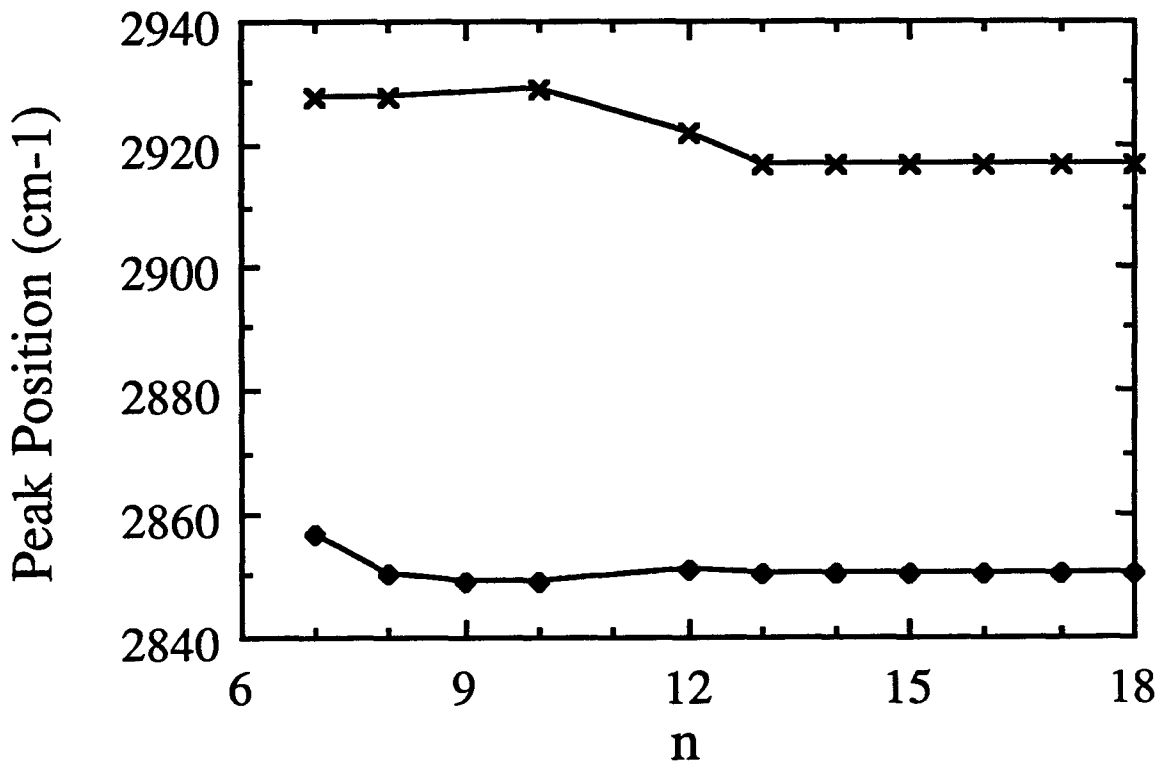

Figure 3. Peak positions of $\nu_s(CH_2)$ (♦) and $\nu_a(CH_2)$ (x) for monolayers of $CH_3(CH_2)_nCOOH$ self-assembled at silver as a function of the methylene group, n, in the alkyl chain.

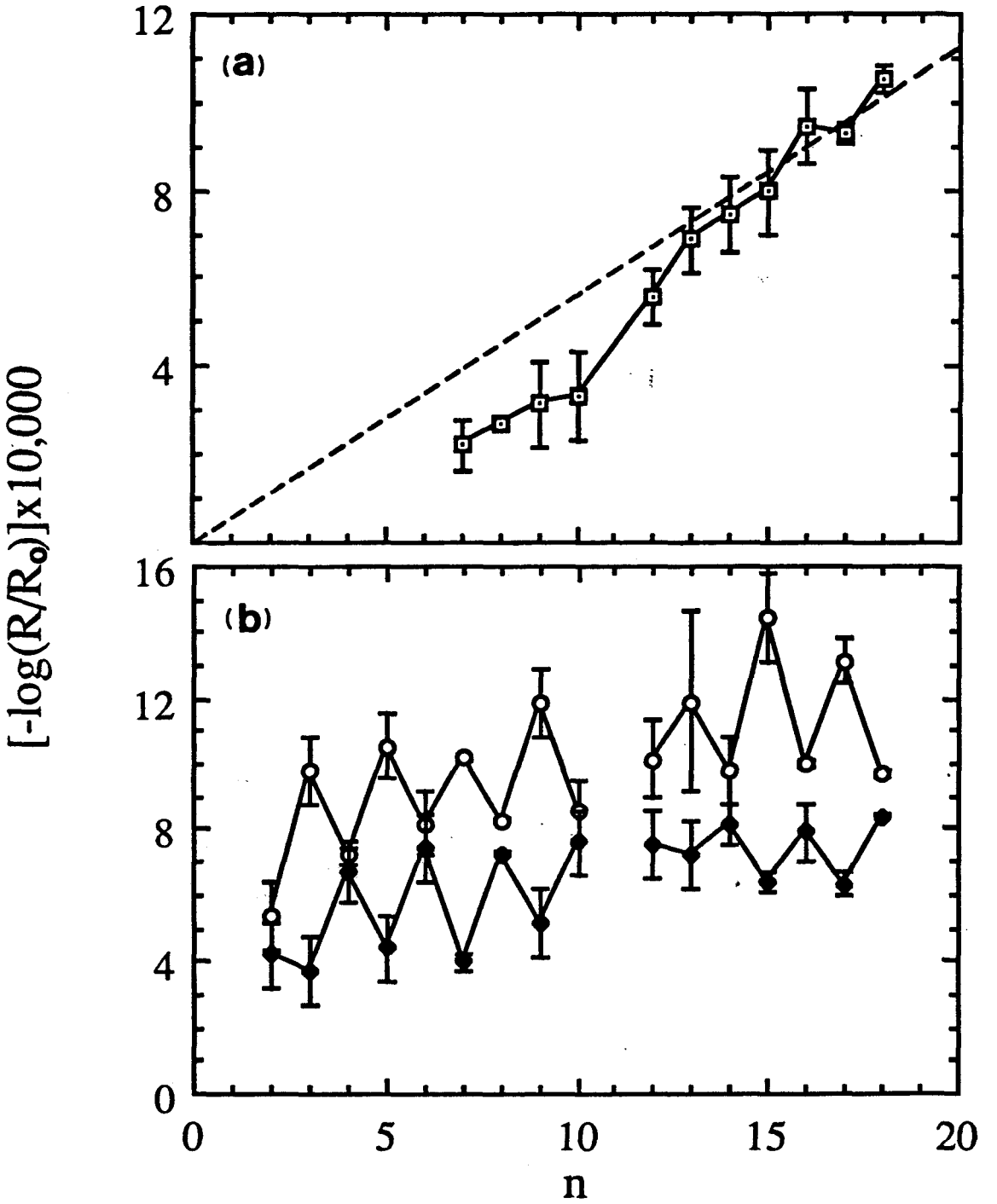

Figure 4. Peak heights of (a) $\nu_s(CH_2)$, (b) $\nu_a(CH_3,ip)$ (o), and $\nu_s(CH_3,FR)$ (♦) for monolayers of $CH_3(CH_2)_nCOOH$ self-assembled at silver as a function of the number of methylene groups, n, in the alkyl chain.

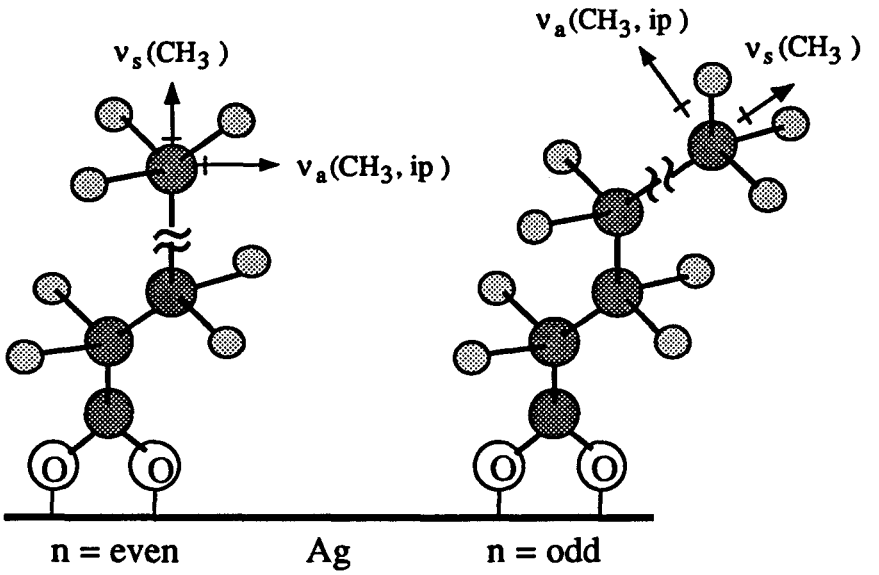

Figure 5. The proposed structure for a carboxylate on silver with an even (right) or odd (left) number of methylene groups in the chain

Three factors could contribute to this deviation from the dependence expected for constant film structure: coverage, chain orientation, and conformational order. The loss of intensity for the shorter chains can be partly accounted for by the loss of coverage with decreasing chain length, as shown in Figure 2. However, the loss of coverage may also lead to larger average chain tilts and conformational disorder. A larger chain tilt would cause an increase in $\nu_s(CH_2)$ intensity. An increase in conformational disorder would be associated with a decrease in $\nu_s(CH_2)$ intensity in isotropic samples [28]. On the other hand, for a surface monolayer with a 20-30° chain tilt, an increase in $\nu_s(CH_2)$ intensity upon randomization of the orientation of the monolayer CH_2 groups is suggested [18]. Although not yet fully understood, these trends indicate that with decreasing hydrocarbon chain length, the total cohesive chain-chain interaction lessens, the coverage decreases, and the chain order decreases.

For n-perfluorocarboxylic acid monolayers, the relatively large size of the fluorine atom (van der Waals radius 1.35 Å) results in a helical chain with a 15-atom repeating unit above 19°C [29,30]. In comparison, the van der Waals radius of hydrogen is 1.2 Å, and hydrocarbon molecules have a planar zigzag carbon chain. Thus, a potential energy barrier of 18.2 kJ mol^{-1} hinders mutual rotation of the CF_3 group in hexafluoroethane compared with a barrier of 12.6 kJ mol^{-1} to free rotation in ethane [31]. Fluorocarbon chains were also shown to be stiffer than hydrocarbon chains by studying the dynamics of end-to-end cyclization [32].

Saturated fluorocarbons have an extremely low intermolecular attraction. The relative weakness of the interaction of a $-CF_2-$ group with perfluorohexane as compared to a $-CH_2-$ group with hexane was shown by the incremental free energies of adsorption ($\Delta\Delta G°$) per $-CF_2-$ and $-CH_2-$ group. The $\Delta\Delta G°$ value for $-CH_2-$ groups at the hexane/water interface is more negative by 200 cal/mol than that at the air/water interface. In comparison, the $\Delta\Delta G°$

value for -CF_2- groups at the perfluorohexane/water interface is more negative than that for the air/water interface by only 60 cal/mol [33]. Taken together, we may expect that the dependence of coverage and chain packing as a function of chain length is smaller for perfluorocarbon molecules than that for hydrocarbon molecules, as consistent with our ellipsometry and contact angle hysteresis data.

Molecular orientation

Infrared reflection spectroscopy was used to determine the orientation of these monolayers. The experimental reflection spectra were compared to theoretical spectra in order to calculate molecular orientations. The theoretical spectra were calculated for a given thickness of a flat, uniform, isotropic layer of bulk material on the silver substrates with classical electromagnetic theory [34]. The application of this theory to reflection spectroscopy is based on boundary value solutions of Maxwell's equations for isotropic and parallel layers of dielectric media [35]. The values of the optical constants of the bulk overlayer material were estimated from transmission spectra of KBr pellets and calculated from the Kramers-Kronig transform [36].

The orientation of the various adsorbate functional groups which have IR active modes can be calculated from reflection spectra because of the anisotropy of the surface electric field. At a grazing angle of incidence with the electric field oriented normal to the surface (p-polarized), only those vibrational modes that have a component of their transition dipole moment normal to the surface will interact strongly with the electric field [26,27]. In this paper, the directions assigned to the chain axis and to the transition dipole moments for various modes are shown in Figure 6, where ϕ is the twist about the chain axis, θ is the tilt from the surface normal, and $\underline{c}$ is the chain axis vector. Before transformation, the chain axis is defined to be normal to the surface. By rotation of an arbitrarily oriented adsorbate

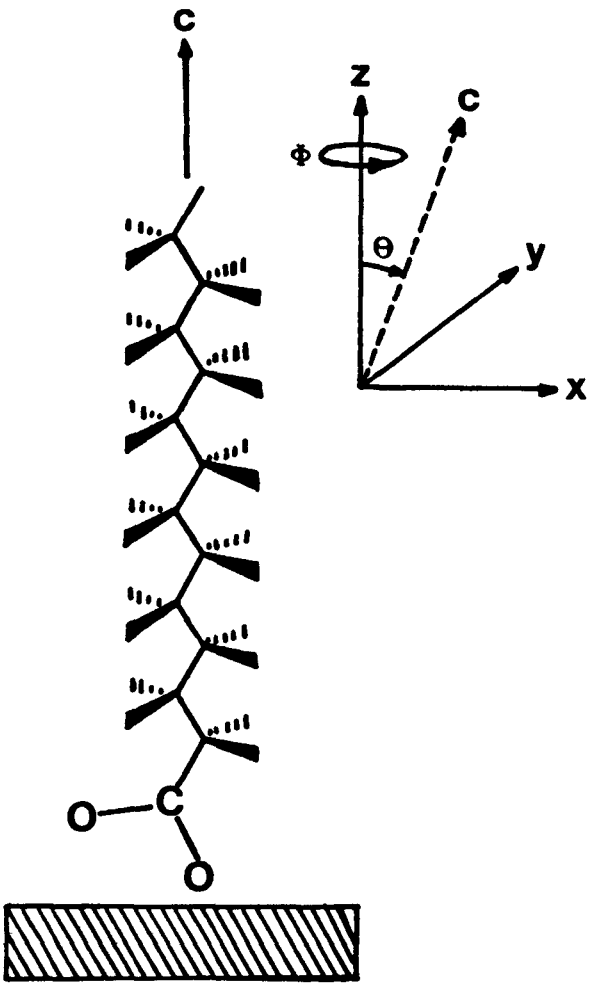

Figure 6. Schematic representation of the average tilt from the surface normal, θ, and average twist about the chain axis, ϕ. Vector ζ represents the direction of the chain axis.

molecule through angles ϕ, θ, and λ, the molecular coordinates after transformation (x', y', z') can be related to those before transformation (x, y, z) by Eulerian transformation [37]:

$$\begin{bmatrix} x' \\ y' \\ z' \end{bmatrix} = \begin{bmatrix} \cos\phi\cos\theta\cos\lambda-\sin\phi\sin\lambda & -\sin\phi\cos\theta\sin\lambda-\cos\phi\sin\lambda & \sin\theta\cos\lambda \\ \cos\phi\cos\theta\sin\lambda+\sin\phi\cos\lambda & -\sin\phi\cos\theta\sin\lambda+\cos\phi\sin\lambda & \cos\theta\sin\lambda \\ -\cos\phi\sin\theta & \sin\phi\sin\theta & \cos\theta \end{bmatrix} \begin{bmatrix} x \\ y \\ z \end{bmatrix} \quad (6)$$

Since the intensity of an infrared active mode is proportional to the square of the scalar product of the incident electric field and the transition dipole moment, it follows that the intensity will vary with orientation of the transition dipole moment at the surface. For a transition dipole moment along the z-axis, the intensity for that mode is 3 times that for the intensity for random orientation. As a result, if the transition dipole moments ($\partial\mu/\partial q$) perpendicular and parallel to $\mathfrak{C}$ are represented by unit vectors (1,0,0), (0,1,0), and (0,0,1), rotation of these unit vectors by angles ϕ and θ gives the following relationships:

$$I_e = 3I_c\cos^2\phi\sin^2\theta \qquad \text{for } \partial\mu/\partial q = (1,0,0) \qquad (7)$$

$$I_e = 3I_c\sin^2\phi\sin^2\theta \qquad \text{for } \partial\mu/\partial q = (0,1,0) \qquad (8)$$

$$I_e = 3I_c\cos^2\theta \qquad \text{for } \partial\mu/\partial q = (0,0,1) \qquad (9)$$

where I_e and I_c are the observed and calculated intensity, respectively, of a given vibrational mode. Thus, by relating the molecular axis of the adsorbate to the orientation of a vibrational mode, the spatial orientation of the surface structure can be determined.

For n-alkanoic acid monolayers, the transition dipole moments of the CH_2 stretching modes are perpendicular to the hydrocarbon chain. Thus, the measured intensities of the CH_2 stretching modes can be used to calculate an average tilt of the chain axis from the surface normal. Figure 7 shows calculated and observed spectra of arachidic acid monolayer on silver. The results of these calculations indicate an average tilt θ of 24-29°, and an average twist ϕ of 44-45° about the chain axis for the n=13-18 chains. Such tilts are in

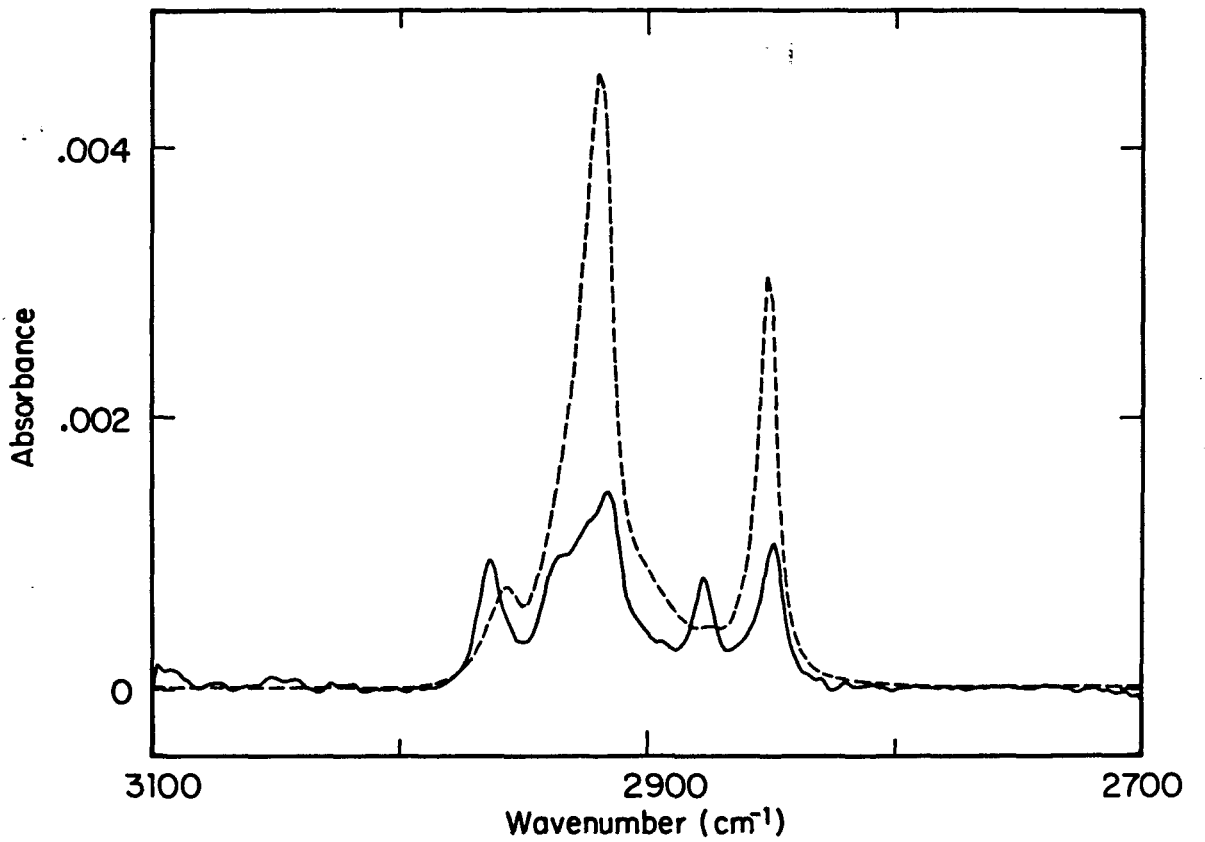

Figure 7. Calculated (---) and observed (—) infrared external reflection spectra for self-assembled arachidic acid at silver. The p-polarized light was incident at 80°.

reasonable agreement with the symmetric binding of the carboxylate head group at silver and the 109.5° dihedral angle of a hydrocarbon chain [11]. The twists of ~45° are comparable to those at aluminum surfaces [38].

For a long perfluorocarbon chain (e.g., those in polytetrafluoroethylene (PTFE)), the transition dipole moment of the CF_2 stretches with A_2 symmetry is parallel to the chain axis, whereas those with E_1 symmetry are perpendicular to the chain axis [39]. However, the finite length of short perfluorocarbon chains results in a small deviation (<3°) in the spatial orientation of the transition dipole moments that are associated with $\nu_a(CF_2)$ mode with E_1 symmetry. The transition dipole moment that is associated with A_2 symmetry deviates by 21-24° for n=6-8 chains. A linear relationship between absorbance and chain length for those modes is not expected. Figure 8 shows calculated and observed spectra of n-perfluorononanoic acid monolayer on silver. The results of the calculations with the $\nu_a(CF_2)$ and $\nu_s(CF_2)$ modes with E_1 symmetry indicate an average tilt of 40° for the n=6-8 chains. Such tilts are in reasonable agreement with the symmetric binding of the carboxylate head group at silver and the 116° C-C-C bond angle of a perfluorocarbon chain [30], which would yield a tilt of ~38°.

The larger tilts of shorter chains can be inferred from IRS data as shown in Figure 9. The $\nu_s(COO^-)$ absorbance of n-alkanoic acids and n-perfluorocarboxylic acids are fairly insensitive with n. For short chain n-alkanoic acid monolayers on silver, the gradual decrease of the $\nu_s(COO^-)$ absorbance indicates that the structures of these monolayers exhibit an increase in average tilt, and/or a decrease in surface coverage. Comparison of the trends in fractional coverages as a function of n may suggest a larger tilt for short chain n-alkanoic acids. In contrast, the $\nu_s(COO^-)$ absorbance mode for n-perfluorocarboxylic monolayers on silver are relatively insensitive to n, except for n=0 chain. Note that the exceptionally small

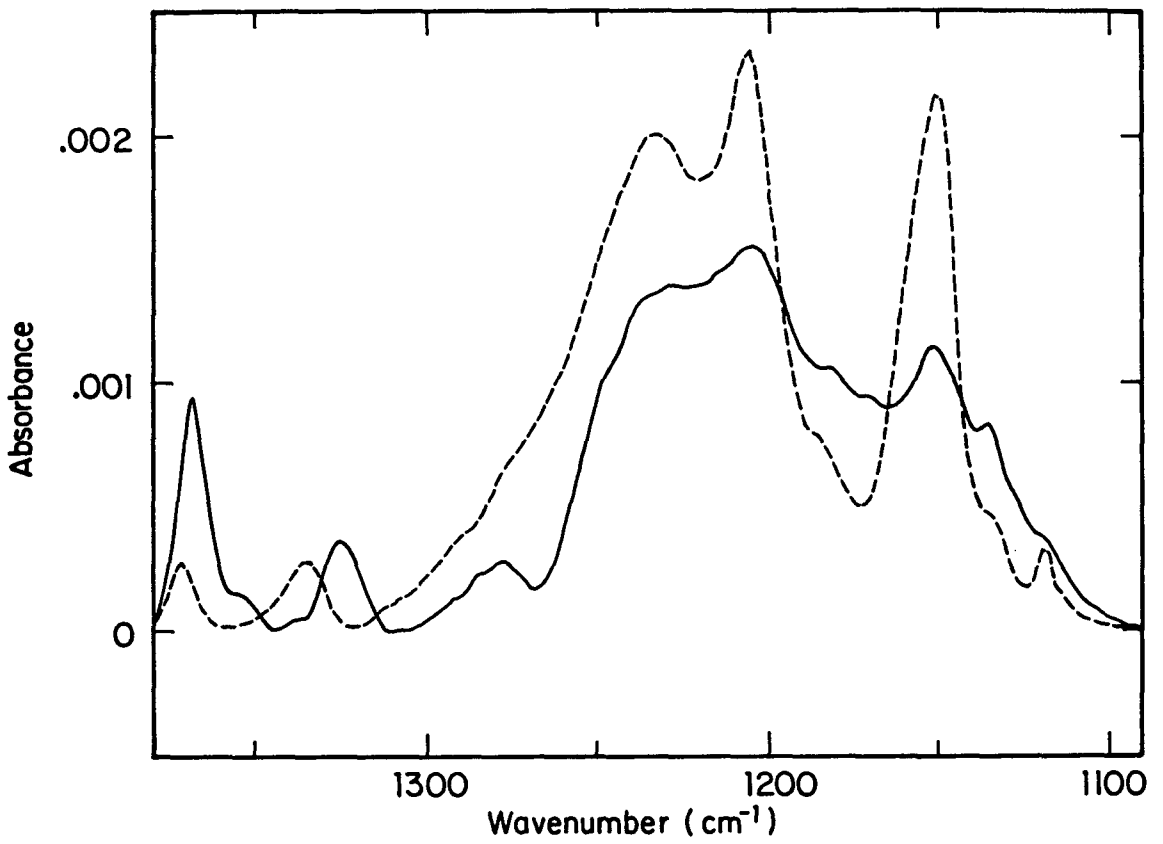

Figure 8. Calculated (---) and observed (—) infrared external reflection spectra for self-assembled n-perfluorononanic acid at silver. The p-polarized light was incident at 80°.

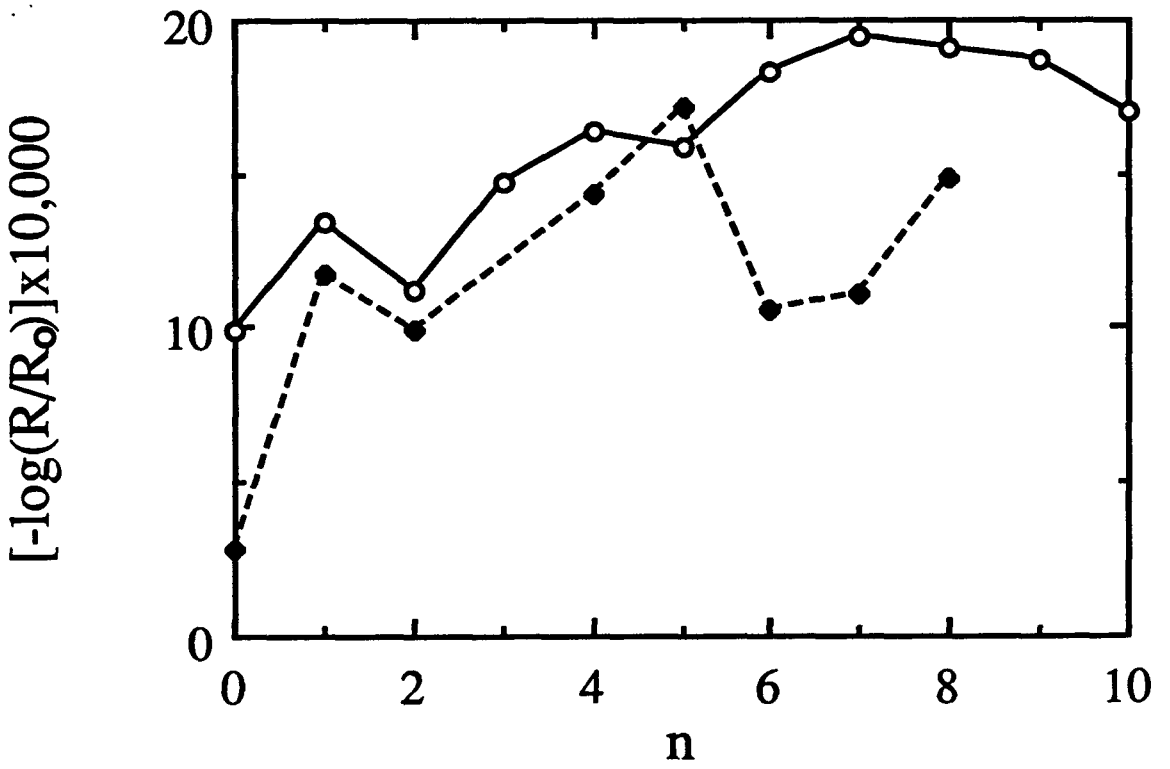

Figure 9. Peak heights of $\nu_s(COO^-)$ for monolayers of $CH_3(CH_2)_nCOOH$ (o) and $CF_3(CF_2)_nCOOH$ (♦) self-assembled at silver as a function of n

$\nu_s(COO^-)$ absorbance for trifluoroacetic acid monolayer on silver suggests a very large tilt of the head from the surface normal. This conclusion of large tilt is supported by the intensities of $\nu_a(CF_3)$ modes which are strong at ~1204 cm^{-1} and weak at ~1143 cm^{-1} [40].

The packing and orientation of individual molecules in a monolayer have been suggested to be a function of the spacing between the heads, the difference in the preferred head-head and tail-tail distances, the length of the tails, and the van der Waals and dipole interactions between the tails [41-44]. In general, in monolayer assemblies where the head-head spacing positions the molecules further apart than the natural spacing of the tails, the chains tilt to maximize attractive van der Waals interactions between molecules [41-43]. These "free-volume-allowed" tilts would then compete with the formation of gauche conformers for excess free volume. For carboxylic acids, the radius of the unhydrated acid molecules is 2.55 Å for all long-chain acid molecules [45]. The radius of the hydrogen tail is 2.42 Å [46], and the radius of the perfluorocarbon tails is 2.99 Å [30,47]. Hence, for n-alkanoic acid, the mismatch of the spacing between head-head and tail-tail distances results in a larger average tilt for shorter chains. In addition, defects could also give rise to disordered chain packing, and hence, a larger average chain tilt.

Wetting characteristics

The wetting properties of these monolayer films, as judged by contact angles, are given as a function of n in Figure 10 for the nonpolar liquid hexadecane and the polar liquids glycerol and water. Across the series the average advancing contact angles in general reach limiting values. The limiting θ_a's for n-alkanoic acid monolayers are comparable to those for an interface terminated with a $-CH_3$ group [48]; whereas the limiting θ_a's for n-perfluorocarboxylic acid monolayers are less than those for an interface terminated with a

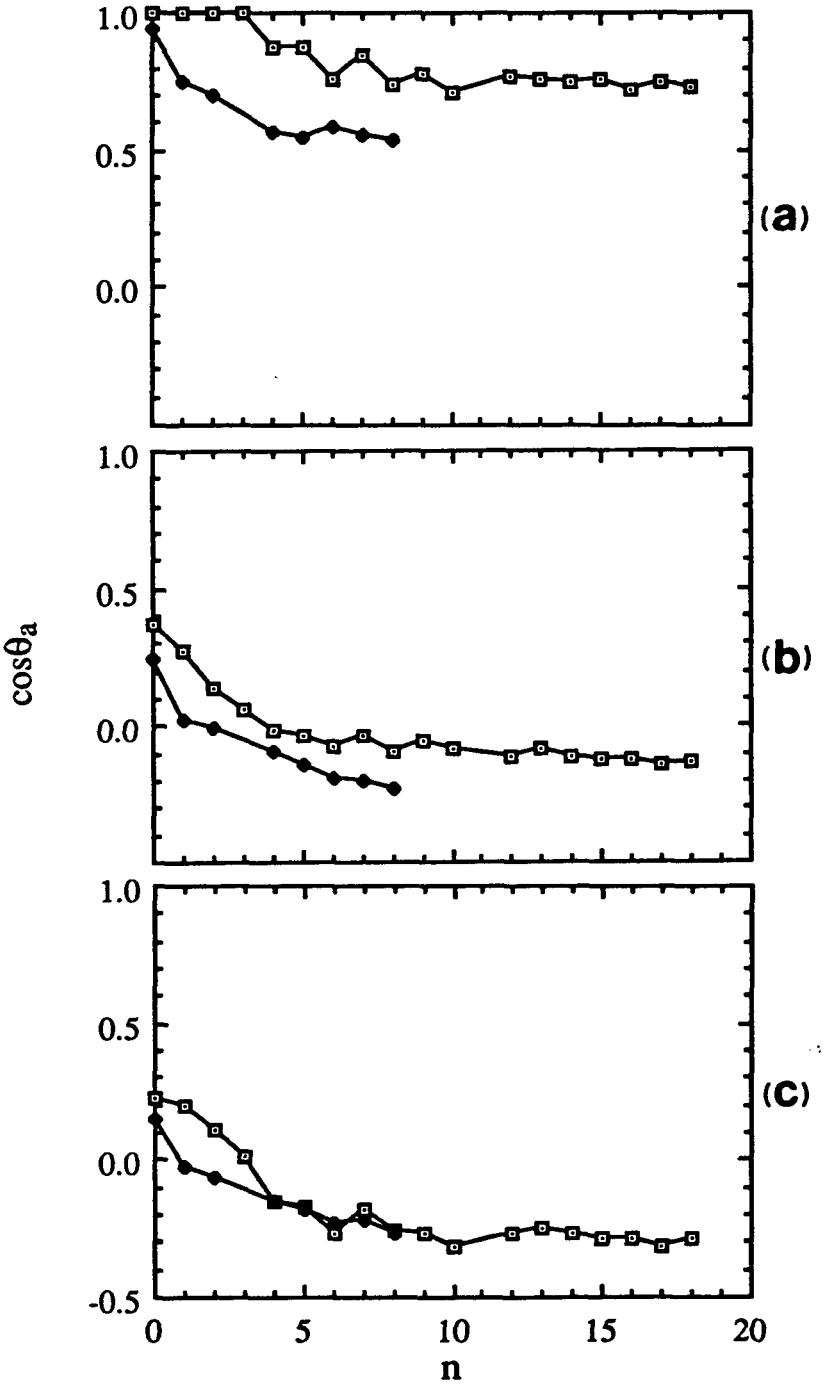

Figure 10. Advancing contact angles of (a) hexadecane, (b) glycerol, and (c) water, on monolayers of $CH_3(CH_2)_nCOOH$ (□) and $CF_3(CF_2)_nCOOH$ (♦) adsorbed at silver.

-CF_3 group [49]. This suggests that the hydrocarbon chains approach a closest-packed structure, whereas the perfluorocarbon chains do not, which agrees with the contact angle hysteresis data described in the previous section. For n-perfluorocarboxylic acid monolayers, with minimum exposure to the ambient laboratory environment, the structures are more densely-packed [12]. At both monolayers, the advancing contact angles for shorter chains were progressively lower, indicative of a decrease in surface free energy.

As shown in Figure 9, the depth sensitivity of a probe liquid to the underlying COO-Ag dipoles and silver plasmons is different with hydrocarbon and fluorocarbon tail. For all three liquids, the thickness of the hydrocarbon layer sufficient to hide the polar carboxylate group from interaction with a probe liquid is larger than that of the fluorocarbon layer. This is attributed to the lower dielectric constant of the perfluorocarbon layer which is more effective in screening the van der Waals interactions between the contacting liquid and the underlying COO-Ag dipoles and silver plasmons [50]. It is also interesting to note that, at large n, contact angles of water on n-alkanoic acid and n-perfluorocarboxylic acid monolayers are comparable, whereas contact angles of hexadecane on n-alkanoic acid monolayers are significantly smaller than those on n-perfluorocarboxylic acid monolayers. The results of glycerol are intermediate between the above two cases. A detailed discussion on this trend with considerations of van der Waals interactions will be reported elsewhere.

The wetting data also indicate an odd-even progression in surface tension for short chain n-alkanoic acid monolayers. The odd-even trend is not significant for long chain n-alkanoic acid. Changes in $\cos\theta_a$'s with an odd-even variation of chain length may arise from a difference in the orientation of the terminal methyl group which screens the van der Waals interactions between the contacting liquid and the underlying COO-Ag dipoles and silver plasmons differently [50]. At longer distances, the interactions are weaker. As a

result, the difference in screening by the terminal methyl groups with different orientations is proportionally smaller. This leads to a smaller odd-even variation as observed in Figure 10.

Formation thermodynamics

A metal oxide displays widely differing types of interactions with organic adsorbates. The analysis presented by Bolger [51] elucidates these specific interactions in terms of the ionic character of the hydroxylated substrate and organic functional group provided by the adsorbate. The ionic character of the substrate is described in terms of the isoelectric point of the surface (IEPS). The surface reactions involved in the established surface charge and the electrical double layer based on an amphoteric dissociation model may be represented as

$$\overline{MO^-} + H^+ \leftrightarrow \overline{MOH} \qquad K_1 = [\overline{MOH}]/[\overline{MO^-}][H^+] \tag{10}$$

$$\overline{MOH} + H^+ \leftrightarrow \overline{MOH_2^+} \qquad K_2 = [\overline{MOH_2^+}]/[\overline{MOH}][H^+] \tag{11}$$

and for

$$\overline{MO^-} + 2H^+ \leftrightarrow \overline{MOH_2^+} \qquad K_1K_2 = [\overline{MOH_2^+}]/[\overline{MO^-}][H^+]^2 \tag{12}$$

At the IEPS, $\overline{MOH_2^+} = \overline{MO^-}$, and $K_1 = K_2$, it follows that

$$\text{IEPS} = \log K_2 \tag{13}$$

From the definition of the pK_a of an acid,

$$HX \leftrightarrow H^+ + X^- \qquad pK_a = -\log([H^+][X^-]/[HX]) \tag{14}$$

The acid-base reaction which involved the hydrated oxide surface and organic acids can be generalized as hydrogen-bond formation and salt formation,

$$\text{—MOH} + HX \rightarrow \text{—M-}\underset{\underset{H}{|}}{O}\cdots H\text{-X} \tag{15}$$

$$\text{—MOH} + HX \rightarrow \text{—M-}OH_2^+\cdots X^- \tag{16}$$

In order to predict the relative probability between reactions 15 and 16, Bolger proposes the following relation:

$$\Delta_A = \log([\overline{MOH_2^+}][\overline{X^-}]/[\overline{MOH}][HX]) \quad (17)$$

Substitution of equations 13 and 14 into equation 17 yields

$$\Delta_A = IEPS - pK_a \quad (18)$$

The strength of the acid-base interactions is expected to increase with Δ_A. Dispersion forces dominate if Δ_A is negative.

For two acids HX_1 and HX_2 with equal concentration competitively adsorbed at a metal oxide surface, from equation 17,

$$\log([\overline{X_1^-}]/[\overline{X_2^-}]) = \Delta_{A1}-\Delta_{A2} \quad (19)$$

With silver, IEPS was estimated to be ~10.4 [52]. The pK_a's for long chain n-alkanoic acid are ~4.5 [53], and pK_a's for long chain n-perfluorocarboxylic acid are about ~2.6 [54]. For equal concentrations of both acids, this calculation indicates that the adsorption of a n-perfluorocarboxylic acid is preferentially favored at silver relative to a n-alkanoic acid by nearly 80 times. The relative binding of adsorbates has been shown to be directly related to the pK_a of the acid group in each molecule, with more acidic species having greater binding to basic surface sites [55]. It is important to note that this analysis considers only acid-base chemistry.

To investigate the effect of the nature of the chain on the coadsorption of n-alkanoic acids and n-perfluorocarboxylic acids, a 2x4 factorial design with two two center points was used [56]. The factors were the immersion time, t, and the mole fraction, X, of n-perfluorodecanoic acid in a mixture of n-perfluorodecanoic acid and n-decanoic acid. The response surface is shown in Figure 11 and is given as $\cos\theta_a$. The monolayer reaches a densely packed structure at an immersion time of 15 minutes. The assumption of

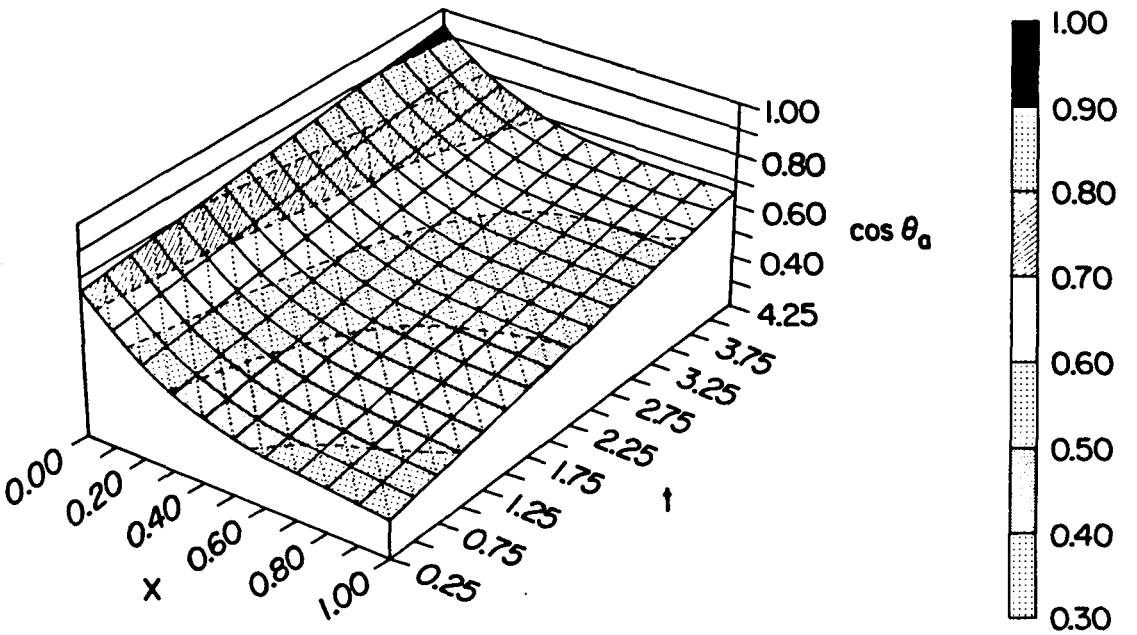

Figure 11. Response surface for competitive adsorption from n-perfluorodecanoic acid/n-decanoic acid mixtures in absolute ethanol. The surface fits the following equation: $\cos\theta_a = 0.740 - 1.232X + 1.369X^2 - 0.055X^3 + 0.045t + 0.041Xt - 0.010X^2t$, where t = time in minutes, and X = mole fraction of n-perfluorodecanoic acid in the mixture.

thermodynamic equilibrium allows us to rationalize the relationships between the concentrations in solution and the compositions of mixed monolayers of these adsorbates on silver. The relative fractional coverages of n-perfluorodecanoic acid to n-decanoic acid at t = 0.25 hr and X = 0.5 was estimated by Cassie's equation to be ~3:1. Treatment of the intensities from the IRS data at 1370 cm^{-1}, assuming the orientation of the chain is independent of coverage, yields the relative fractional coverages of n-perfluorodecanoic acid to n-decanoic acid at t = 0.25 hr and X = 0.5 to be ~2:1. The results show that n-perfluorodecanoic acid preferentially adsorbs at the silver surface. However, the ratio is far below that estimated by consideration of only the acid-base chemistry of the carboxylate head group and the silver substrate. Thermodynamically, it is shown that stronger cohesive interactions between hydrocarbon chains favor adsorption of the longer chains [57]. As a result, weaker intermolecular attractions between perfluorocarbon chains lead to a relative fractional coverage lower than that expected. The weaker intermolecular attractions of saturated fluorocarbon chains are also revealed by the shift of peak position of $\nu_s(CH_2)$. The crystalline-like packing in the pure monolayer ($\nu_s(CH_2)$ peak position 2852 cm^{-1}) is changed to be more liquid-like in the mixed monolayers ($\nu_s(CH_2)$ peak position 2858 cm^{-1}) [24]. This also suggests that the mixed monolayers do not phase-segregate into macroscopic islands.

Furthermore, n-perfluorodecanoic acid is a stronger acid than n-decanoic acid and is therefore a better leaving group in ethanol from a mechanistic perspective. Thermodynamically, the component with the lower solubility will be preferentially adsorbed into the monolayer. Therefore, the nature of the solvent influences both the relative solubilities and the preference for adsorption. Taken together, the extent of the preference varies with the pK_a of the acid, the cohesive interactions between the chains, and the nature of the solvent.

As shown in Figure 11, at longer times, the contact angles decline with increased exposure to the self-assembly solution. Analysis of the self-assembly solutions by ICP-AES revealed a graduate increase in its silver content, suggesting a slow dissolution of the surface silver complex. The observed dissolution arises from the labile nature of the surface structure. Dissolution of n-alkanoic acid films adsorbed at copper from ethanol and hexadecane has also been observed in our laboratory and reported in the literature [58]. Because of this competition with polar solvents, it is suggested that carboxylic acid groups are ineffective in bond durability with most very high or low IEPS oxides, probably because the acid-base forces are large enough to cause corrosion or chemical attack of metal surface [51].

CONCLUSIONS

As a result of differences in head group acidity, head-head to tail-tail distances, and intermolecular attractions, the formation and structure of n-alkanoic and n-perfluorocarboxylic acid monolayers on silver have their own characteristics with respect to reactivity, orientation, packing density, and intermolecular environment. These properties, in general, indicate the tendency of these monolayers toward more disordered and less densely packed structures for short chains. The bulkier, more rigid structure, and the "mutual-phobia" [59] characteristics of perfluorocarbon chains lead to less appreciable changes in monolayer properties with respect chain length variation. Due to higher acidity of the head group, n-perfluorodecanoic acid preferentially adsorbs at a silver surface relative to n-decanoic acid. However, further detailed studies are necessary to investigate the effect of chain length on the adsorption competition, as the trade off between acid-base reactivity and intermolecular attraction may take place when a critical chain length is reached. Further studies concerning the influence of solvent to the extent of the preferential adsorption are currently in progress.

REFERENCES

1. Whitesides, G. M.; Laibinis, P. E. Langmuir **1990**, 6, 87-96.
2. Stewart, K. R.; Whitesides, G. M.; Godfried, H. P.;Silvera, I. F. Rev. Sci. Instrum. **1986**, 57, 1381-1383.
3. Wasserman, S. R.; Whitesides, G. M. J. Mater. Res. **1989**, 4, 886-892.
4. Zisman, W. A.In Friction and Wear; Davies, R., Ed.; Elsevier: New York, 1959.
5. Novontny, V.; Swalen, J. D.; Rabe, J. P. Langmuir **1989**, 5, 485-489.
6. Notoga, T.; Poling, G. W. Corrosion **1979**, 35, 193-200.
7. Murray, R. W. In Electroanalytical Chemistry; Bard, A. J., Ed.; Marcel Dekker: New York, 1984; Vol. 13.
8. Ringsdrof, H.; Schlarb, B.;Vengmer, J. Angew. Chem. Int. Ed. Engl. **1988**, 27, 113-158.
9. Zisman, W. A. In Contact Angle: Wettability and Adhesion; Gould, R. F., Ed.; Advances in Chemistry 43; American Chemical Society: Washington, DC, 1964; Chapter 1.
10. Sexton, B. A.; Madix, R. J. Surf. Sci. **1981**, 105, 177-195.
11. Schlotter, B. A.; Porter, M. D.; Bright, T. B.; Allara, D. L. Chem. Phys. Lett. **1986**, 132, 93-98.
12. Chau, L. K.; Porter, M. D. Chem. Phys. Lett. **1990**, 167, 198-204.
13. Griffith, R. L. J. Chem. Phys. **1943**, 11, 499-505.
14. Blakeslee, A. E.; Hoard, J. L. J. Am. Chem. Soc. **1956**, 78, 3029-3033,
15. Griffin, R. G.; Ellett, J. D., Jr.; Mehring, M.; Bullitt, J. G.; Waugh, J. S. J. Chem. Phys. **1972**, 57, 2147-2155.
16. Bewick, A.; Thomas, B. J. Electroanal. Chem. **1975**, 65, 911-931.
17. Widrig, C. A.; Chung, C.; Porter, M. D. manuscript in preparation,

Department of Chemistry, Iowa State University.

18. Porter, M. D.; Bright, T. B.; Allara, D. L.; Chidsey, C. E. D. J. Am. Chem. Soc. **1987**, 109, 3559-3568.
19. Winge, P. K.; Fassel, V. A.; Edelson, M. C. Spectrochim. Acta **1988**, 43B, 85-91.
20. Fenstermaker, C. A.; McCrackin, F. L. Surf. Sci. **1969**, 16, 85-96.
21. Allara, D. L.; Nuzzo, R. G. Langmuir **1985**, 1, 45-52.
22. Cassie, A. B. D. Discuss. Faraday Soc. **1948**, 3, 11-16.
23. Dettre, R. H.; Johnson, R. E., Jr. J Phys. Chem. **1965**, 69, 1507-1515.
24. Snyder, R. G.; Strauss, H. L.; Elliger, C. A. J. Phys. Chem. **1982**, 86, 5145-5150.
25. Hill, I. R.; Levin, I. W. J. Chem. Phys. **1979**, 70, 842-851.
26. Greenler, R. G. J. Chem. Phys. **1966**, 44, 310-315.
27. Pearce, H. A.; Shepard, N. Surf. Sci. **1976**, 59, 205-217.
28. Snyder, R. G. Macromolecules **1990**, 23, 2081-2087.
29. Clark, E. S.; Muus, L. T. Z. Krist. **1962**, 117, 119-127.
30. Bunn, C. W.; Howells, E. R. Nature **1954**, 174, 549-551.
31. Banks, R. E.; Tatlow, J. C. J. Fluorine Chem. **1986**, 33, 227-346.
32. Eaton, D. F.; Smart, B. E. J. Am. Chem. Soc. **1990**, 112, 2821-2823.
33. Mukerjee, P.;Handa, T. J. Phys. Chem. **1981**, 85, 2298-2303.
34. Allara, D. L.; Baca, A.;Pryde, C.A. Macromolecules **1978**, 11, 1215-1220.
35. Hanson, W. N. J. Opt. Soc. Am. **1968**, 58, 380-390.
36. Burns, G. Solid State Physics; Academic Press: Orlando, 1985; Chapter 13.
37. Wilson, E. B.; Decius, J. C.; Cross, P. C. Molecular Vibrations; McGraw Hill: New York, 1950; p 285.
38. Allara, D. L.; Nuzzo, R. G. Langmuir **1985**, 1, 52-66.
39. Moyniham, R. E. J. Am. Chem. Soc. **1959**, 81, 1045-1050.

40. Spinner, E. J. Chem. Soc. **1964**, 4217-4226.

41. Langmuir, I. J. Chem. Phys. **1933**, 1, 756-776.

42. Epstein, H. T. J. Phys. Colloid Chem. **1950**, 54, 1053-1069.

43. Safran, S. A.; Robbins, M. O.; Garoff, S. Phys. Rev. A **1986**, 33, 2186-2189.

44. Ulman, A.; Eilers, J. E.; Tillman, N. Langmuir **1989**, 5, 1147-1152.

45. Adam, N. K. Physics and Chemistry of Surfaces, 3rd Ed.; Oxford University Press: London, 1941.

46. Muller, A. Proc. Roy. Soc. (London) **1927**, 114, 542-561.

47. Pauling, L. The Nature of the Chemical Bond; Cornell University Press: Ithaca, 1960.

48. Bain, C. D.; Troughton, E. B.; Tao, Y.-T.; Evall, J.; Whitesides, G. M.; Nuzzo, R. G. J. Am. Chem. Soc. **1989**, 111, 321-335.

49. Chidsey, C. E. D.; Loiacono, D. N. Langmuir **1990**, 6, 682-691.

50. Chau, L. K.; Porter, M. D. manuscript in preparation, Department of Chemistry, Iowa State University.

51. Bolger, J. C. In Adhesion Aspects of Polymeric Coatings; Mittal, K. L., Ed.; Plenum: New York, 1983.

52. Chau, L. K.; Porter, M. D. submitted for publication in J. Colloid Interface Sci.

53. Noller, C. R. Chemistry of Organic Compounds; Saunders: Philadelphia, 1966.

54. Arrington, C. H.; Patterson, G. D. J. Phys. Chem. **1953**, 57, 247-250.

55. Holmes-Farley, S. R. Langmuir **1988**, 4, 766-774.

56. Box, G. E. P.; Hunter, W. G.; Hunter, J. S. Statistics for Experimenters; Wiley: New York, 1978.

57. Bain, C. D.; Whitesides, G. M. J. Am. Chem. Soc. **1989**, 111, 7164-7175.

58. Walker, D. C.; Ries, H. E., Jr. In Contact Angle, Wettability and Adhesion; Gould, R. F., Ed.; Advances in Chemistry Series 43; American Chemical Society:

Washington, DC, 1964; Chapter 20.

59. Mukerjee, P.; Yang, A.Y. S. J. Phys. Chem. **1976**, 80, 1388-1390.

SECTION IV. DEPTH SENSITIVITY OF WETTING: CONSIDERATION OF LONDON-VAN DER WAALS INTERACTIONS IN CONTACT ANGLE MEASUREMENTS

Depth Sensitivity of Wetting:
Consideration of London-van der Waals Interactions in Contact Angle Measurements

Lai-Kwan Chau and Marc D. Porter

Department of Chemistry and Ames Laboratory - USDOE

Iowa State University

Ames, Iowa 50011

ABSTRACT

Wetting studies of a liquid on series of structurally different organic monolayer films show that van der Waals interactions decay as the square of the distance between two semiinfinite parallel flat slabs at small separations (<100 Å). The depth sensitivity of wetting is quantitatively correlated to the van der Waals interactions between a liquid and an underlying functional group of a solid surface. A comparison of relative depth sensitivities of various liquids are made. The correlation of limiting contact angles to van der Waals interactions at various interfaces is also discussed, as well as the structural implications of the variation of the spatial orientation of the methyl terminal group.

INTRODUCTION

Wettability phenomena are complex and their interpretation at a microscopic level is not fully understood. In spite of the lack of microscopic theories, the spreading of a liquid on a solid has provided a wealth of information on the properties of interfaces. Studies have shown qualitatively that the wettability of a solid is determined by the structure of its outermost few angstroms [1-4]. As an example, a phenyl ring is sufficient to hide an underlying polar amide group from interaction with water, suggesting that a relatively small, nonpolar group can bury a polar group and that wettability must be sensitive to molecular-scale details of interfacial structure [5]. The high sensitivity of wetting as a probe of interfacial structure has been compared with X-ray photoelectron spectroscopy (XPS). Results indicate that the size of alkyl groups required to mask polar functionality in wetting is small compared to the thickness of hydrocarbon required to significantly attenuate XPS signals [3,6]. Furthermore, it has been shown that the depth sensitivity of different probe liquids (hexadecane, glycerol, and water) to the underlying polar ether group varies from ~2Å to ~5 Å [7]. A more quantitative knowledge of the influence of the depth of functional groups beneath the surface to different probe liquids on wetting would be invaluable in understanding the intermolecular forces acting at these interfaces.

In macroscopic systems, three different phenomena contribute to van der Waals (VW) interactions: (1) randomly orienting dipole-dipole (or orientation) interactions, described by Keesom; (2) randomly orienting dipole-induced dipole (or induction) interactions, described by Debye; (3) fluctuating dipole-induced dipole (or dispersion) interactions, described by London [8]. All three interaction energies between atoms or small molecules decay very rapidly distance (x), as x^{-6}. Between macroscopic bodies, Hamaker showed that the dispersion energy between two semiinfinite parallel flat slabs decays with distance as x^{-2} for relatively short distances ($x < 100$ Å) [9] and as x^{-3} at greater distances due to retardation

[10]. Here we present experimental results to verify Hamaker's theory at relatively short distances and develop quantitative relations between the depth sensitivity of wetting and the London-van der Waals interactions at the macroscopic interfaces. The correlation between limiting contact angles and the van der Waals interactions at various solid-liquid interfaces will also be addressed.

RESULTS AND DISCUSSION

Van der Waals interactions at macroscopic interfaces

When a small liquid droplet contacts with a flat solid surface, two distinct equilibrium regimes as shown in Figure 1 may be found: partial wetting with a finite equilibrium contact angle ($\theta \neq 0$), or complete wetting ($\theta = 0$). In cases of partial wetting, three phases are in contact at a line: the solid S, the liquid L, and the corresponding equilibrium vapor V. The equilibrium can be expressed quantitatively in terms of the well-known Young relation [11]:

$$\gamma_{SV}^{\bullet} - \gamma_{SL} = \gamma_{LV}^{\bullet}\cos\theta \qquad (1)$$

where $\gamma_{SV}^{\bullet}$ and $\gamma_{LV}^{\bullet}$ are the respective solid and liquid surface tensions in equilibrium with the saturated liquid vapor, γ_{SL} is the interfacial tension between liquid and solid, and θ is the equilibrium contact angle between the liquid and the solid surfaces. Assuming that van der Waals interactions control the energetics at the liquid-solid interface, then the energy to bring into contact the regions L and S can be represented as:

$$\gamma_{SL} = \gamma_{SV}^{\bullet} + \gamma_{LV}^{\bullet} - V_{SL} \qquad (V_{SL} > 0) \qquad (2)$$

where $-V_{SL}$ describes the attractive VW interactions between the regions L and S. Substituting equation 2 into equation 1 yields,

$$\gamma_{LV}^{\bullet}(1+\cos\theta) = V_{SL} \qquad (3)$$

Since V_{SL} is a function of separation distance, x, between regions S and L, its decay with x can be evaluated by varying the chain length of self-assembled monolayers. Assuming a similar structure for the same series of monolayers, variation in the chain length, n, of the tail provides angstrom-scale control over the position of the underlying functional group. The array of tails then acts as a dielectric layer.

Next consider monolayers of n-alkanethiols [$CH_3(CH_2)_nSH$] and n-carboxylic acids [$CX_3(CX_2)_nCOOH$, where X = H or F] on gold or silver surfaces, as shown in Figure 2a, and ω-mercapto ethers [$CH_3(CH_2)_nO(CH_2)_{16}SH$] on gold, as shown in Figure 2b, VW

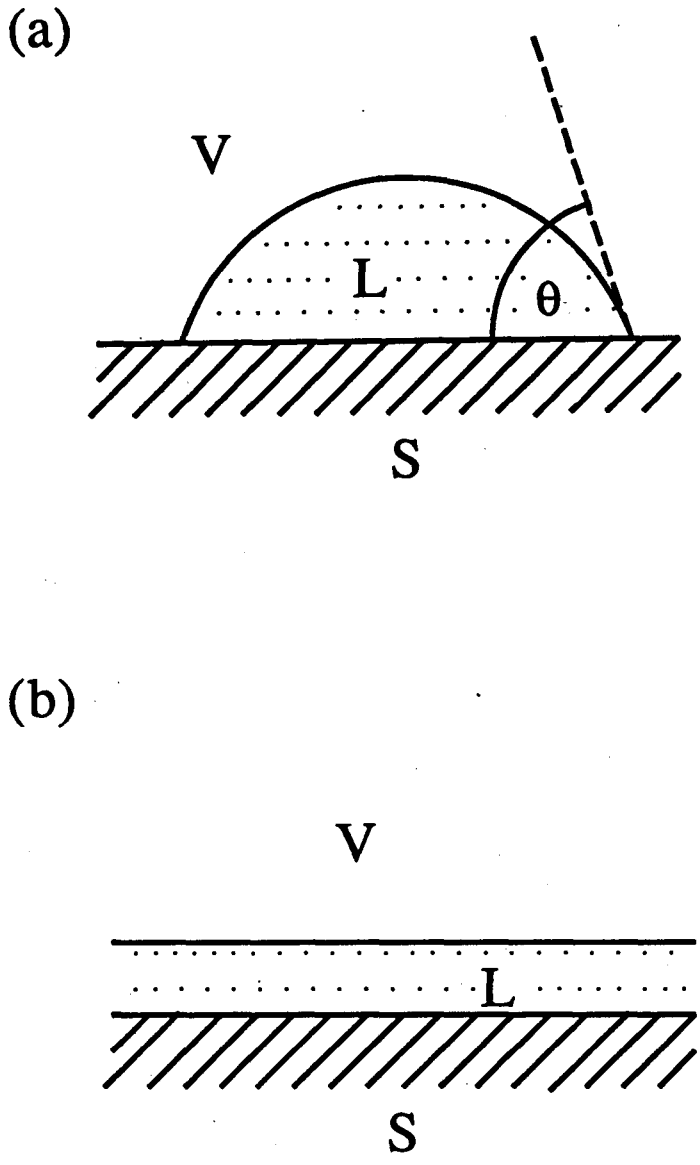

Figure 1. A liquid drop in equilibrium over a horizontal surface: (a) partial wetting ($\theta \neq 0$), and (b) complete wetting ($\theta = 0$).

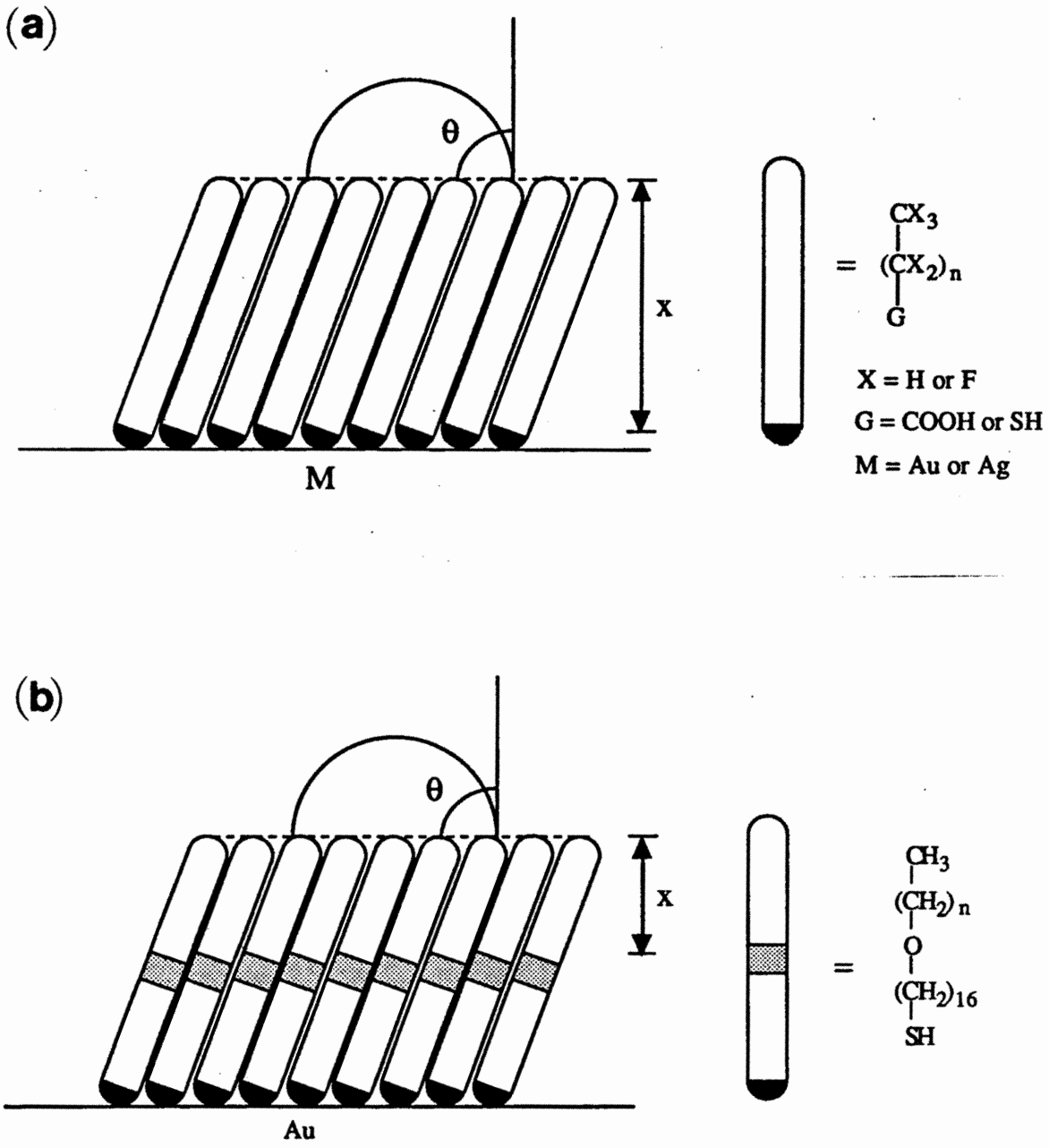

Figure 2. A schematic illustration of a liquid drop on a monolayer of (a) $CX_3(CX_2)_nG$ on gold or silver, where X = H or F, and G = COOH or SH, and (b) $CH_3(CH_2)_nO(CH_2)_{16}SH$ on gold.

interactions between the regions S and L can be separated into two parts: (1) VW interaction of a contacting liquid with the perfluorocarbon tail or the hydrocarbon tail, denoted by superscript T; (2) VW interaction of a contacting liquid with the underlying functional group of interest, denoted by superscript G. Thus, equation 3 can be represented as:

$$\gamma_{LV}^{\circ}(1+\cos\theta) = V_{SL}^{G} + V_{SL}^{T} \tag{4}$$

Assuming the change of V_{SL}^{T} with different n is negligible compared to the change of V_{SL}^{G} with varying n, V_{SL}^{T} is considered essentially constant. Then, at large n (i.e., large x), V_{SL}^{G} decays to almost zero. Let θ_{∞} be the limiting contact angle (i.e., the contact angle of a probe liquid on a monolayer with large n), equation 4 can then be written as

$$\gamma_{LV}^{\circ}(1+\cos\theta_{\infty}) = V_{SL}^{T} \tag{5}$$

Substituting equation 5 into equation 4 yields,

$$\gamma_{LV}^{\circ}(\cos\theta-\cos\theta_{\infty}) = V_{SL}^{G} \tag{6}$$

In accord with Hamaker's treatment [9] for semiinfinite parallel flat slabs, the VW interaction decays as the square of the separation distance at fairly close range (i.e., in the nonretarded regime). Coupled with the consideration of the tails as dielectric media between regions L and S, V_{SL}^{G} can be expressed as

$$V_{SL}^{G} = A/12\pi\kappa x^{2} \tag{7}$$

where A is the Hamaker constant and κ is the dielectric constant of the medium between the slabs. Thus, equation 6 can be expressed as

$$\gamma_{LV}^{\circ}(\cos\theta-\cos\theta_{\infty}) = A/12\pi\kappa x^{2} \tag{8}$$

The Hamaker constant was originally linked solely to London-van der Waals interactions, but recent efforts have shown that it applies to all three electrodynamic interactions in condensed systems, that is, to the sum of the dispersion, orientation, and induction interactions [8]. However, in condensed media, the dispersion interaction is usually the only significant term [12]. Taking logarithm of equation 8 on both sides gives,

$$\log(\cos\theta-\cos\theta_\infty) = \log(A/12\pi\kappa\gamma_{LV}^{\bullet}) - 2\log x \qquad (9)$$

A plot of $\log(\cos\theta-\cos\theta_\infty)$ versus log x should give a slope of -2 and an intercept equal to $\log(A/12\pi\kappa\gamma_{LV}^{\bullet})$.

To substantiate Hamaker's result for semiinfinite parallel flat slabs separated by relatively short distances, contact angle data of hexadecane on series of structurally different monolayers with varying chain lengths were examined. These monolayers include: (1) $CH_3(CH_2)_nSH$ on gold [13], (2) $CH_3(CH_2)_nSH$ on silver [14], and (3) $CF_3(CF_2)_nCOOH$ on silver [15]. The chain tilts of these monolayers are 31°, 13°, and 40°, respectively, from surface normal. The values of n from these monolayers for estimating the limiting contact angles are 17, 16, and 8, respectively. Figures 3a-c show plots of $\log(\cos\theta-\cos\theta_\infty)$ versus log x for hexadecane on these monolayers. Each plot shows a slope of about -2 and an intercept of about -15. The intercepts of about -15 give values for A on the order of magnitude of $\sim 1\times10^{-12}$ erg, which agree with the theoretical prediction [9]. The scatter in the data may arise from the change of surface coverage with chain length, the change of molecular tilt with chain length, or the orientation dependence of the $-CH_3$ or the $-CF_3$ group with the odd-even variation of chain length (see below). With glycerol and water as the probe liquids, slopes of about -2 are also observed for the plots of $\log(\cos\theta-\cos\theta_\infty)$ versus log x for these monolayers. In general, the data support Hamaker's prediction that VW interactions for semiinfinite parallel flat slabs decays as the square of the distance at fairly close range.

Depth sensitivity of wetting

Since VW interactions in contact angle measurements are relatively long-range in nature, different probe liquids may sense different depths beneath the surface. The sensing depths of different probe liquids in contact angle measurements has been correlated

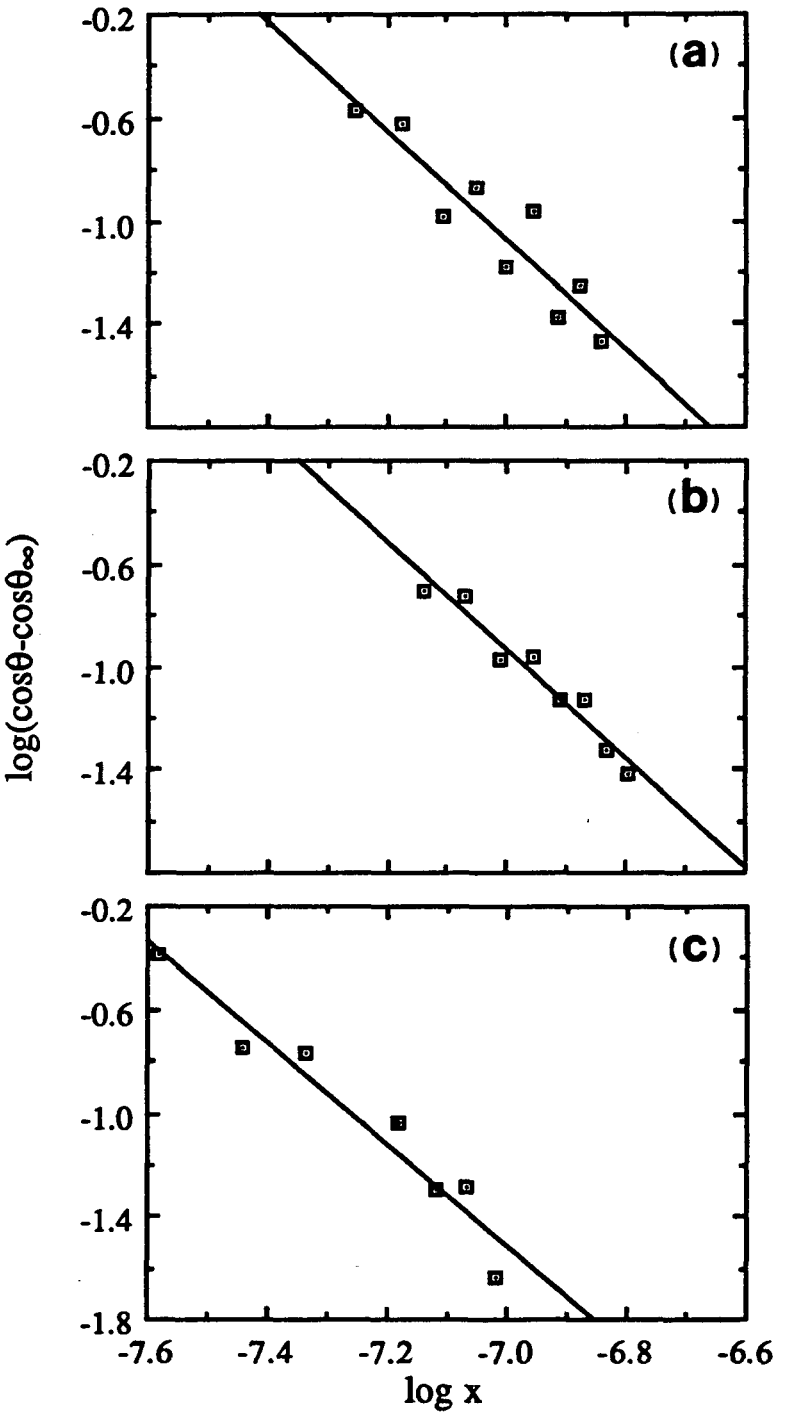

Figure 3. Plots of $\log(\cos\theta-\cos\theta_\infty)$ versus log x for hexadecane on (a) monolayers of $CH_3(CH_2)_nSH$ on gold (slope = -2.12, y-intercept = -15.89); (b) monolayers of $CH_3(CH_2)_nSH$ on silver (slope = -2.12, y-intercept = -15.74); and (c) monolayers of $CF_3(CF_2)_nCOOH$ on silver (slope = -1.95, y-intercept = -15.17).

qualitatively by Bain and Whitesides, and two mechanisms have been proposed [7]. However, a quantitative correlation is lacking. This section presents a quantitative correlation of the depth sensitivity of a probe liquid with its physical properties via the consideration of VW interactions.

As is apparent in equation 8, the VW interactions decay as x^{-2} at fairly close range and its rate of decay is a function of γ_{LV}°, A, and κ. If surface sensitivity (SS) is defined as $d(\cos\theta)/dx$, or depth sensitivity (DS) is defined as $dx/d\cos\theta$, then from equation 8,

$$SS = d(\cos\theta)/dx = -A/6\pi\kappa\gamma_{LV}^{\circ}x^3 \tag{10}$$

$$DS = dx/d(\cos\theta) = -6\pi\kappa\gamma_{LV}^{\circ}x^3/A \tag{11}$$

If the two slabs are composed of two different substances S and L,

$$A = \pi^2 q_S q_L \lambda_{SL} \tag{12}$$

where q's are the atom densities and λ's are the London-van der Waals constants; both are annotated by the appropriate suffix. We also note that λ is approximately expressed by

$$\lambda_{SL} = 3\alpha_S\alpha_L I_S I_L/2(I_S+I_L) \tag{13}$$

where α's are the polarizabilities, and I's are the ionization potentials of the isolated molecule as indicated by each suffix. Further, polarizability may be calculated by the Lorentz-Lorenz equation:

$$\alpha = 3v(n^2-1)/4\pi N_o(n^2+2) \tag{14}$$

where n is refractive index, v is molar volume, and N_o is Avogadro's number. Combining equations 12, 13, and 14 yields

$$A = 27(n_S^2-1)(n_L^2-1)I_S I_L/32(n_S^2+2)(n_L^2+2)(I_S+I_L) \tag{15}$$

Substituting equation 15 into equation 11 gives,

$$DS = -64\pi\kappa\gamma_{LV}^{\circ}x^3(n_S^2+2)(n_L^2+2)(I_S+I_L)/9I_S I_L(n_S^2-1)(n_L^2-1) \tag{16}$$

To compare the depth sensitivities of two different probe liquids A and B, from equation 16, we write

$$(DS)_A/(DS)_B = (\gamma_{LV}^{\circ})_B((n_L)_A^2-1)((n_L)_B^2+2)(I_L)_A(I_S+(I_L)_B) + (\gamma_{LV}^{\circ})_A((n_L)_B^2-1)((n_L)_A^2+2)(I_L)_B(I_S+(I_L)_A) \quad (17)$$

In contact angle measurements, hexadecane is a commonly used probe liquid which interacts with a solid only by dispersion interaction. Other probe liquids listed in Table I interact either by the dispersion interaction or by both the dispersion and polar interactions. In order to compare depth sensitivities of different probe liquids, hexadecane is chosen as the reference with a depth sensitivity of unity. Table I lists the relative depth sensitivities (RDS) of some commonly used probe liquids in contact angle measurements as calculated from equation 17. The ionization potential (IP) of the ether group is approximated by the IP of $(n\text{-}C_3H_7)_2O$, which is equal to 9.27eV [16].

The depth sensitivity of a probe liquid is also related to the dielectric constant of the medium between the slabs, i.e., the dielectric constant of the tail. Since perfluorocarbon chain has a lower dielectric constant than that of the perhydridocarbon chain, it is expected that the depth sensitivity of a probe liquid is larger at a perhydridocarbon chain than at a perfluorocarbon chain.

The above discussion has taken only dispersion interaction into account. In fact, three distinct types of forces contribute to the total long-range interaction: the induction force, the orientation force, and the dispersion force. Dispersion force generally exceeds the dipole dependent induction and orientation forces except for small highly polar molecules [12]. In addition, in the interaction between dissimilar molecules of which one is nonpolar, the VW energy is almost completely dominated by the dispersion contribution [12]. The induction force ranks lowest in importance of the VW forces and is generally negligible [17]. Hence, the contribution of polar interactions in the calculated RDS listed Table I can be ignored since the ether group in the monolayer is not a highly polar functional group.

Table I. Relative depth sensitivity (RDS) of liquids on monolayers of $CH_3(CH_2)_nO(CH_2)_{16}SH$ on gold

liquid	γ_{LV}*(dyne/cm)	η_L^2	I_L(eV) [a]	RDS
perfluoro-n-heptane	13.6	1.605	13.38 [b]	0.66
carbon disulfide	32.3	2.490	10.08	0.90
cyclohexane	25.3	2.034	9.88	0.92
n-propanol	23.8	1.920	10.20	0.93
benzene	29.0	2.179	9.25	0.99
hexadecane	27.6	2.026	10.08 [c]	1.00
methylene iodide	50.8	3.031	9.46	1.20
pyridine	38.0	2.270	9.32	1.23
formamide	58.2	2.095	10.25	1.99
glycerol	63.4	2.136	10.85 [d]	2.06
water	72.8	1.755	12.59	3.02

[a] IP values from reference 16.

[b] Estimated by using the IP value of C_3F_8.

[c] Estimated by using the IP value of n-heptane.

[d] Estimated by using the IP value of methanol.

The qualitative correlation of depth sensitivities of hexadecane, glycerol and water on monolayers of $CH_3(CH_2)_nO(CH_2)_{16}SH$ on gold reveals that the sensitivity of the contact angle of hexadecane to the ether group in that monolayer system extents only ~2 Å, whereas water senses the ether group down to ~5 Å beneath the surface [5]. This correlation agrees with our calculated results. However, the proposed mechanism that the greater sensing depth of water may reflect its penetration through short alkyl chains at the surface of the monolayer is probably relatively unimportant, as suggested by our calculated results. The relatively similar depth sensitivities of the three probe liquids on monolayers of $CF_3(CF_2)_nCOOH$ on silver [14] may be due to the highly polar nature of the carboxylate group in the monolayers. This leads to a strong orientation interaction of the carboxylate group with polar probe liquids, such as water and glycerol, and causes an increase in the value of A. As a result, the difference between the depth sensitivities of the three probe liquids is not appreciable.

Limiting contact angles

At large n, as V_{SL}^G decays to almost zero, V_{SL}^T and as a consequence θ_∞ reach limiting values. This limiting contact angle is a characteristic of the composition of the molecular surface. It is interesting to compare values of θ_∞ for various liquids on different molecular surfaces. Table II lists the values of θ_∞ for the nonpolar liquid hexadecane and polar liquids glycerol and water on surfaces terminated with a $-CH_3$ group or $-CF_3$ group. As is apparent, for the two different molecular surfaces, the difference in θ_∞'s for a liquid decreases in the order of hexadecane, glycerol, and water. From equation 5,

$$\cos\theta_\infty = V_{SL}^T/\gamma_{LV}^\bullet - 1 \qquad (18)$$

Following the treatment of Hamaker, V_{SL}^T in this case is assumed to be at an equilibrium distance, x_0 (i.e., two surfaces in contact). The best empirical value for x_0 is reported to be 1.58±0.08 Å [8,18]. Hence,

Table II. Limiting contact angles of various liquids on molecular surfaces terminated with a $-CH_3$ or $-CF_3$ group

Materials	θ_{∞}(hexadecane)	θ_{∞}(glycerol)	θ_{∞}(water)	References
$CF_3(CF_2)_7(CH_2)_5SH/Au$	79°	---	118°	19
$CF_3(CF_2)_8COOH/Ag$	70°	103°	108°	15
$CH_3(CH_2)_{21}SH/Au$	47°	---	112°	20
$CH_3(CH_2)_{18}COOH/Ag$	43°	98°	107°	21

Table III. Comparison of $A/\gamma_{LV}^{\bullet}$ values on various interfaces (Unit: cm^2)

Liquid	$A/\gamma_{LV}^{\bullet}$(-CH_3 surface)	$A/\gamma_{LV}^{\bullet}$(-CF_3 surface)
hexadecane	16.0×10^{-15}	4.0×10^{-15}
glycerol	7.8×10^{-15}	1.9×10^{-15}
water	5.3×10^{-15}	1.3×10^{-15}

$$\cos\theta_\infty = A/12\pi x_o^2\gamma_{LV}^{\bullet} - 1 \qquad (19)$$

Table III lists the calculated values of $A/\gamma_{LV}^{\bullet}$ at the six different interfaces. Note that the surfaces terminated with a $-CH_3$ group or $-CF_3$ group are approximated by the physical properties of hexadecane and perfluoro-n-heptane, respectively. As is apparent in Table III, the difference in $A/\gamma_{LV}^{\bullet}$ values decreases in the order of hexadecane, glycerol, and water, which explains the trend of θ_∞ listed in Table II. As a result, the value of the limiting contact angle is governed by the van der Waals interactions at the solid-liquid interface.

Odd-even progression

The wetting data as shown in Figure 4 show an odd-even variation in contact angle for monolayers of $CH_3(CH_2)_nSH$ on gold [13] and $CH_3(CH_2)_nCOOH$ on silver [21]. The odd-even variation is more significant for short chain than for long chain. For simplicity, we refer to a chain with an odd number of $-CH_2-$ or $-CF_2-$ groups as an "odd chain" and a chain with an even number of $-CH_2-$ or $-CF_2-$ groups as an "even chain". For monolayers of $CH_3(CH_2)_nSH$ on gold, odd chain monolayers have θ's that are markedly greater than those that are composed of chains with one less methylene group. In contrast, for monolayers of $CH_3(CH_2)_nCOOH$ on silver, even chain monolayers have θ's that are markedly greater than those that are composed of chains with one less methylene group. Changes in θ's with an odd-even variation of chain length may arise from a difference in the orientation of the terminal methyl group, as shown in Figure 5. The permanent dipole moment of the methyl group, which has a component perpendicular to the surface and opposite in direction to the S-Au or COO-Ag dipoles, will screen the VW interactions between the probe liquid and the underlying S-Au or COO-Ag dipoles. Methyl dipoles of odd chain $CH_3(CH_2)_nSH$ monolayers on gold and even chain $CH_3(CH_2)_nCOOH$ monolayers on silver are almost perpendicular to the surface, while methyl dipoles of even chain $CH_3(CH_2)_nSH$ monolayers

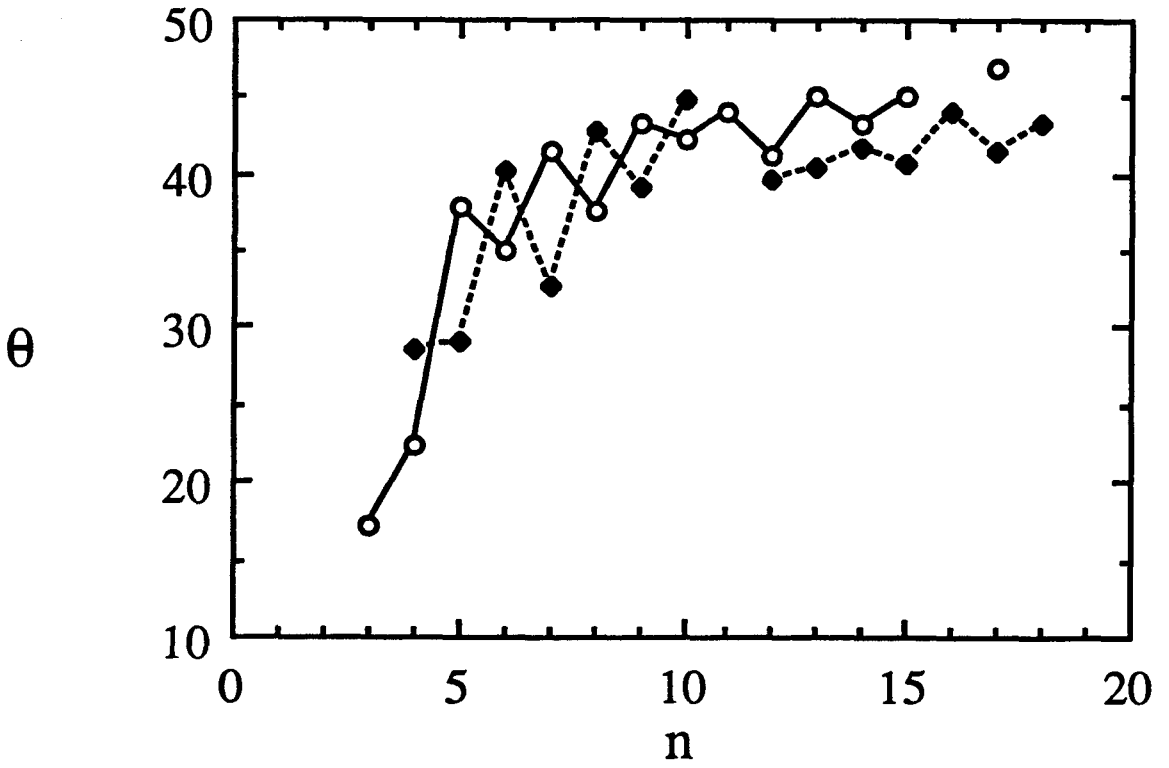

Figure 4. Contact angles of hexadecane on monolayers of $CH_3(CH_2)_nSH$ adsorbed at gold (o) and $CH_3(CH_2)_nCOOH$ adsorbed at silver (♦)

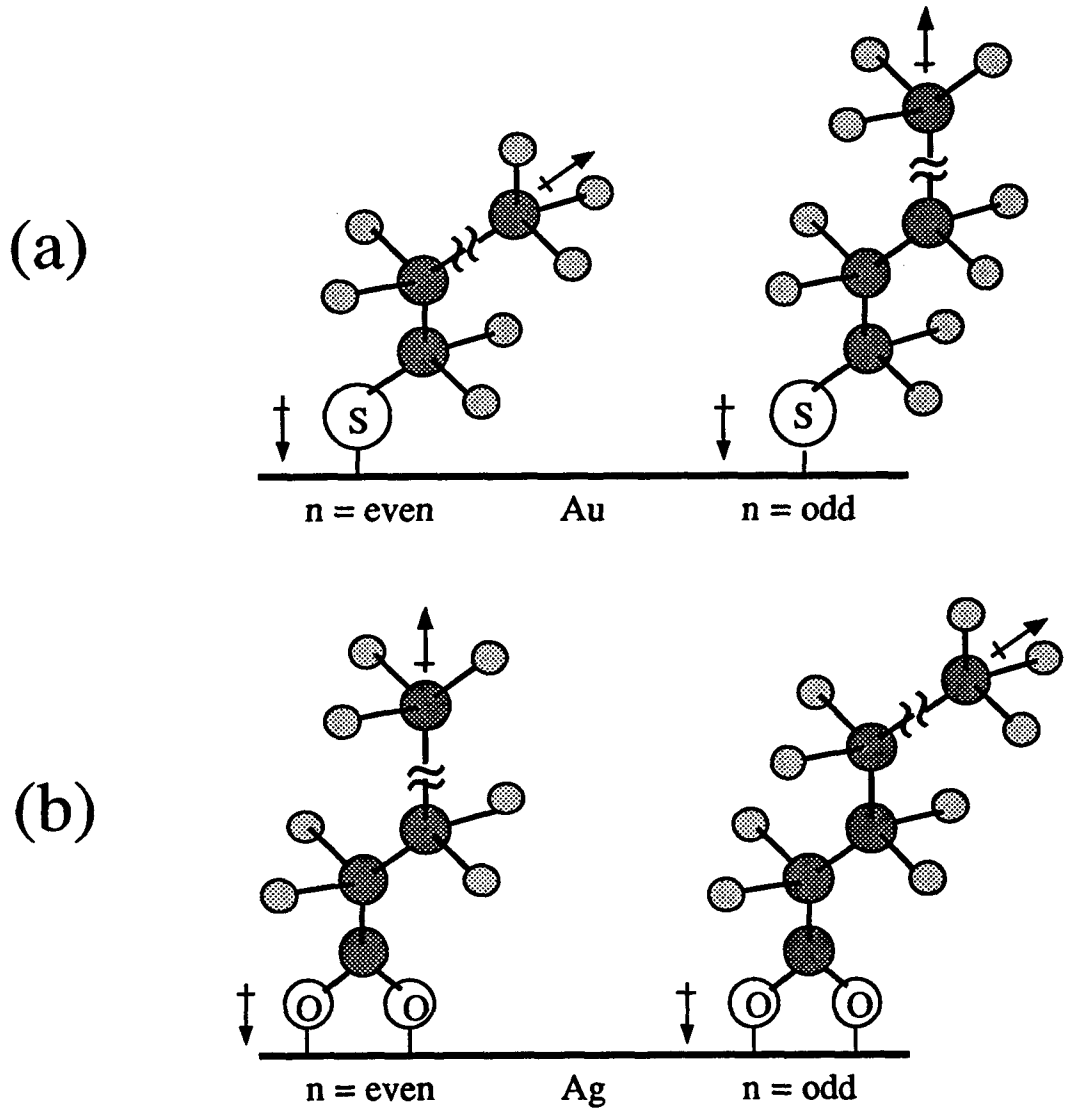

Figure 5. Proposed structures for (a) n-alkanethiolate monolayers on gold, and (b) n-alkanoate monolayers on silver, with an even (right) and odd (left) number of methylene groups in the chain. Directions of the -CH_3, S-Au, and COO-Ag permanent dipole moments are indicated by the arrows.

on gold and odd chain $CH_3(CH_2)_nCOOH$ monolayers on silver have smaller components perpendicular to the surface. Thus, the VW interactions between the probe liquid and the underlying structures are screened more effectively by the methyl dipoles of odd chain $CH_3(CH_2)_nSH$ monolayers on gold and even chain $CH_3(CH_2)_nCOOH$ monolayers on silver and result in relatively greater θ's.

At larger separation distances, the VW interactions between the probe liquid and the underlying dipoles are weaker. Consequently, the difference in screening by the terminal methyl groups with different orientations is proportionally smaller. This leads to a smaller odd-even variation as observed in Figure 5.

CONCLUSIONS

The wettability of a liquid on a solid surface is related to the microscopic composition and structure of the solid surface. Our results show that the van der Waals interactions between two semiinfinite parallel flat slabs decay as the square of the separation distance at fairly close range. As a result, the depth sensitivity of a liquid to an underlying functional group of a solid surface depends on the van der Waals (dispersion, orientation, and induction) interactions between the liquid and the functional group of interest. In addition, the limiting contact angle depends on the van der Waals interactions between the liquid and the molecular surface. The relative depth sensitivity of several representative liquids were calculated and compared, based on the consideration of dispersion interaction only. More sophisticated calculations of depth sensitivity are necessary for interactions between polar liquids and highly polar functional groups underlying solid surfaces with additional considerations of polar interactions.

REFERENCES

1. Zisman, W. A. in Contact Angles, Wettability, and Adhesion; Fowkes, F. M. Ed.; Advances in Chemistry Series 43; American Chemical Society: Washington, DC, 1964; pp 1-51.
2. Whitesides, G. H.; Laibinis, P. E. Langmuir **1990**, 6, 87-96.
3. Wilson, M. D.; Furguson, G. S.; Whitesides, G. M. J. Am. Chem. Soc. **1990**, 112, 1244-1245.
4. Dubois, L. H.; Zegarski, B. R.; Nuzzo, R. G. J. Am. Chem. Soc. **1990**, 112, 570-579.
5. Wilson, M. D.; Whitesides, G. M. J. Am. Chem. Soc. **1988**, 110, 8718-8719.
6. Bain, C. D.; Whitesides, G. M. J. Phys. Chem. **1989**, 93, 1670-1673.
7. Bain, C. D.; Whitesides, G. M. J. Am. Chem. Soc. **1988**, 110, 5897-5898.
8. van Oss, C. J.; Chaudhury, M. K.; Good, R. J. Chem. Rev. **1988**, 88, 927-941.
9. Hamaker, H. C. Physica **1937**, 4, 1058-1072.
10. Casimir, H. B. G.; Polder, D. Phys. Rev. **1948**, 73, 360-372.
11. Adamson, A. W. Physical Chemistry of Surfaces, 4th Ed.; Wiley: New York, 1982; pp 338-340.
12. Israelachvili, J. N. Intermolecular and Surface Forces; Academic Press: San Diego, 1985; Chapter 6.
13. Walczak, M. M.; Chung, C.; Stole, S. M.; Widrig, C. A.; Porter, M. D. unpublished results, Department of Chemistry, Iowa State University.
14. Walczak, M. M.; Chung, C.; Stole, S. M.; Widrig, C. A.; Porter, M. D. submitted for publication in J. Am. Chem. Soc.
15. Chau, L. K.; Porter, M. D. Chem. Phys. Lett. **1990**, 167, 198-204.
16. Rosenstock, H. M.; Draxl, K.; Steiner, B. W.; Herron, J. T.

J. Phys. Chem. Ref. Data **1977**, 6, supplement no. 1.

17. Kaelble, D. H. Physical Chemistry of Adhesion; Wiley-Interscience; New York, 1971; Chapter 2.
18. Israelachvili, J. N. Intermolecular and Surface Forces; Academic Press: San Diego, 1985; Chapter 11.
19. Chidsey, C. E. D.; Loiacono, D. N. Langmuir **1990**, 6, 682-691.
20. Bain, C. D.; Troughton, E. B.; Tao, Y.-T.; Evall, J.; Whitesides, G. M.; Nuzzo, R. G. J. Am. Chem. Soc. **1989**, 111, 321-335.
21. Chau, L. K.; Wolff, K. M.;Porter, M. D. manuscript in preparation, Department of Chemistry, Iowa State University.

SECTION V. OPTICAL SENSOR FOR CALCIUM: PERFORMANCE, STRUCTURE, AND REACTIVITY OF CALCICHROME IMMOBILIZED AT AN ANIONIC POLYMER FILM

Optical Sensor for Calcium: Performance, Structure, and Reactivity of Calcichrome Immobilized at an Anionic Polymer Film

Lai-Kwan Chau and Marc D. Porter

Ames Laboratory - USDOE and Department of Chemistry

Iowa State University

Ames, Iowa 50011

ABSTRACT

A calcium-selective optical sensor has been fabricated by the electrostatic immobilization of calcichrome at a porous anion-exchange polymer film. The change in the optical properties of the bound indicator as a function of Ca(II) concentration was monitored in a single-beam diffuse reflection mode at a pH of 12.1. Advantageous features of this design include a short response time (<15 s), high selectivity, facile construction, and compatibility with commercially available instrumentation. The rapid response results from the porous microstructure of the anion exchange polymer, which facilitates the mass transport of analyte and counter ions between solution and polymer film. The optical response is linear for a Ca(II) concentration between 3 and 30 mM with a detection limit of 3 mM. Immobilization alters both the acid and chelation strength of the indicator. Possible causes of these reactivity differences are discussed, based on insights provided by infrared internal reflection and photoacoustic spectroscopies. Equations to determine the metal complex formation constant and acid dissociation constants of the immobilized reagent from diffuse reflectance spectra are developed.

INTRODUCTION

Thin films of organic polymers have been used extensively for the development and construction of a wide variety of sensors based either on electrochemical or optical detection schemes [1-4]. Central to both of these schemes is the control of the selectivity and/or sensitivity of an analysis by the synthetic manipulation of the chemical and physical properties of the polymeric film. For electrochemical sensors, strategies to control the composition of "redox" and ion exchange polymers have been employed to mediate the electron-transfer of large biomolecules [5-7] and to preconcentrate metal ions [8,9]. One approach to control selectivity has focused on the careful alteration of the permselectivity of cellulosic polymers [10,11]. Permselective films have the additional advantage of precluding the adsorption of macromolecules that may foul the electrode surface, enhancing the long term stability of the sensor.

As has been briefly summarized [12], the design and construction of optical sensors have focused to a large degree on approaches for the attachment of a colorimetric reagent to a host polymeric support. Immobilization schemes include the attachment of acid-base and metallochromic indicators with a covalent linkage [13-16], the electrostatic immobilization of sulfonate- and carboxylate-functionalized indicators at ion exchange polymers [17], and the adsorption of dyes onto cellulosic films [18]. Such sensors have exhibited a wide range of performance characteristics (e.g., sensitivity, stability, and response time), which are intimately linked to the composition and microstructure of the polymeric film. It is therefore apparent that the optimization of the performance characteristics of both optical and electrochemical sensors represents a complex mixture of fundamental and practical issues. To this end, future progress will require an increasingly interdisciplinary research strategy, drawing from specialties such as synthesis, materials characterization, theory, and instrumentation.

This paper describes the construction, performance characteristics, and structural and reactivity details of an optical sensor for the selective determination of Ca(II). The sensor was fabricated by the electrostatic immobilization of calcichrome (2,8,8'-trihydroxy-1,1'-azonaphthalene-3,6,3',6'-tetrasulfonic acid) at a porous anion exchange polymer film. The change in the optical properties of the immobilized reagent were monitored in a diffuse reflection mode in the visible spectral region. Relevant features of this design include a short equilibration time (<15 s), high selectivity, facile construction, and compatibility with commercially available instrumentation. The rapid response results from the porous microstructure of the anionic polymer which facilitates the mass transport of analyte and counter ions between solution and polymer film. Immobilization, however, alters both the acid and chelation strength of the indicator. Possible causes of the reactivity differences are discussed and substantiated by structural descriptions of the bound indicator that are deduced from infrared internal reflection and photoacoustic spectroscopic data. Equations to determine the metal complex formation constant and acid dissociation constants of the immobilized reagent from diffuse reflectance spectra are developed and used to assist the characterization of the chemical properties of the sensor. Considerations for the potential application of this sensor to environmental, industrial, and clinical purposes are also briefly discussed.

THEORY

This section describes the requisite formulization for obtaining the conditional formation constants and acid dissociation constants for immobilized colorimetric indicators with diffuse reflection spectroscopy in both single-and double-beam modes. It begins with use of Kubelka-Munk theory [19] to develop equations that relate the experimentally measured intensities of the diffusely reflected light to the equilibrium between a solution phase metal ion and an immobilized metallochromic indicator. An analogous method for the determination of the acid dissociation constant(s) of an immobilized indicator is also presented.

Determination of the formation constant for a metal complex with diffuse reflection spectroscopy

The general reaction for the equilibrium between a solution phase metal ion, M^{n+}, and an immobilized ligand, L^{m-}, is

$$M^{n+} + L^{m-} = ML^{n-m} \qquad (1)$$

where ML^{n-m} is the immobilized metal complex. Assuming activity coefficients of unity for both solution and immobilized species, the conditional formation constant, K_f, for the chelation of the metal and ligand is

$$K_f = \overline{ML} / [M]\,\overline{L} \qquad (2)$$

where [M] is the equilibrium solution concentration of the metal ion, and $\overline{L}$ and $\overline{ML}$ are the respective equilibrium concentrations of the immobilized ligand and the immobilized metal complex. Equation 2 can also be written with respect to $\overline{ML}$ and the initial concentrations of the metal ion in solution, $[M]_o$, and the immobilized ligand, $\overline{L}_o$, to give

$$K_f = \overline{ML} / ([M]_o - \overline{ML})(\overline{L}_o - \overline{ML}) \qquad (3)$$

Upon expansion and rearrangement, equation 3 yields

$$1/K_f = [M]_o \overline{L} / \overline{ML} - [M]_o - \overline{L}_o + \overline{ML} \quad (4)$$

If experimental conditions are such that

$$\overline{L}_o - \overline{ML} \ll [M]_o \overline{L}_o / \overline{ML} - [M]_o$$

i.e., $\overline{ML} \ll [M]_o$, then equation 4 reduces to

$$1/K_f = [M]_o \overline{L}_o / \overline{ML} - [M]_o \quad (5)$$

For diffuse reflection measurements, the Kubelka-Munk (K-M) function provides an empirical approach for relating the observed signal quantitatively to the sample concentration. The K-M function, $f(R_\infty)$, is defined as

$$f(R_\infty) = (1-R_\infty)^2/2R_\infty \quad (6)$$

where R_∞ is the absolute diffuse reflectance of an infinitely thick sample. This function is related to the concentration of an absorbing sample species, C, by

$$f(R_\infty) = \varepsilon C/s \quad (7)$$

where ε is the molar absorptivity of the sample species and s is the scattering coefficient. For a nonabsorbing M^{n+}, $f(R_\infty)$ can be expressed using equation 7 as

$$f(R_\infty) = \varepsilon_{ML} \overline{ML} /s + \varepsilon_L(\overline{L}_o - \overline{ML})/s \quad (8)$$

where ε_{ML} and ε_L are the molar absorptivities of $\overline{ML}$ and $\overline{L}$, respectively. If $f(R_\infty')$ represents the K-M function for L_o, equation 8 becomes

$$f(R_\infty) = (\varepsilon_{ML}-\varepsilon_L) \overline{ML} /s + f(R_\infty') \quad (9)$$

The general expression for the Kubelka-Munk function in equation 6 can also be used to formulate $f(R_\infty)$ in terms of $f(R_\infty')$, which through subtraction of $f(R_\infty')$ and rearrangement gives

$$f(R_\infty) - f(R_\infty') = (R_\infty'-R_\infty)(1-R_\infty R_\infty')/2R_\infty R_\infty' \quad (10)$$

For measurements that result in $R_\infty R_\infty' \ll 1$, equation 10 simplifies to

$$f(R_\infty) - f(R_\infty') = (R_\infty'-R_\infty)/2R_\infty R_\infty' \quad (11)$$

Combining equations 9 and 11 then results in an expression that relates R_∞ and R_∞' with $\overline{ML}$

$$(R_\infty'-R_\infty)/2R_\infty R_\infty' = (\varepsilon_{ML}-\varepsilon_L)\,\overline{ML}\,/s \qquad (12)$$

To relate equations 5 and 12 to measurements in a single-beam mode, a comparison to a reference intensity is necessary to compensate for instrument fluctuations (e.g., long term drift of the intensity of the light source). One approach for compensation is to use the reflected intensity at an isosbestic point as a reference [16]. For a diffuse reflectance measurement, the diffuse reflectance ratios for the free (R_n') and complexed (R_n) forms of an immobilized indicator can be expressed as

$$R_n = J_n/J_r \qquad (13)$$

$$R_n' = J_n'/J_r \qquad (14)$$

where J_n, J_n', are the experimentally measured intensities of the diffusely reflected light at the sampling wavelength and J_r is that at an isosbestic point. Additionally, as most experimental measurements do not determine the absolute diffuse reflectance of a sample, it is usual to relate the observed signal to a suitable reference material [20]. These relative quantitites are given as

$$r_\infty = R_\infty/\sigma_{std} \qquad (15)$$

$$r_\infty' = R_\infty'/\sigma_{std} \qquad (16)$$

where σ_{std} is the absolute diffuse reflectance of the reference material and is equal to unity for a perfect diffuse reflector. Dividing both the numerators and denominators in equations 13 and 14 by σ_{std} yields

$$R_n = R_\infty\sigma_{std}/J_r \qquad (17)$$

$$R_n' = R_\infty'\sigma_{std}/J_r \qquad (18)$$

Combining equations 5, 12, 17 and 18 results in

$$(1/R_n - 1/R_n')^{-1} = s\sigma_{std}/2(\varepsilon_{ML}-\varepsilon_L)J_r\,\overline{L}_o K_f[M]_o + s\sigma_{std}/2(\varepsilon_{ML}-\varepsilon_L)J\,\overline{L}_o \qquad (19)$$

In the conventional double beam mode, a comparable derivation gives

$$(1/r_\infty - 1/r_\infty')^{-1} = s/2(\varepsilon_{ML}-\varepsilon_L)\sigma_{std}\,\overline{L}_o K_f[M]_o + s/2(\varepsilon_{ML}-\varepsilon_L)\sigma_{std}\,\overline{L}_o \qquad (20)$$

In both instances, a plot of $(1/R_n - 1/R_n')^{-1}$ or $(1/r_\infty - 1/r_\infty')^{-1}$ vs $1/[M]_o$ is linear, which allows the calculation of K_f by dividing the y-intercept by the slope.

Determination of acid dissociation constants for an immobilized species with diffuse reflection spectroscopy

The general reaction for the acid dissociation of an immobilized ligand is

$$\overline{H_nL^{m-}} = \overline{H_{n-1}L^{(m+1)-}} + H^+ \qquad (21)$$

Where $\overline{H_nL^{m-}}$ and $\overline{H_{n-1}L^{(m+1)-}}$ are the immobilized forms of a conjugate-acid-base pair, respectively. The acid dissociation constant for equation 21 can be written as

$$K_a = [\overline{H_{n-1}L^{(m+1)-}}][H^+]/[\overline{H_nL^{m-}}] \qquad (22)$$

Since equation 7 shows that concentration is proportional to $f(R_\infty)$, the pK_a for equation 22 can then be expressed as

$$pK_a = pH - \log\{(f(R_{\infty 1}) - f(R_\infty))/(f(R_\infty) - f(R_{\infty 2}))\} \qquad (23)$$

where $f(R_{\infty 1})$ and $f(R_{\infty 2})$ are the K-M function at pH values which result only in $\overline{H_nL^{m-}}$ or $\overline{H_{n-1}L^{(m+1)-}}$, respectively, and $f(R_\infty)$ is the K-M function at intermediate pH values where both $\overline{H_nL^{m-}}$ and $\overline{H_{n-1}L^{(m+1)-}}$ are present.

If one or more sets of isosbestic points exist, equation 22 can be expressed following earlier arguments as

$$pK_a = pH - \log\{(1/R_{n1} - 1/R_n)/(1/R_n - 1/R_{n2})\} \qquad (24)$$

where R_{n1} and R_{n2} are the diffuse reflectance ratios at pH values which result only in $\overline{H_nL^{m-}}$ and $\overline{H_{n-1}L^{(m+1)-}}$, respectively, and R_n is that at intermediate pH values where both $\overline{H_nL^{m-}}$ and $\overline{H_{n-1}L^{(m+1)-}}$ are present.

EXPERIMENTAL

Sensor construction

The sensor was constructed by the electrostatic immobilization of calcichrome at a N-0030 anion exchange film (RAI Research Corporation, Hauppauge, NY). This film is a porous (pore size > 10 mm) organic polymer with ~1.5 meq/g of quaternary ammonium cationic exchange sites. The films scatter light analogously to the mats commonly employed as references for diffuse reflection spectroscopy. Immobilization was accomplished by immersing a film into an aqueous 0.1 mM calcichrome solution for 24 h at 25°C. Under these conditions, the concentration of immobilized calcichrome was ~6mM (1.2 mmoles/g dry film). This value was determined by the optical quantitation of the difference in the amount of colorimetric reagent in solution before and after immobilization. The thickness of an immersed membrane was ~800 mm.

Flow cell

The optical sensor and flow cell are shown in Figure 1. The incident light was carried to the cell through 400-mm diameter optical fibers (Ensign-Bickford Optics Co. Avon, CT). The fiber diameter with cladding is ~730 mm. Optical fibers also collected and transmitted the diffusely reflected light to the entrance slit of a monochromator. The optical fiber bundle consisted of 10 fibers, which were arranged in a vertical orientation, with half used to transmit the incident light to the thin film and half used to transmit the diffusely reflected light to the entrance slit of a monochromator. The optical fibers were sealed into slotted Plexiglass cylinders and mounted to the cell with setscrews. The solution cavity was defined by the front window of the cell, the silicone rubber gasket, and the thin film sensor. The window was sealed into place with silicone rubber cement. The front and back plates of the cell were machined from Plexiglass to respective thicknesses of 1.2 and 2.0 cm. The solution inlet and

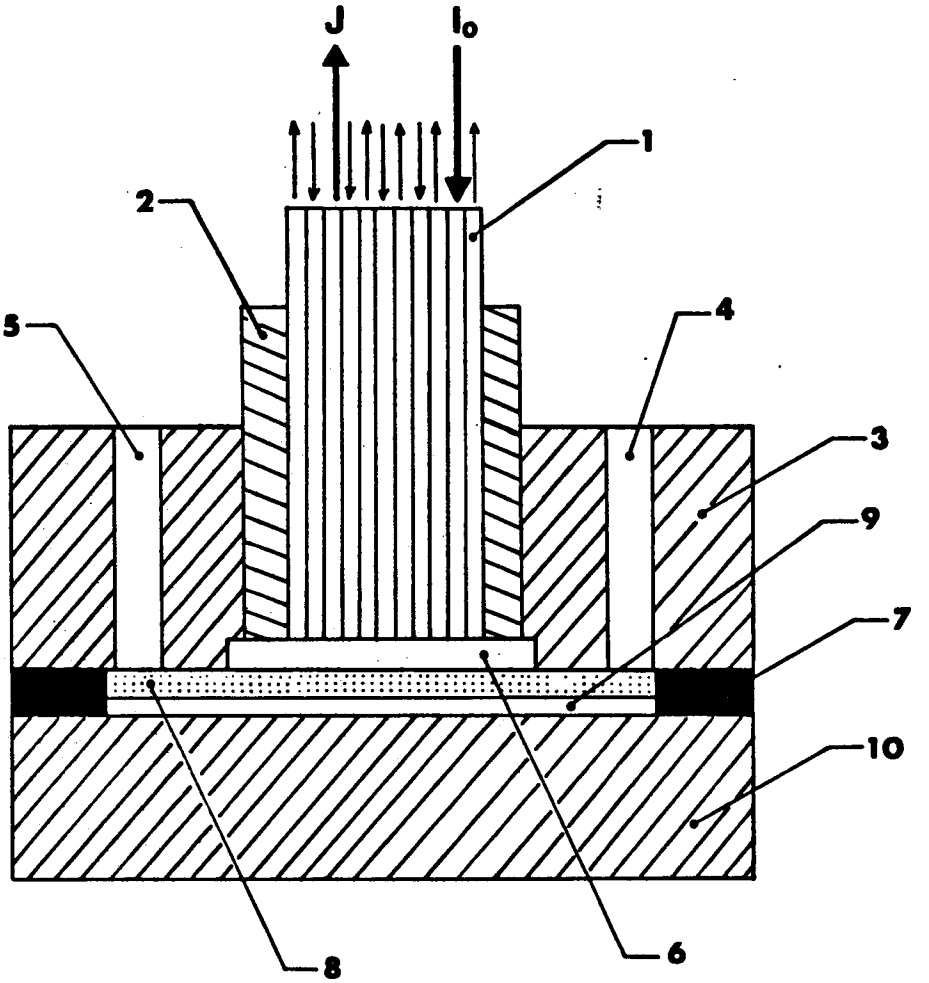

Figure 1. Flow cell construction: (1) optical fiber, (2) fiber mounting cylinder, (3) front plate, (4) solution inlet channel, (5) solution outlet channel, (6) front window, (7) slotted gasket, (8), thin film Ca(II)-sensor, (9) diffuse white reflector, (10) back plate.

outlet channels were drilled to a diameter of 0.2 cm and connected to Teflon tubing with flanged fittings. The cell was sealed with a 0.15 cm thick silicone rubber gasket of which an inner portion was removed to define the solution channel. The time required to affect a complete change (99.9%) of the solution in the cell was 1.22±0.18 s (standard deviation, n = 17).

Under these experimental conditions, values for $R_\infty R_\infty'$ were less than 0.01, which correspond to an error of less than 1% for the approximation in developing equation 11 from equation 10. In addition, by using calcium concentrations greater than 0.06 M, the approximation in arriving at equation 5 from equation 4 results in an error of less than 10% in the determination of K_f.

Instrumentation

A Xenon arc lamp (Oriel Corp., Stamford, CT) was used as a light source. The collected light was dispersed with a 0.22-m grating monochromator and monitored with a digital photometer (Spex DPC-2, SPEX, Edison, NJ) in a photon counting mode. The pH of the solutions was measured with a 140 A Accumet pH meter (Fischer Scientific, Pittsburgh, PA). Infrared spectra of solid and dissolved calcichrome were collected with a Nicolet 740 Fourier transform infrared spectrometer (Madison, WI). A CIRCLE cell (Spectra Tech, Inc., Stamford, CT) with a ZnSe internal reflection element was used to acquire the solution IR spectra. The y-axis of the solution spectra is given as $-\log(R/R_0)$, where R is the single beam spectrum of calcichrome at a given pH and R_0 is that of the same solution without calcichrome. This method of data presentation effectively compensates for small changes in the absorptivity of the aqueous solvent as a function of pH below ~1550 cm^{-1}; however, the large absorbance of the solvent precluded an effective compensation at the higher energies of the carbonyl and C=C stretching regions. Photoacoustic spectra of both the calcichrome

modified film and the unmodified film were collected with a Perkin-Elmer 1800 Fourier transform infrared spectrometer (Norwalk, CT) and a MTEC 200 photoacoustic detector (Ames, IA).

Reagents

The pH of the solutions was controlled by varying the amounts of NaOH or HCl, or by citrate or phosphate buffers (McIlvaine buffers). All solutions were prepared with deionized water. Calcichrome (Pfaltz and Bauer, CT) was used as received. The ionic strength of the solutions was maintained with 0.2 M KCl.

RESULTS AND DISCUSSION

Diffuse reflectance spectra of the sensor

Diffuse reflectance spectra of immobilized calcichrome before and after complexation with Ca(II) are shown in Figure 2. Both spectra were taken at pH 12.1, and are given as relative reflectances, i.e., R_s/R_u, where R_s is the diffuse reflectance of the free or complexed forms of the immobilized indicator and R_u is that of the unmodified film. The free form of immobilized calcichrome exhibits a reflectance minimum near 620 nm, whereas that for the immobilized Ca(II):calcichrome complex is slightly above 540 nm. These reflectance minima are red shifted about 20 nm relative to the absorbance maxima of their solution analogs [21]. On the basis of a comparison to the transmission spectra of the solution form of the indicator [21], a set of isosbestic points in the reflectance spectra were also observed at 556 and 425 nm. The shifts in the reflectance minima for immobilized calcichrome arise primarily from optical dispersion effects that are inherent to diffuse reflection measurements [19].

Response to Ca(II)

Both the K-M function and the diffuse reflectance ratio of the sensor as a function of Ca(II) concentration at 670 nm are shown in Figure 3. The reflected intensity at the isosbestic point at 556 nm was used as the reference. The K-M function is linear up to Ca(II) concentration of ~30 mM, leveling off at higher concentrations because of saturation of the chelating sites of the thin film sensor. The plot of diffuse reflectance ratio vs. Ca(II) concentration is sigmoidal, also exhibiting a linear region approximately between 3 and 30 mM. The detection limit, defined as the concentration which gave a signal that was four times the standard deviation of the blank, was estimated at 3 mM. Efforts are currently underway to lower the detection limit both by increasing the light collection efficiency and by

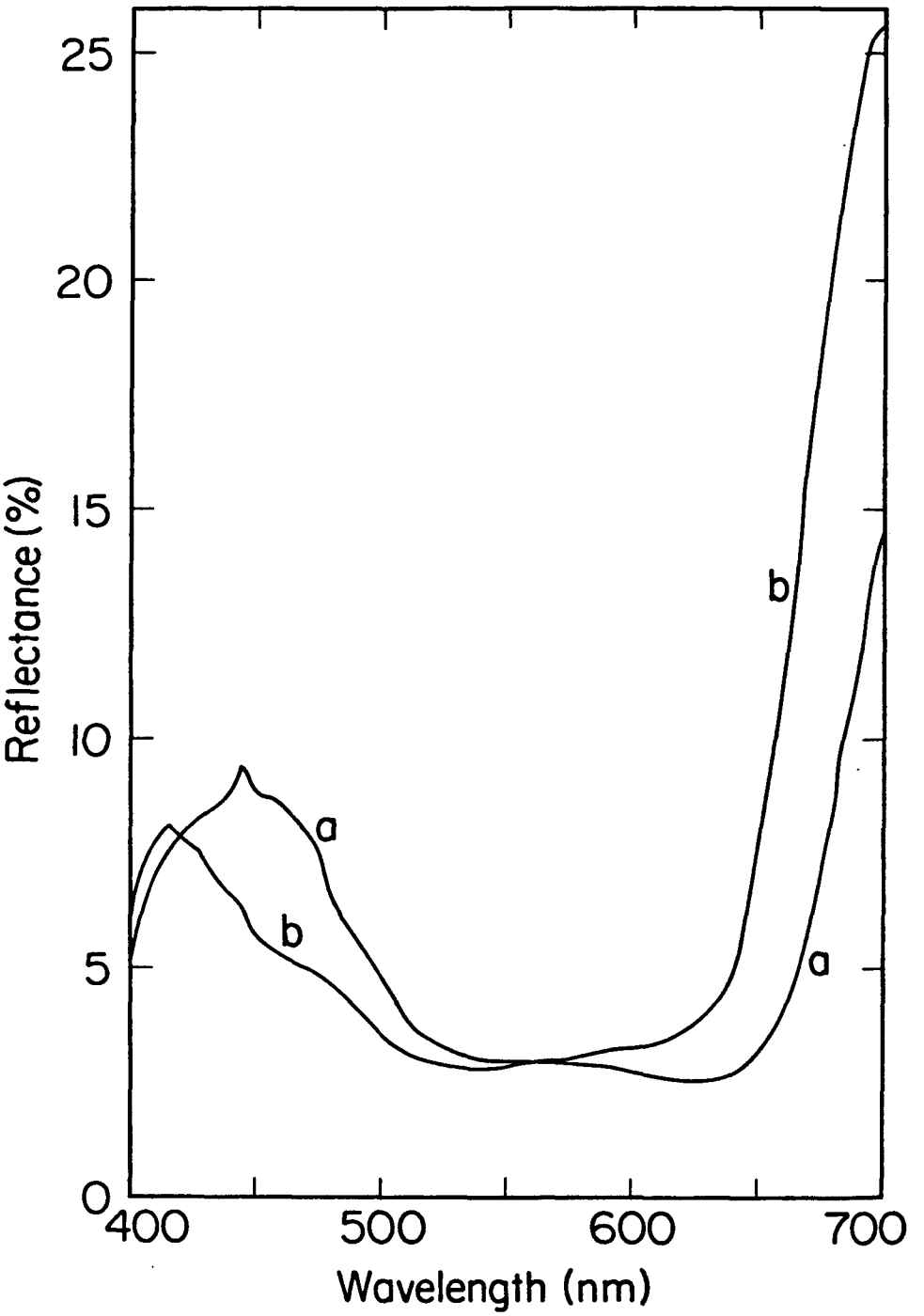

Figure 2. Diffuse reflectance spectra of (a) immobilized calcichrome, (b) immobilized Ca(II)-calcichrome complex ([Ca(II)] = 0.2 M), at pH 12.1 in the flow cell.

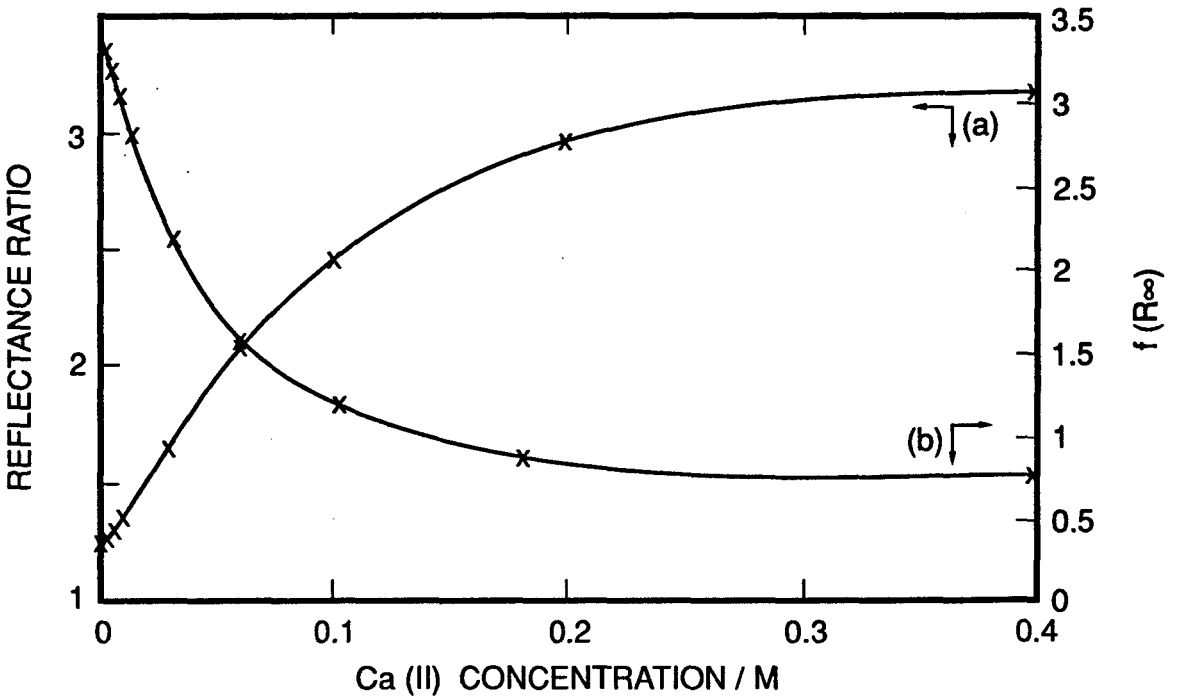

Figure 3. (a) Diffuse reflectance ratio and (b) K-M function of the Ca(II) sensor as a function of Ca(II) concentration at pH 12.1

reducing stray light [22]. The latter improvement should also increase the dynamic range of the measurement [23].

Response time

The optical response of the sensor to a rapid change in Ca(II) concentration is shown in Figure 4. The wavelength used for these measurements was 670 nm. Both the blank ([Ca(II)]= 0.0 M) and calcium-containing solution ([Ca(II)]=0.20 M) were buffered at pH 12.1. Upon injection of analyte solution, the diffuse reflectance ratio increases rapidly, corresponding to the formation of the immobilized metal complex. Equilibration (99.9% completion) is achieved in ~13 s, with the response reaching 63% of the maximum value in less than 4 s. The response of this sensor is 5-10 times more rapid than those of other metal ions [24-29], and is roughly 20 times more rapid than those of other Ca(II) sensors [30,31]. Comparable improvements in response times have been observed for pH sensors that were constructed at a porous microstructure [18], further demonstrating an advantage of designing sensors based on porous polymeric materials.

Interferences

In addition to Ca(II), the solution form of calcichrome complexes with a variety of other metal ions, including Cu(II), Cd(II), Zn(II), V(IV), Mg(II), and Ba(II) [32]. However, near pH 12 calcichrome complexes only with Mg(II), Ba(II), and Ca(II). Tests for the possible interference of each of the latter metal ions with the response from the sensor were conducted over a broad range of concentrations (up to saturated solutions) at pH 12.1. In all instances, the response of the sensor was virtually indistinguishable (<1% change in reflectance at 670 nm) from that obtained with a blank pH 12.1 solution. Thus, the sensor

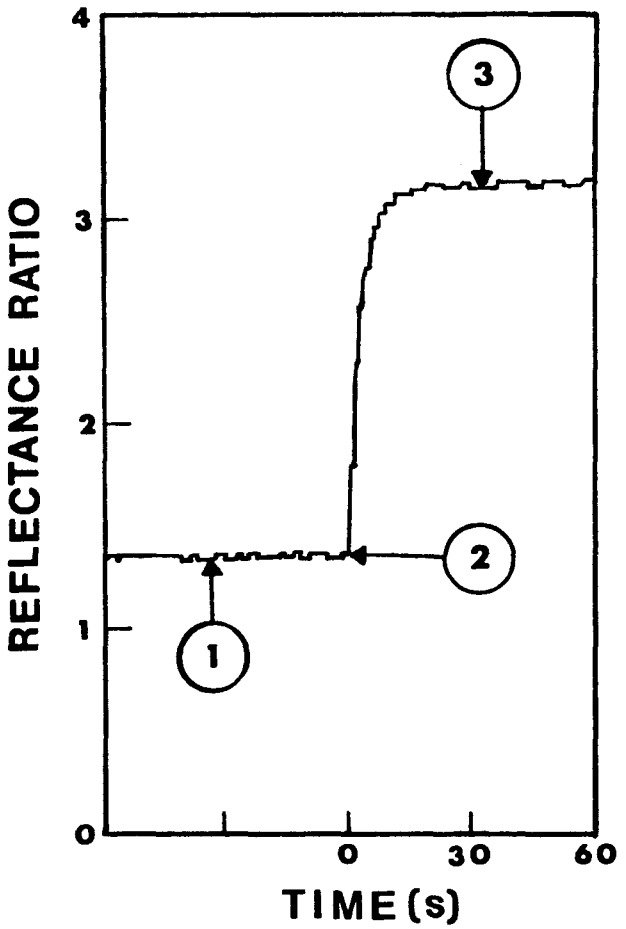

Figure 4. Response time of the Ca(II)-sensor: (1) equilibrated response at pH 12.1 solution, (2) injection of a 0.2 M Ca(II) solution at pH 12.1, (3) equilibrated response at the 0.2 M Ca(II) solution at pH 12.1.

exhibits a high selectivity for Ca(II), suggesting its applicability to a variety of applications (vide infra).

Stability

The stability of the sensor was tested by the replicate injection of a calcium-containing solution under constant irradiation at 670 nm. Freshly prepared sensors were subject to photobleaching during the first few minutes of light exposure which was accompanied by a small decrease in the intensity of the diffusely reflected light. However, the signal stabilized after the first few minutes of light exposure, with no observable degradation in response to calcium over a period of several weeks. Other variables that may affect the response of the sensor, such as temperature, will be tested in the near future.

Reactivity of the solution form of calcichrome

In several instances, the complexation of a metallochromic indicator with a metal ion proceeds with the loss of one or more protons from the indicator. The design of optical sensors for metal ion determinations therefore requires a detailed understanding of those factors that can influence both the acid-base reactivity and chelation capability of an immobilized indicator. One approach for gaining insights into the molecular level details of such interfaces is through a comparison of the structures and reactivities of the solution and immobilized forms of the indicator. This and the next section examine the details of the reactivities of the solution and immobilized forms of calcichrome through measurements of acid dissociation and metal association constants and through structural information provided by infrared internal reflection and photoacoustic spectroscopies.

In aqueous solution, calcichrome has two titratable naphtholic protons with pK_a's of 7.19±0.05 and 11.63±0.05 at 25°C [21]. The reaction scheme is given in equation 25, and

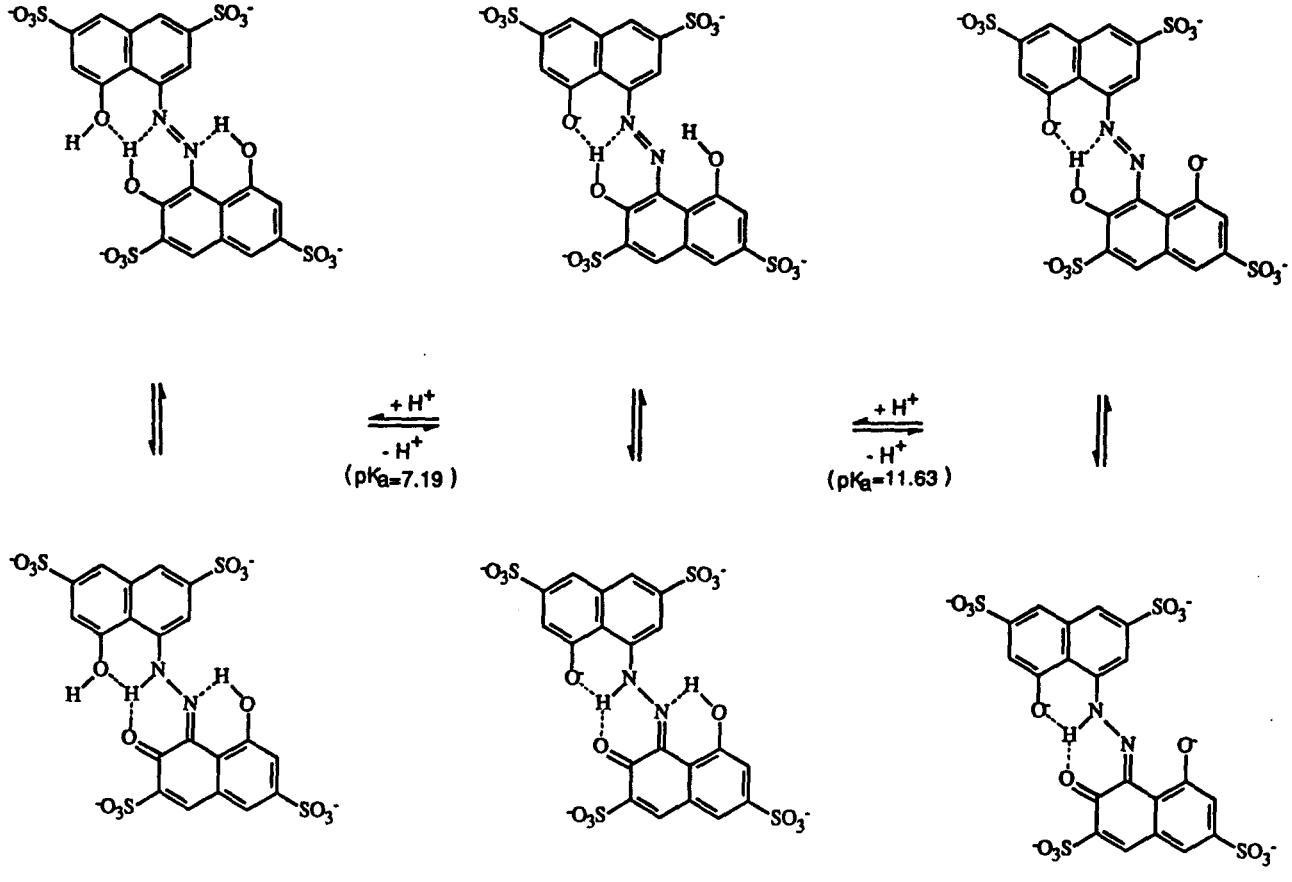

(25)

includes both the acid-base and the tautomeric equilibria for each proton dissociation step. Based on considerations of intramolecular hydrogen bonding, which is revealed by ^{1}H- and ^{13}C-NMR [21] and supported by molecular models, acid dissociation proceeds by the successive loss of protons from the hydroxy groups at the 8' and 8 positions. The naphtholic proton of the hydroxy group at the 2 position does not dissociate in aqueous solution as a result of extensive hydrogen bonding with the azo nitrogen at the 1' position and possibly with the oxygen of the hydroxy group at the 8' position. Both resonance stabilization and hydrogen bonding contribute to the differences in the acid strengths of the naphtholic protons at the 8' and 8 positions.

Identification of the predominant tautomeric species of dissolved calcichrome was aided by the analysis of the infrared internal reflection spectra shown in Figure 5. These spectra were taken at pH values representative of each of the protonated forms of the indicator. As such, the spectra at pH 5.1 and 8.2 are essentially those of the triprotic and diprotic forms of the indicator, respectively. The spectrum at pH 12.1 represents a mixture of the diprotic and monoprotic forms of the indicator. Peak positions and band assignments for these spectra are given in Table I.

All of the bands shown in Figure 5 are affected to varying degrees by a change in pH, complicating the mode assignments and subsequent molecular level interpretation. The bands at ~1290 and 1335 cm^{-1} and the shoulder on the low energy side of an unassigned band slightly above 1350 cm^{-1} are attributed respectively to the O-H bending modes (δ(O-H)) of the naphtholic protons at the 2, 8, and tentatively, 8' positions. Changes in these bands reflect the deprotonation process as well as conformational rearrangements about the azo linkage and/or alterations in intramolecular hydrogen bonding. For example, δ(O-H) for the naphtholic proton at the 8 position shifts to slightly lower energies between a pH of 5 and 8, whereas its absorbance decreases to a level only slightly distinguishable from the background

Table I. Peak positions (cm^{-1}) and vibrational mode assignments for the solution and immobilized forms of calcichrome[a]

solution form				solid form	immobilized form	band assignment[b]
pH 5.1	pH 8.2	pH 12.0	Ca(II) complex (pH 12.0)	(Na salt)		
1042	1040	1040	1039	1044	1037	$\nu_s(SO_3^-)$
1196	1196	1195	1207	1193	1202	$\nu_a(SO_3^-)$
--	1270	1268	1263	--	1269	δ'(NH)
1293	sh	--	--	1277	--	δ(OH)
1335	1334	--	--	1335	1322	δ(OH)
1371	1368	1365	1363	1367	1342	
--	1392	1391	1379	--	1384	ν_s(C=N-N)
--	1442	1438	1419	--	1425	ν_a(C=N-N)
1474	--	--	--	--	1475	ν(C=C)
				1519	1501	ν(C=C)
				--	1567	δ(NH)
				1603	1599	ν(C=C)
				1635	1645	ν(C=O)

[a] Band assignments based on those reported in references 33-35.

[b] Key: ν_a = asymmetric stretch; ν_s = symmetric stretch; δ = bending; δ' = deformation; sh = shoulder.

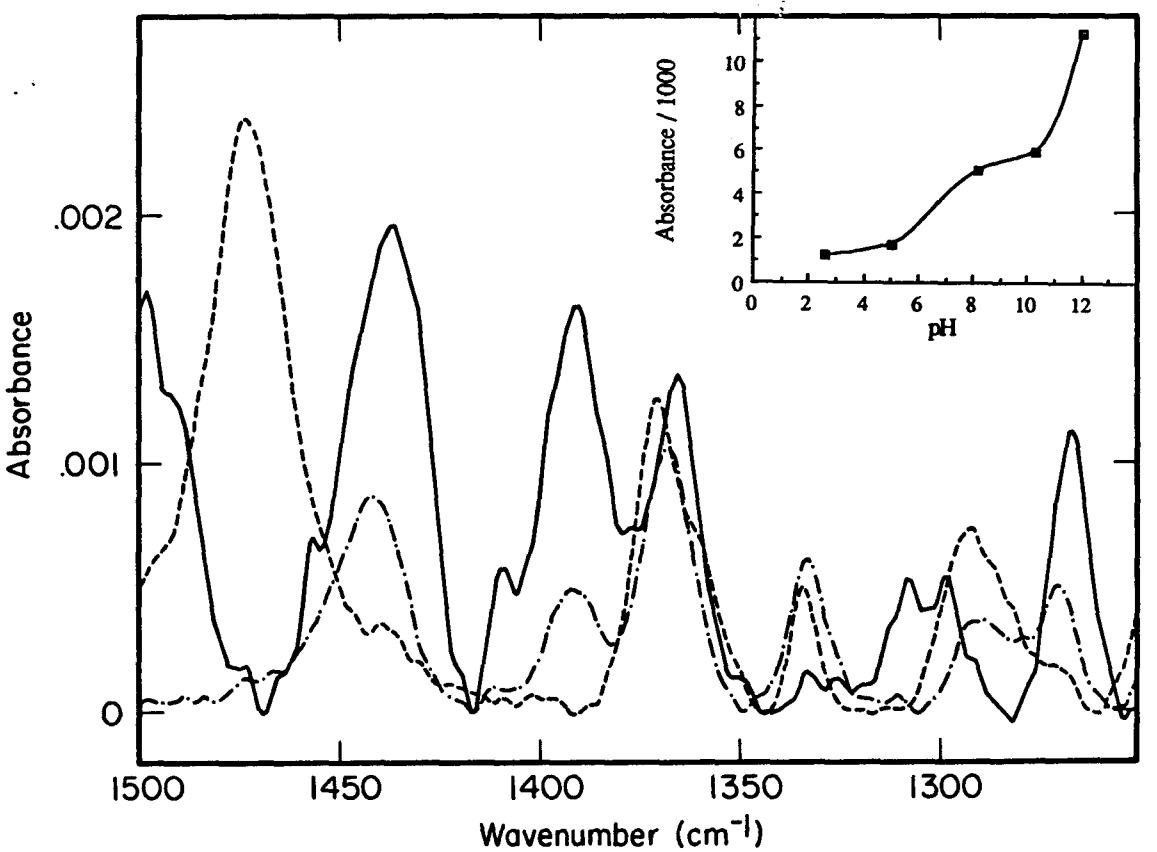

Figure 5. Infrared internal reflection spectra of calcichrome solution at (a) pH 5.1 (---), (b) pH 8.2 (-·-·-), (c) pH 12.0 (—). Inset: absorbance of δ'(NH) as a function of pH.

noise at pH 12. The absorbance decrease is caused by the loss of a proton from the diprotic form of calcichrome. Shifts in peak position are ascribed to the changes in conformation and hydrogen bonding that arise from the stepwise deprotonation process (vide infra). Decreases in the absorbance of the δ(O-H) of the hydroxy group at the 2 position reflect the transfer of the proton from the hydroxy group to an azo nitrogen as a result of the increased formation of the hydrazone form. The disappearance of δ(OH) for the naphtholic proton at the 8' position between a pH of 5 and 8 is consistent with the loss of a proton from the triprotic form of calcichrome.

Several of the bands shown in Figure 5 exhibit changes that arise from alterations in the relative amounts of the azo and hydrazone forms in each of the tautomeric equilibria. The increase in the absorbance of the N-H deformation mode (δ'(N-H)) at 1270 cm^{-1} with increasing pH, as shown in the inset of Figure 5, indicates a shift towards the hydrazone form of the indicator. The appearance and subsequent growth with increasing pH of the bands at ~1440 and 1390 cm^{-1}, which are assigned respectively to the asymmetric (ν_a(C=N-N)) and symmetric (ν_s(C=N-N)) stretching modes, further confirms the increasing presence of the hydrazone form of the indicator. The structural implications of the pH dependence of the band at 1475 cm^{-1} are as yet unclear.

The change from the azo to hydrazone form of calcichrome is induced by an alteration in the hybridization of the azo nitrogen at the 1' position from sp^2 to sp^3. This rehybridization leads to a nonplanar structural arrangement of the two naphthalene rings [36], an arrangement which is required for the formation of the Ca(II)-calcichrome complex. The conditional formation constant for the complex at pH 12.3 is 8.0 x 10^3 [21]. Evidence for the nonplanar structure of the metal complex is provided by the presence of δ'(N-H) in the infrared spectrum of the Ca(II)-calcichrome complex in Figure 6. The shifts of δ'(N-H), ν_a(C=N-N), and ν_s(C=N-N) toward lower energies are consistent with the donation of

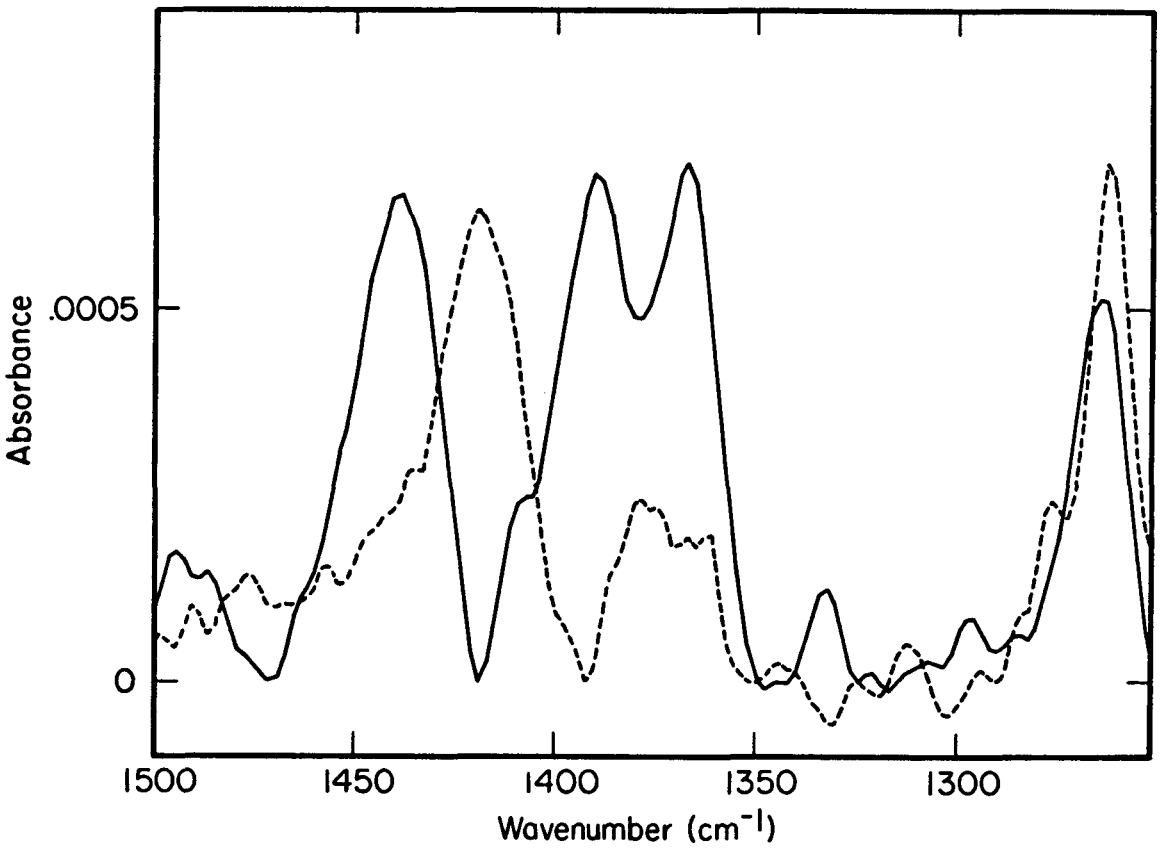

Figure 6. Infrared internal reflection spectra of solutions of (a) calcichrome (—) and (b) Ca(II)-calcichrome (---) at pH 12.0

electron density for the formation of the complex. From these data, I is proposed as the structure for the Ca(II)-calcichrome complex.

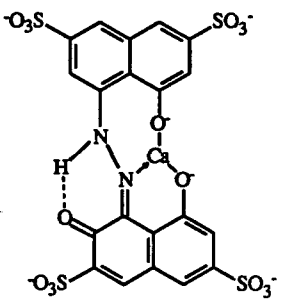

I

Reactivity of immobilized calcichrome

The reactivity of the immobilized form of calcichrome at the anion exchange film was determined by the approaches described in the Theory section. Plots of the relevant data for equations 19 and 24 gave K_f' for the Ca(II)-calcichrome complex of 32±8 at pH 12.3 and pK_a's of 5.3±0.3 and 10.7±0.3. In both complexation and acid-base dissociation, the immobilized and solution forms of the indicator are markedly different, with immobilized calcichrome acting as a stronger acid but weaker ligand than its solution analog. Such differences can arise from a variety of effects. For instance, the cation exchange polymer film known as Nafion acts as a strong acid with a strength that is comparable to CF_3SO_3H [37]. This leads to the complete protonation of bases such as p-nitroaniline (pKa = 1.0) upon their incorporation into the Nafion matrix. By analogy, an anion exchange polymer based on quaternary amines will behave as a strong base, promoting the acid dissociation of an immobilized reagent as observed for calcichrome. The lower pK_a values of immobilized calcichrome suggest that the complexation process may be facilitated at a lower pH in the anion exchange film.

Another factor that may influence the reactivity of the immobilized indicator is the hydrophobic/hydrophilic nature of the polymeric support. Hydrophobic environments have been shown to favor hydroxyl forms of tautomeric equilibria for azo structures comparable to calcichrome, whereas hydrophilic environments favor keto forms [36]. For example, upon incorporation into the hydrophobic cavity of α- and β-cyclodextrins from aqueous solutions, the tautomeric equilibrium of 4-phenylazo-1-naphthol (as the 4-phenyl sulfonic acid) shifts from the less acidic hydrazone form to the more acidic azo form [38]. This change results in a structure with lower polarity, and is induced by the nonpolar microenvironment of the cyclodextrin cavity. In contrast, hydrophilic environments, such as that of a quaternized polymer film, favor the more polar, less acidic hydrazone form of the tautomeric equilibrium. The presence of the hydrazone form of calcichrome in the anion exchange resin is supported by the three infrared photoacoustic spectra (IR-PAS) shown in Figure 7. Figures 7a and 7b are IR-PAS for the calcichrome-modified anion exchange membrane, and the unmodified anion exchange membrane, respectively. Figure 7c is the difference spectrum for the subtraction of Figure 7b from Figure 7a. The presence of the hydrazone form of calcichrome is indicated by δ'(N-H) at 1269 cm^{-1}, δ(N-H) at 1567 cm^{-1} and ν(C=O) at 1645 cm^{-1}. Additionally, a transmission spectrum of a thin-sectioned dry film in the visible region exhibited an absorbance maximum at 593 nm, indicating nearly full conversion of the immobilized calcichrome to its hydrazone form. Hence, immobilized calcichrome has the same hydrazone form as its Ca(II) complex. These interactions between calcichrome and the anion exchange resin appear to favor the formation of the Ca(II)-calcichrome complex.

The above discussion, although providing a qualitative explanation for the apparent increase in the acid strength of the immobilized form of calcichrome, fails to account for the low K_f' for the sensor. However, an examination of the mode of attachment between the indicator and support provides a plausible explanation. Calcichrome contains four sulfonic

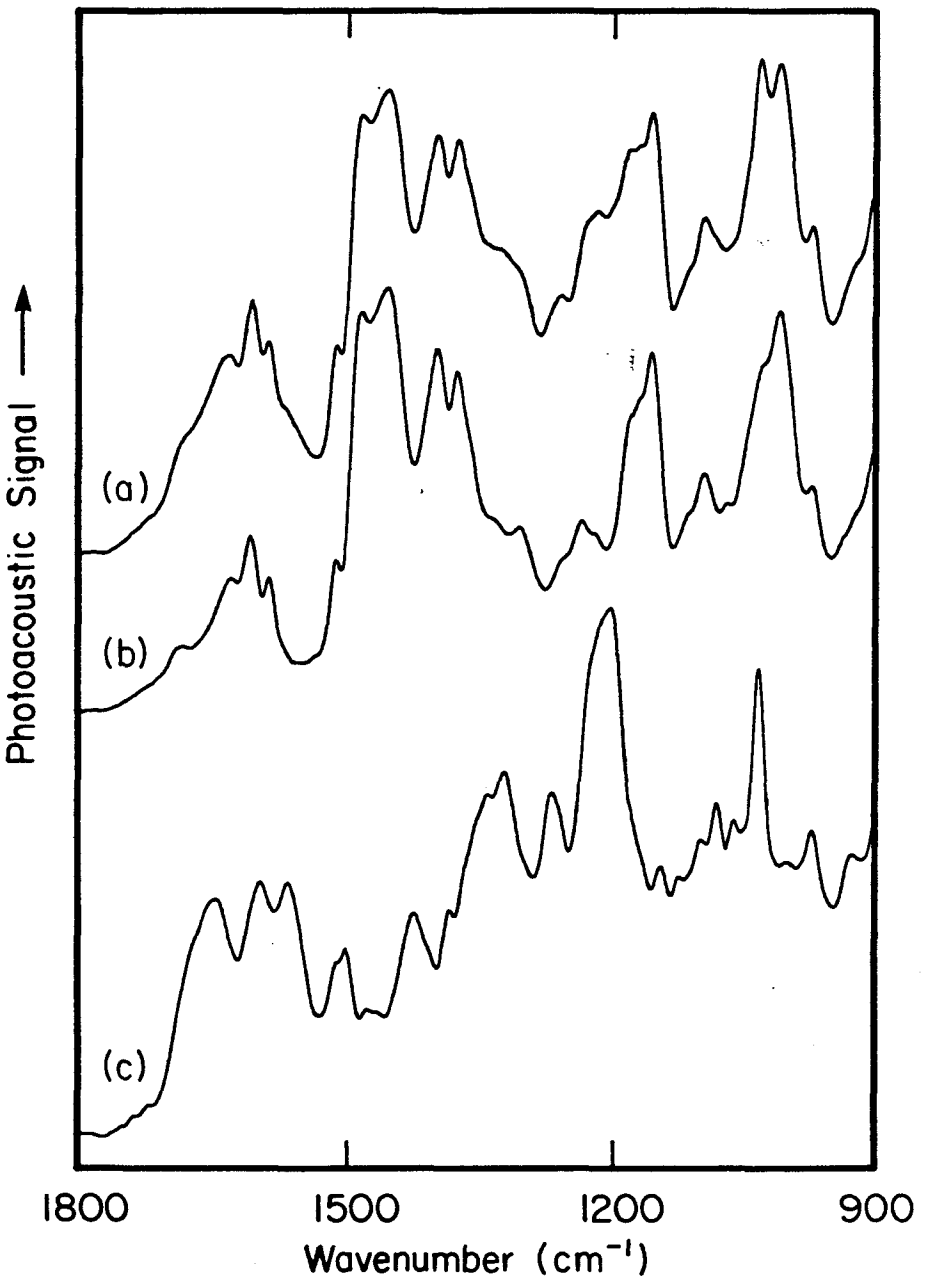

Figure 7. Infrared photoacoustic spectra of (a) calcichrome modified anion exchange membrane, (b) unmodified anion exchange membrane, (c) immobilized calcichrome at the anion exchange membrane. The y-axis for part c is 3 times that of parts a and b.

acid groups, each of which are capable of binding electrostatically with a cationic site of the polymeric support. Since immobilized calcichrome molecules may exist in different conformations in the matrix, rotation about the C-N axis may be necessary to achieve a conformation that is favorable for complex formation. Hence, tethering by more than one linkage would markedly hinder complexation. By the same reasoning, metallochromic reagents which are tethered through a single linkage may more readily undergo the structural rearrangements required for complexation, exhibiting more comparable reactivities of the solution and immobilized forms. More comparable reactivities have been observed for the binding of Mg(II) and Zn(II) by the solution and immobilized forms of quinolin-8-ol-5-sulfonate [24], a ligand which is naturally fixed in a configuration favorable for complex formation.

CONCLUSIONS

The construction of an optical sensor with a variety of attractive performance characteristics for the determination of Ca(II) has been demonstrated. Both the sensitivity and rapid response suggest several interesting applications (e.g., clinical assays, compliance environmental monitoring and control of industrial processing). However, most of these situations will require that the composition of the analyte solution be altered to a more basic pH. One approach for accomplishing a change in pH would be to couple the sensor with instrumentation for flow injection analysis (FIA). With FIA, the pH of the analyte can be readily manipulated by premixing the analyte solution with a small volume of a buffer solution. Premixing of analyte with FIA has been successfully employed in the development of instrumentation for pH measurement in solutions with low ionic strengths [39]. These and other opportunities are presently under investigation and should offer a facile means to adjust the pH to the level needed for the functioning of the calcichrome-based Ca(II) optical sensor.

This study also points to the need to consider the influence of immobilization on the reactivity of an indicator. Both the apparent acid-base and chelation strengths for an indicator can be markedly altered by immobilization [12]. The apparent acid-base reactivity for calcichrome is affected by the basic nature of the anion exchange film, whereas immobilization appears to hinder the structural rearrangement necessary for chelation. The latter suggests the possible use of a calcichrome analog with fewer sulfonic acid moieties as an approach for enhancing the reactivity and hence, sensitivity of the sensor. The flexibility to tune the reactivity of immobilized calcichrome by using a calcichrome analog with fewer sulfonic acid moieties and/or adjusting the number of cationic sites in the polymeric matrix may enable the design of a sensor to suit the needs of a specific application. Efforts to develop further insights into the fundamental interactions that govern reactivity of such sensors are currently underway.

REFERENCES

1. Durst, R. A.; Blubaugh, E. A. In Fundamentals and Applications of Chemical Sensors; Schuetzle, D., Hammerle, R., Butler, J. W., Eds.; ACS Symposium Series 309; American Chemical Society: Washington, DC, 1986; Chapter 14.
2. Seitz, W. R. CRC Crit. Rev. Anal. Chem. **1988**, 19, 135-173.
3. Janata, J.; Bezegh, A. Anal. Chem. **1988**, 60, 62R-74R.
4. Johnson, D. C.; Ryan, M. D.; Wilson, G. S. Anal. Chem. **1988**, 60, 147R-162R.
5. Lau, A.; Miller, L.J. Am. Chem. Soc. **1983**, 105, 5271.
6. Lundrum, H. L.; Salmon, R. T.; Haukridge, F. M. J. Am. Chem. Soc. **1977**, 99, 3154-3158.
7. Degani, Y.; Heller, A. J. Am. Chem. Soc. **1989**, 111, 2357-58.
8. Guadalupe, A.; Abruna, H. Anal. Chem. **1985**, 57, 142.
9. Baldwin, R. P.; Christensen, J. K.; Kryger, L. Anal. Chem. **1986**, 58, 1790-1798.
10. Sittampalam, G.; Wilson, G. S. Anal. Chem. **1983**, 55, 1608-1610.
11. Wang, J.; Hutchins, L. D. Anal. Chem. **1985**, 57, 1536-1541.
12. Stole, S. M.; Jones, T. P.; Chau, L. K.; Porter, M. D. In Chemical Sensors and Microinstrumentation; Murray, R. W., Dessy, R. E., Heineman, W. R., Janata, J., Seitz, W. R., Eds.; ACS Symposium Series 403; American Chemical Society: Washington, DC., 1989, Chapter 19.
13. Saari, L. A.; Seitz, W. R. Anal. Chem. **1982**, 54, 823-824.
14. Munkholm, C.; Walt, D. R.; Milanovich, F. P.; Miller, S. M. Anal. Chem. **1986**, 58, 1427-1430.
15. Kawabata, Y.; Tsuchida, K.; Ishibashi, N. Anal. Sci. **1987**, 3, 7-9.
16. Peterson, J. I.; Goldstein, S. R.; Fitzgerald, R. V.; Buckhold, D. K. Anal. Chem. **1980**, 52, 864-869.

17. Zhujun, Z.; Seitz, W. R. Anal. Chim. Acta **1984**, 100, 47-55.

18. Jones, T. P.; Porter, M. D. Anal. Chem. **1988**, 60, 404.

19. Wendlandt, W. W.; Hecht, H. G. Reflectance Spectroscopy; Interscience: New York, 1966; Chapter III.

20. Guthrie, A. J.; Narayanaswamy, R.; Russell, D. A. Analyst **1988**, 113, 457-461.

21. Chau, L. K.; Pruski, M.; Porter, M. D. Anal. Chim. Acta **1989**, 217, 31.

22. Skogerboe, K. J.; Yeung, E. S. Anal. Chem. **1987**, 59, 1812-1815.

23. Coleman, J. T.; Eastham, J. F.; Sepaniak, M. J. Anal. Chem. **1984**, 56, 2246-2249.

24. Saari, L. A.; Seitz, W. R. Anal. Chem. **1983**, 55, 667-670.

25. Saari, L. A.; Seitz, W. R. Analyst, **1984**, 109, 655-657.

26. Zhujun, Z.; Weitz, W. R. Anal. Chim. Acta **1985**, 171, 251-258.

27. Zhujun, Z.; Mullin, J. L.; Seitz, W. R. Anal. Chim. Acta **1986**, 184, 251-258.

28. Alder, J. F.; Ashworth, D. C.; Narayanswamy, R.; Moss, R. E.; Sutherland, I. O. Analyst, **1987**, 112, 1191-1192.

29. Carroll, M. K.; Bright, F. V.; Hieftje, G. M. Anal. Chem. **1989**, 61, 1768-1772.

30. Ashworth, D. C.; Huang, H. P.; Narayanaswamy, R. Anal. Chim. Acta **1988**, 213, 251-257.

31. Suzuki, K.; Tohda, K.; Tanda, Y.; Ohzora, H.; Nishihama, S.; Inoue, H.; Shirai, T. Anal. Chem. **1989**, 61, 382-384.

32. Close, R. A. ; West, T. S. Talanta **1960**, 5, 221-230.

33. Socrates, G. Infrared Characteristic Group Frequencies; Wiley: New York, 1980.

34. Nolting, F.; Zetzsch, C. Spectrochimica Acta **1988**, 44A, 845-848.

35. Jones, T. P; Porter M. D. Appl. Spectrosc. **1989**, 43, 908-911.

36. Zollinger, H. Color Chemistry: Syntheses, Properties and Applications of Organic Dyes and Pigments; VCH: Weinheim, 1987; Chapter 7.

37. Sondheimer, S. J.; Bunce, N. J.; Lemke, M. E.; Fyfe, C. A. Macromolecules 1986, 19, 339-343.

38. Ball, P.; Nicholis, C. H. Dyes and Pigments, 1982, 3, 5-26.

39. Woods, B. A.; Ruzicka, J.; Christian, G. D.; Charlson, R. J. Anal. Chem. 1986, 58, 2496-2502.

SUMMARY, DISCUSSION, AND PROSPECTUS

Probing the characteristics of the molecular structure of monomolecular and thin polymer films will produce technological and scientific benefits. Such a picture forms the basis for molecular engineering, not just of the chemical structure of the individual molecules but also of the collective properties of an ensemble of molecules. An understanding of the microscopic interfacial interactions will be important to the design of an ideal molecular arrangement, containing the requisite distribution of functional groups. As an example, for best water resistant, the adhesive or coating should have only enough functional groups to occupy all available surface sites. Additional polar groups increase water permeability and swelling and can therefore decrease resistance to water displacement [75]. Therefore, the required concentration of polar groups in a thin polymer film to achieve optimum bonding to metal oxide surfaces is a subject of interest. Further, reactivity of a sensing molecule in a thin polymer film may be markedly altered by immobilization [76]. All of these issues require an understanding of the intermolecular forces to enhance the design of these materials.

Some important aspects of the structure of these organized molecular films on hydrophilic solid surfaces include: (1) Trans/gauche isomerization in the carbon tail; (2) in-plane order; (3) tilt ordering; and (4) substrate effects [77]. Wide application of molecular films to science and technology, however, has been hindered by a number of problems and a certain lack of understanding of some of the key fundamental processes. Some of these more important obstacles include: (1) Characterization methods need to be developed further, and existing surface analytical techniques need to be refined and tested on organic films; (2) integrity and stability of films must be improved to overcome some of the problems related to their soft and almost fluidlike behavior; (3) deleterious impurities and defects must be identified and removed. Therefore, newer and better methods for their characterization to

enhance the understanding of the intermolecular forces, involving mechanical, electronic, chemical, and biological processes, will be the key to progress.

Wetting phenomena are complex and their interpretation is to some extent still controversial. Wettability plays a major role in a number of technological, environmental and biological phenomena. In addition, contact angle measurements provide a convenient probe of the structure of the interface. The utility of this method is based on its high sensitivity to local surface structure and on its ability to detect certain types of reactions, such as those involving ionization of functional groups. An important motivation underlying these studies is to answer one of the fundamental questions of molecular-level structure of matter and its macroscopic physical properties. Monomolecular and thin polymer films provide models for relating molecular-level structure of surfaces and thier wetting properties. These models can be further delineated by the calculation of intermolecular forces at these macroscopic interfaces and would eventually lead to better understanding of wetting phenomena.

LITERATURE CITED

1. Williams, D. J. Angew. Chem. Int. Ed. Engl. **1984**, 23, 690-703.
2. Swalen, J. D. Thin Solid Films **1988**, 160, 197-208.
3. Seitz, W. R. CRC Crit. Rev. Anal. Chem. **1988**, 19, 135-173.
4. Arnold, M. A.; Meyerhoff, M. E. CRC Crit. Rev. Anal. Chem. **1988**, 20, 149-196.
5. Moriizumi, T. Thin Solid Films **1988**, 160, 413-429.
6. Kawabata, Y.; Tsuchida, K.; Imasaka, T.; Ishibashi, N. Anal. Sci. **1987**, 3, 7-9.
7. Durst, R. A.; Blubaugh, E. A. in Fundamentals and Applications of Chemical Sensors; Schuetzle, D., Hammerle, R., Eds.; American Chemical Society: Washington, DC, 1986; Chapter 14.
8. Sugawara, M.; Kojima, K.; Sazawa, H.; Umezawa, Y. Anal. Chem. **1987**, 59, 2842-2846.
9. Bezegh, K.; Bezegh, A.; Janata, J.; Oesch, U.; Xu, A.; Simon, W. Anal. Chem. **1987**, 59, 2846-2848.
10. McCallum, J. J. Analyst **1989**, 114, 1173-1189.
11. Ballantine, D. S., Jr.; Wohltjen, H. Anal. Chem. **1989**, 61, 704A-715A.
12. Lupinski, J. H.; Moore, R. S. in Polymeric Materials for Electronics Packaging and Interconnection; Lupinski, J. H., Moore, R. S., Eds.; ACS Symposium Series 407; American Chemical Society: Washington, DC, 1989; Chapter 1.
13. Seibold, R. W.; Lamoureux, R. T.; Goodman, S. H. in Electronic Packaging Materials Science III; MRS Symposium Proceedings Vol. 108; Materials Research Society: Pittsburgh, 1988; pp 141-152.
14. Vincett, P. S.; Roberts, G. G. Thin Solid Films **1980**, 68, 135-171.
15. Reichmanis, E.; Thompson. L. F. Chem. Rev. **1989**, 89, 1273-1289.
16. Wrobel, J. J. Solid State Technology **1989**, June, 103-105.

17. Whitesides, G. M.; Laibinis, P. E. Langmuir **1990**, 6, 87-96.

18. Murray, R. W. In Electroanalytical Chemistry; Bard, A. J., Ed.; Marcel Dekker: New York, 1984; Vol. 13.

19. Ringsdroff, H.; Schlarb, B.; Vengmer, J. Angew. Chem. Int. Ed. Engl. **1988**, 27, 113-158.

20. Stewart, K. R.; Whitesides, G. M.; Godfried, H. P.; Silvera, I. F. Rev. Sci. Instrum. **1986**, 57, 1381-1383.

21. Wasserman, S. R.; Whitesides, G. M. J. Mater. Res. **1989**, 4, 886-892.

22. Zisman, W. A. In Friction and Wear; Davies, R., Ed.; Elsevier: New York, 1959.

23. Novontny, V.; Swalen, J. D.; Rabe, J. P. Langmuir **1989**, 5, 485-489.

24. Notoga, T.; Poling, G. W. Corrosion **1979**, 35, 193-200.

25. Gaines, G. L. Insoluble Monolayers at Liquid-Gas Interfaces; Interscience: New York, 1966.

26. Bigelow, W. C.; Pickett, D. L.; Zisman, W. A. J. Colloid Sci. **1946**, 1, 513-538.

27. Chollet, P.-A. Thin Solid Films **1978**, 52, 343-360.

28. Haller, I. J. Am. Chem. Soc. **1978**, 100, 8050-8055.

29. Sagiv, J. J. Am. Chem. Soc. **1980**, 102, 92-98.

30. Wasserman, S. R.; Tao, Y. T.; Whitesides, G. M. Langmuir **1989**, 5, 1074-1087.

31. Wasserman, S. R.; Whitesides, G. M.; Tidswell, I. M.; Ocko, B. M.; Pershan, P. S.; Axe, J. D. J. Am. Chem. Soc. **1989**, 111, 5852-5861.

32. Tillman, N.; Ulman, A.; Penner, T. L. Langmuir **1989**, 5, 101-111.

33. Duvault, Y.; Gagnaire, A.; Gardies, F.; Jaffrezic-Renault, N.; Martelet, C.; Morel, D.; Serpinet, J.; Duvault, J.-L. Thin Solid Films **1990**, 185, 169-179.

34. Gun, J.; Iscovici, R.; Sagiv, J. J. Colloid Interface Sci. **1984**, 101, 201-213.

35. Allara, D. L.; Nuzzo, R. G. Langmuir **1985**, 1, 45-52.

36. Allara, D. L.; Nuzzo, R. G. Langmuir **1985**, 1, 52-66.

37. Schlotter, N. E.; Porter, M. D.; Bright, T. B.; Allara, D. L. Chem. Phys. Lett. **1986**, 132, 93-98.

38. Chau, L. K.; Porter, M. D. Chem. Phys. Lett. **1990**, 167, 198-204.

39. Allara, D. L.; Nuzzo, R. G. J. Am. Chem. Soc. **1983**, 105, 4481-4483.

40. Nuzzo, R. G.; Zegarski, B. R.; Dubois, L. H. J. Am. Chem. Soc. **1987**, 109, 733-740.

41. Nuzzo, R. G.; Fusco, F. A.; Allara, D. L. J. Am. Chem. Soc. **1987**, 109, 2358-2368.

42. Porter, M. D.; Bright, T. B.; Allara, D. L.; Chidsey, C. E. D. J. Am. Chem. Soc. **1987**, 109, 3559-3568.

43. Nuzzo, R. G.; Dubois, L. H.; Allara, D. L. J. Am. Chem. Soc. **1990**, 112, 558-569.

44. Troughton, E. B.; Bain, C. D.; Whitesides, G. M.; Nuzzo, R. G.; Allara, D. L.; Porter, M. D. Langmuir **1988**, 4, 365-385.

45. Strong, L.; Whitesides, G. M. Langmuir **1988**, 4, 546-558.

46. Bain, C. D.; Troughton, E. B.; Tao, Y. T.; Evall, J.; Whitesides, G. M.; Nuzzo, R. G. J. Am. Chem. Soc. **1989**, 111, 321-235.

47. Bain, C. D.; Evall, J.; Whitesides, G. M. J. Am. Chem. Soc. **1989**, 111, 7155-7164.

48. Bain, C. D.; Whitesides, G. M. J. Am. Chem. Soc. **1989**, 111, 7164-7175.

49. Bain, C. D.; Biebuyck, H. A.; Whitesides, G. M. Langmuir **1989**, 5, 723-727.

50. Diem, T.; Czajka, B.; Weber, B.; Regan, S. L. J. Am. Chem. Soc. **1986**, 108, 6094-6095.

51. Ulman, A.; Tillman, N. Langmuir **1989**, 5, 1418-1420.

52. Chidsey, C. E. D.; Loiacono, D. N. Langmuir **1990**, 6, 682-691.

53. Chidsey, C. E. D.; Bertozzi, C. R.; Putvinski, T. M.; Mujsce, A. M.

J. Am. Chem. Soc. **1990**, 112, 4301-4306.

54. Sandroff, C. J.; Garoff, S.; Leung, K. P. Chem. Phys. Lett. **1983**, 96, 547-551.
55. Joo, T. H.; Kim, K.; Kim, M. S. J. Phys. Chem. **1986**, 90, 5816-5819.
56. Practical Surface Analysis by Auger and X-ray Photoelectron Spectroscopy; Briggs, D., Seah, M. D., Eds.; John Wiley & Sons: New York, 1983.
57. Greenler, R. G. J. Chem. Phys. **1966**, 44, 310-315.
58. Greenler, R. G. J. Chem. Phys. **1969**, 50, 1963-1968.
59. Pons, S.; Davidson, T.; Bewick, A. J. Electroanal. Chem. **1984**, 160, 63-71.
60. Porter, M. D.; Bright, T. B.; Allara, D. L.; Kuwana, T. Anal. Chem. **1986**, 58, 2461-2465.
61. Udagawa, A.; Matsui, T.; Tanaka, S. Appl. Spectrosc. **1986**, 40, 794-797.
62. Dluhy, R. A. J. Phys. Chem. **1986**, 90, 1373-1379.
63. Archer, R. A. J. Opt. Soc. Am. **1962**, 52, 970-977.
64. Greenler, R. G.; Slager, T. L. Spectrochim. Acta **1973**, 29A, 193-201.
65. Campion, A. Ann. Rev. Phys. Chem. **1985**, 36, 549-572.
66. Benninghoven, A.; Rudenauer, F. G.; Werner, H. W. Secondary Ion Mass Spectrometry: Basic Concepts, Instrumental Aspects, Applications and Trends; Wiley: New York, 1987.
67. Fay, M. J.; Proctor, A.; Hoffmann. D. P.; Hercules, D. M. Anal. Chem. **1988**, 60, 1225A-1243A.
68. Heinz, F. T.; Reider, G. A. Trends Anal. Chem. **1989**, 8, 235-242.
69. Binnig, G.; Rohrer, H. Angew. Chem. Int. Ed. Engl. **1987**, 26, 606-614.
70. Binnig, G.; Quate, C. F.; Gerber, C. Phys. Rev. Lett. **1986**, 56, 930-933.
71. Holmes-Farley, S. R.; Reamey, R. H.; McCarthy, T. J.; Deutch, J.; Whitesides, G. M. Langmuir **1985**, 1, 725-740.

72. Bain, C. D.; Whitesides, G. M. J. Am. Chem. Soc. **1988**, 110, 5897-5898.

73. Cassie, A. B. D. Discuss Faraday Soc. **1948**, 3, 11-16.

74. Dettre, R. H.; Johnson, R. E., Jr. J. Phys. Chem. **1965**, 69, 1507-1515.

75. Bolger, J. C. In Adhesion Aspects of Polymeric Coatings; Mittal, K. L., Ed.; Plenum: New York, 1983.

76. Stole, S. M.; Jones, T. P.; Chau, L. K.; Porter, M. D. Chemical Sensors and Microinstrumentation; Murray, R. W., Dessy, R. E., Heineman, W. R., Janata, J., Seitz, W. R., Eds; ACS Symposium Series 403; American Chemical Society: Washington, DC, 1989; Chapter 19.

77. Garoff, S. Proc. Natl. Acad. Sci. USA **1987**, 84, 4729-4732.

ACKNOWLEDGMENTS

The author gratefully appreciates his advisor Dr. Marc D. Porter for guidance. Praises are expressed for the wonderful collaboration with Kristy M. Wolff and Dr. Marek Pruski. The acquisition of the Auger spectroscopy data by Dr. Albert J. Bevelo and infrared photoacoustic spectra by Dr. Roger W. Jones, silver content analysis by Royce K.Winge and Daniel Wiederin, and helpful discussions with Dr. Lorraine M. Siperko, Tsan-Chuen Leung, Dr. Tim-On Man, Man-Kit Leung, and Han-Wah Man are acknowledged. Thanks are expressed for the financial support provided by Ames Laboratory - USDOE, IBM Corporation, and a graduate research fellowship from Phillips Petroleum.

APPENDIX. CALCICHROME: A RE-EXAMINATION OF ITS STRUCTURE AND CHEMICAL PROPERTIES BY SOLID- AND LIQUID-STATE NMR, INFRARED SPECTROSCOPY, AND SELECTIVE CHEMICAL DEGRADATION

Calcichrome: A Re-Examination of Its Structure and Chemical Properties by Solid and Liquid State NMR, Infrared Spectroscopy, and Selective Chemical Degradation

Lai-Kwan Chau, Marek Pruski,

and Marc D. Porter

Ames Laboratory - USDOE and Department of Chemistry

Iowa State University

Ames, Iowa 50011

ABSTRACT

Nuclear magnetic resonance and infrared spectroscopies have been used to unravel the controversies regarding the structures of calcichrome and calcion. Together with the identification of the products from selective chemical cleavage reactions, these data indicate that structures of both compounds are equivalent with a molecular formula of $C_{20}H_{14}N_2O_{15}S_4.3H_2O$ (2,8,8'-trihydroxy-1,1'-azonaphthelene-3,6,3',6'-tetrasulfonic acid). The compound has two titratable phenolic protons in aqueous solution with pK_a values of 7.19±0.05 and 11.63±0.05 at 25°C. As a ligand, the compound forms a colored complex with Ca(II) at a 1:1 stoichiometric ratio (pH 12.3) with a formation constant of 8.0×10^3 at 25°C. The free form of the ligand at pH 12.3 has an absorption maximum of 1.44×10^4 L mol^{-1} cm^{-1} at 599 nm, whereas the complexed form has a maximun molar absorptivity of 1.37×10^4 L mol^{-1} cm^{-1} at 522 nm.

INTRODUCTION

The construction and performance characteristics of an optical sensor for the selective determination of Ca(II) were recently studied in this laboratory. The sensor was fabricated by the electrostatic immobilization of the metallochromic indicator calcichrome at an anion exchange polymer film. During an assessment of the general applicability of this approach for sensor construction, it was found that calcichrome was one of the few solution phase indicators which maintained its chelating capability after immobilization. Attempts to probe the fundamental details regarding these differences in reactivity were hindered, in part, by the extensive controversy regarding the structure of calcichrome. The present work represents a re-examination and clarification of the structure and solution properties of this chelate.

The synthesis of calcichrome, which is formed by the self-coupling of diazotised 1-amino-8-hydroxy-naphthalene-3,6-disulphonic acid (H-acid), was first reported in a German patent in 1896 [1]. Subsequently, the ligand was used as a spectrophotometric reagent for the determination of calcium [2-5] and numerous other metal ions [6-9]. Close and West [3] named the compound calcichrome and postulated the cyclic tris-azo structure shown by **I**. Lukin et al. [10] dismissed structure **I** and postulated a bis-azo structure **II**, which is commonly referred to as calcion. Although neither structure was supported by definitive analytical evidence, **II** has since found general acceptance in the literature.

Mendes-Bezerra and Stephen [11], based on spectrophotometric, chromatographic, polarographic, and microanalytical evidence, concluded that the structures of calcion and calcichrome were identical. Stead [12], from ^{1}H-NMR, elemental analyses, and synthetic derivatizations, concluded that the structure of the compound was neither **I** nor **II**, but was the mono-azo structure shown by **III**. Nevertheless, Einaga and Ishii [9], based on potentiometric titrations and elemental analyses, supported the structure proposed by Close

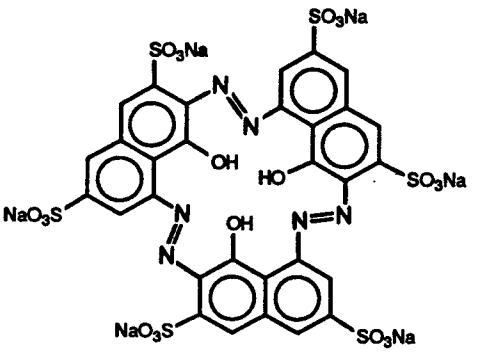

(I)

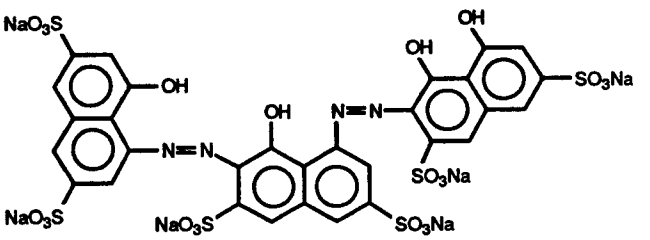

(II)

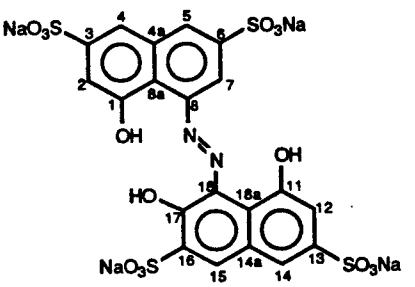

(III)

and West [3]. Clearly, several discrepancies exist concerning the structure of the product of this self-coupling reaction.

In this article, the results of a multi-faceted effort to resolve the ambiguities concerning the composition, structure, and chemical properties of calcichrome and calcion are reported. Evidence from nuclear magnetic resonance (^{1}H and ^{13}C) and infrared spectroscopies indicate that the structures of calcichrome and calcion are identical. (Hereafter, the product of this self-coupling reaction is referred to as calcichrome unless specified otherwise.) This conclusion was substantiated by a structural identification of the products of selective chemical cleavage reactions. The molecular spectroscopic characterizations further point to an enolic form of **III** as the structure of the ligand. Characterization of the solution reactivity of calcichrome indicates that this metallochromic indicator has two titratable phenolic protons in aqueous solution (pK_a values of 7.19±0.05 and 11.63±0.05) and forms a 1:1 stoichiometric complex with Ca(II) with a formation constant of 8.0×10^3 at 25°C.

EXPERIMENTAL

Chemicals

Calcichrome (Pfaltz and Bauer) was used without further purification. Calcion (Sigma Chemical Co.) was further purified by adsorption chromatography on a silica gel column (length 45 cm, inner diameter 2.5 cm); an ethanol/aqueous 2M ammonia solution (9:1) was employed as the eluent. Eluates were evaporated and dried under vacuum. Each reagent exhibited a single spot when tested by thin-layer chromatography at silica gel with a variety of different mobile phases. All aqueous solutions were prepared with distilled, deionized water.

Instrumentation

The ^{1}H-NMR spectra of calcichrome and its cleavage products were obtained in DMSO-d_6 or D_2O with a Nicolet 300 MHz spectrometer. The low solubility of the ligand prohibited ^{13}C-NMR characterization in solution.

A home-built 100 MHz spectrometer was used to obtain high-resolution ^{13}C-NMR spectra of solid calcichrome [13]. A Varian XL-100-15 magnet, which was equipped with a double-tuned single-coil probe, was operated at 25.15 MHz and 100.06 MHz for ^{13}C and ^{1}H, respectively. Samples (~200 mg) were spun at ~4.5 KHz in a windmill-type Kel-F rotor. The rotor was equipped with a 12-psi air drive and a 40-psi air bearing. The ^{13}C NMR spectra were obtained by cross-polarization (CP) with strong proton decoupling and magic angle spinning (MAS). The radiofrequency field strengths were 50 kHz for both CP and proton decoupling. Typically, 10000 scans were co-added with 2000 data points in each of the two channels of a quadrature detector. A 16K Fourier transformation of the free induction decay signal was performed on a Vax computer with zero- and first-order phase corrections.

Absolute intensities of the proton signal were measured to estimate the concentration and mobility of water molecules. This experiment was performed with a home-built 56-MHz spectrometer [14]. To minimize the artifacts after pulse excitation, the following alternating sequence was used to monitor the transverse decay of magnetization along y in the rotating frame. First, a 90°x pulse was applied, which was followed by data collection. After $5t_1$, a 180°y, τ, 90°x sequence was used, where $t_2 < t << t_1$. The signal following the second 90°x pulse was phase corrected by multiplying by -1 prior to its addition to memory. The deadtime of the probe-receiver system was 4 μs. The data were accumulated with a dual time base; the first 1000 channels operated with a 0.2-μs dwell time, whereas that of the second 1048 channels was 20 μs. Acquisition of data in this manner allowed both the short (t_2 ~20 μs) and long (t_2 ~1 ms) decays to be monitored with a negligible loss of information for either component.

A Varian DMS 200 UV-Visible spectrophotometer was used to characterize the composition and to determine the formation constant of the Ca(II) complex. A Model 130 Corning glass-electrode pH meter was used for pH measurements. Infrared spectra were obtained with a Nicolet 740 FT-IR spectrometer with the sample dispersed in a KBr matrix.

RESULTS AND DISCUSSION

Spectral studies

^{1}H-NMR. The ^{1}H-NMR spectrum of calcichrome in DMSO-d_6 is shown in Figure 1. The position and integration of the peaks between 7.1 and 8.3 ppm indicate that these features represent a total of seven aromatic protons. Three additional singlets are present downfield at 11.8, 12.0, and 17.1 ppm; integration indicates that each singlet corresponds to a single phenolic proton. These latter protons are labile, as verified by their absence in D_2O, and experience intramolecular hydrogen bonding. The position of the singlet at 17.1 ppm suggests that this phenolic proton is involved in extensive hydrogen bonding (vide infra). Examination of the three previously proposed structures clearly shows that these data fit only that expected for (III). Furthermore, the ^{1}H-NMR spectra of calcichrome and calcion are identical, confirming the structural equivalence of the two compounds.

^{13}C-NMR. Solid state ^{13}C NMR spectra of calcichrome are shown in Figures 2A-C. Figure 2A is a CP/MAS spectrum obtained with a 2-ms cross-polarization contact time. Because typical time constants for proton-carbon cross polarization in organic solids are less than 0.5 ms [15], Figure 2A represents a spectrum of the ^{13}C nuclei in the sample. Before any attempt to make peak assignments, two additional CP/MAS experiments were performed to discriminate between those features which originate from nonprotonated ^{13}C and those from protonated ^{13}C, respectively. The spectrum shown in Figure 2B was obtained with the ^{1}H-^{13}C heteronuclear dipolar-dephasing (DD) technique [16]. In this experiment, data acquisition was delayed for 100 μs after the proton contact time. During this delay, dipolar dephasing occurs due to the interruption of proton-carbon decoupling. Because the rate of ^{13}C magnetization decay depends on the strength of the heteronuclear dipolar interactions, this technique eliminates the ^{13}C signal from nuclei which exhibit strong proton coupling. Thus, only those resonances representing ^{13}C nuclei which are not bound

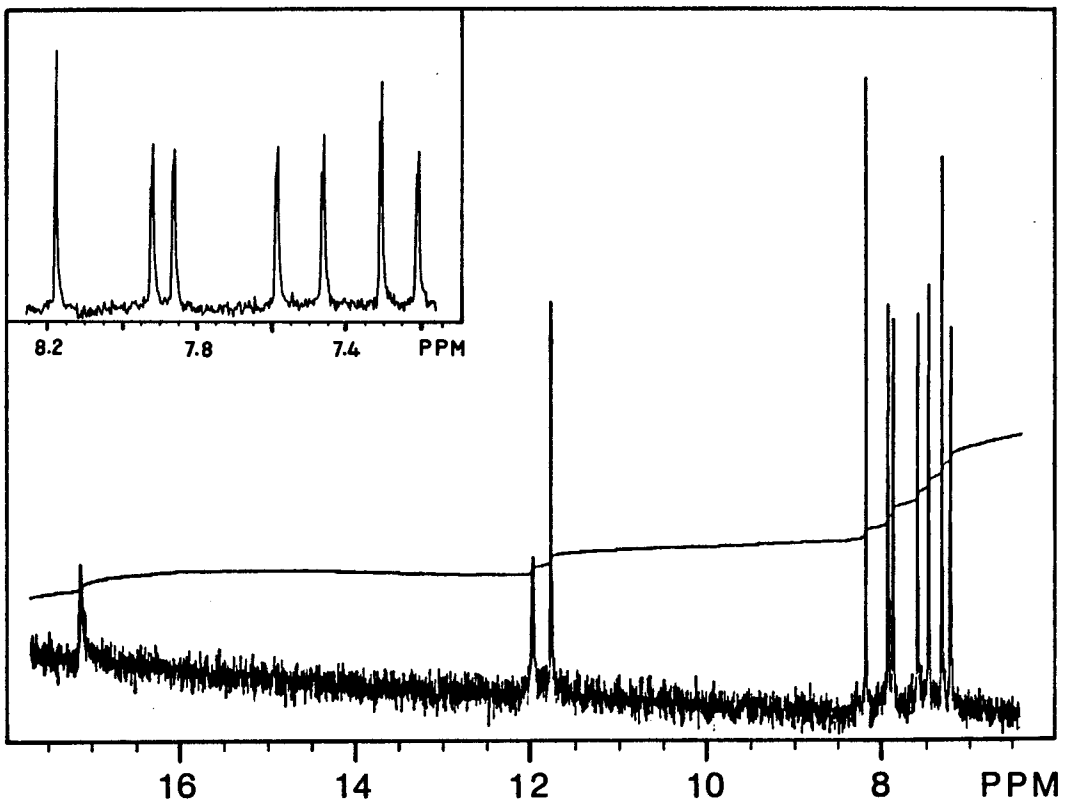

Figure 1. Spectra (^{1}H-NMR) of calcichrome in DMSO-d_6. Inset: Expansion of region between 7.1 and 8.3 ppm.

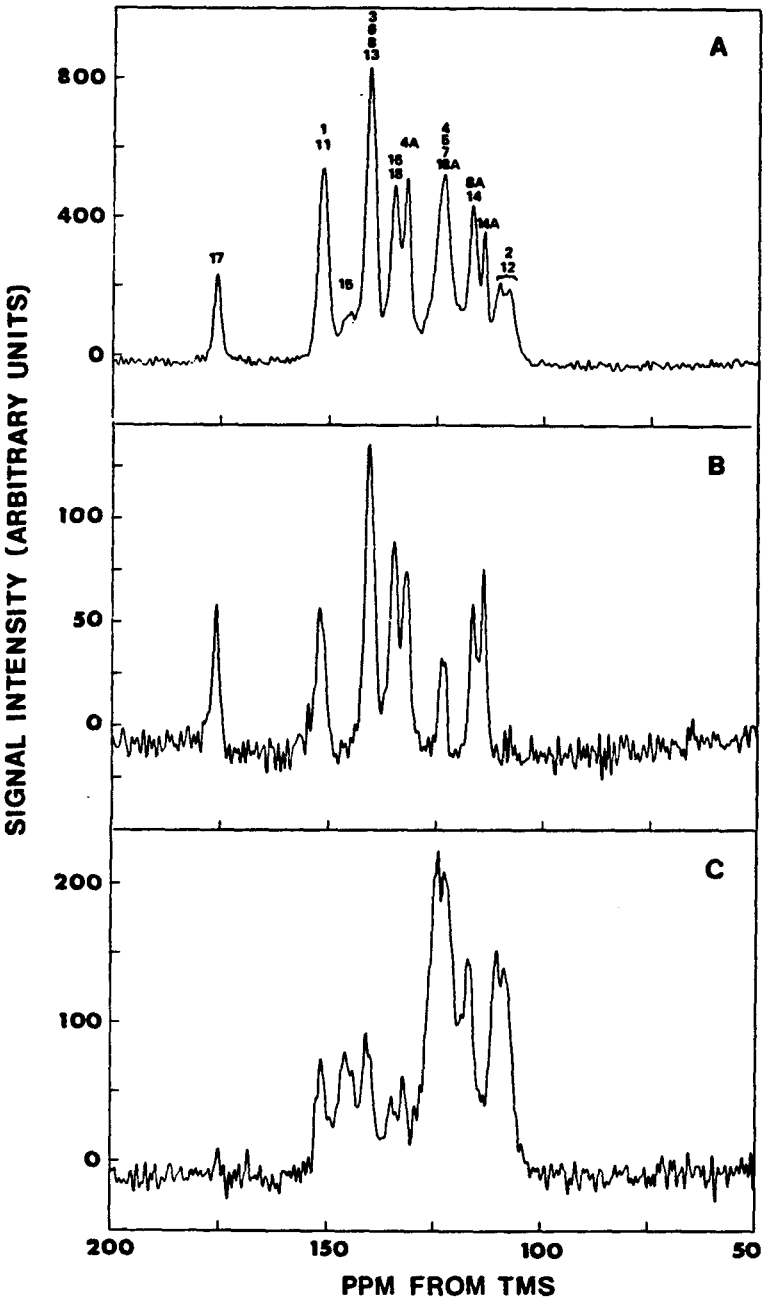

Figure 2. Spectra (CP/MAS ^{13}C NMR) of calcichrome: (A) spectrum recorded with a 2-ms contact time; (B) dipolar dephased spectrum with a dephasing delay of 60 μs; and (C) spectrum with a 50-μs contact time.

to ^{1}H are present in Figure 2B. In Figure 2C, the ^{13}C-NMR spectrum for a very short contact time (50 μs) is presented. Because the rate at which various carbons are polarized by protons varies dramatically with environment and molecular motion, ^{13}C signals for nuclei which are not bound directly to 1H are strongly suppressed. As such, Figure 2C represents a spectrum in which the signals for those ^{13}C nuclei which are bound directly to ^{1}H are preferentially enhanced. Thus, a comparison between these three spectra greatly facilitates peak assignments.

Peak assignments were made by comparing the observed spectra in Figure 2 with those calculated by two different additivity schemes [17-20]. In both cases, 1-hydroxynapthalene-3,6-disulphonic acid was chosen as the parent molecule for constructing the ^{13}C-NMR spectrum for each of the three proposed structures [18]. As judged from the relative peak intensities and the number of protonated and nonprotonated carbons, the simulation of structure **III** provided the most reasonable fit with the spectrum in Figure 2A. Furthermore, with the exception of the feature at 175 ppm, the simulated peak positions for structure **III** provided the best agreement with those observed. Peak assignments based on these arguments are labeled in Figure 2A and designated by the carbon numbering scheme for **III**.

The feature at 175 ppm, which is outside the normal value of isotropic chemical shifts for aromatic carbons, indicates the presence of a carbonyl carbon, where the proton resides in, perhaps, a bridged structure (vide infra).

Infrared spectroscopy. Infrared (IR) spectroscopy provides an alternative approach to probe the molecular structure of calcichrome. An IR spectrum for calcichrome, which was dispersed in KBr, between 1800 and 750 cm^{-1}, is shown in Figure 3. Several characteristic vibrational modes are readily apparent and are assigned in the Figure. The feature at 1635 cm^{-1} is representative of a quinone carbonyl stretch [21,22]. This latter

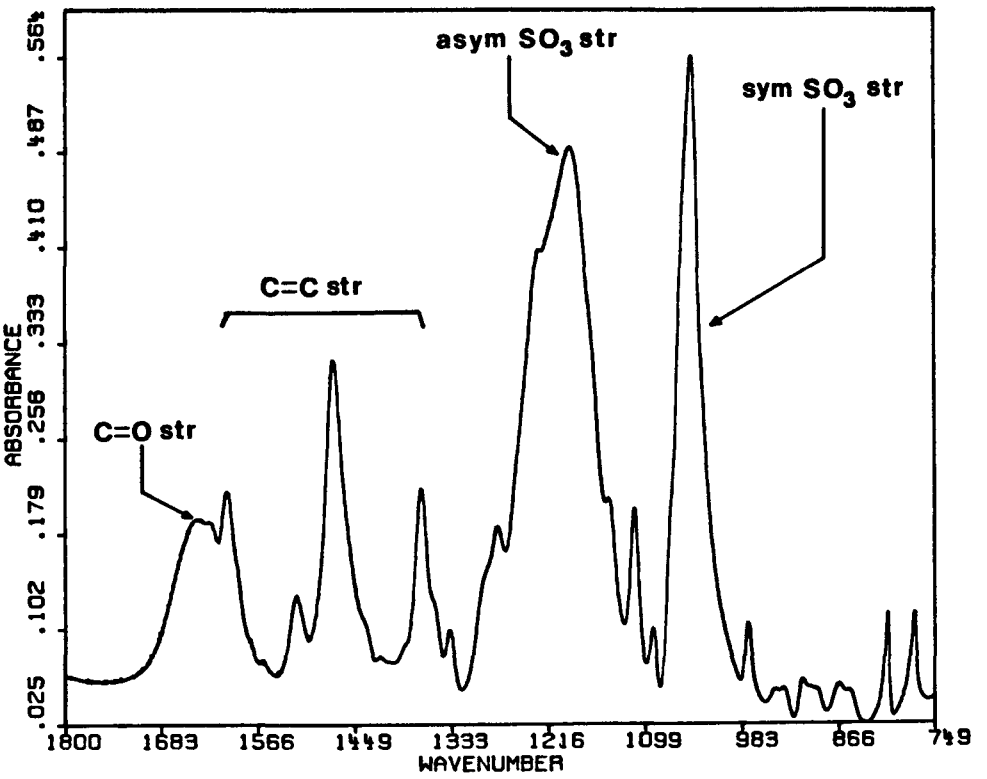

Figure 3. Infrared spectrum of calcichrome dispersed in a KBr matrix (4 cm^{-1} unapodized resolution)

feature, combined with earlier evidence from ^{1}H- and ^{13}C-NMR, suggests the following bridged structure for solid-phase calcichrome **IV**. As with the NMR data, a comparison of the IR spectrum of calcichrome with calcion supports the structural equivalence of these two compounds.

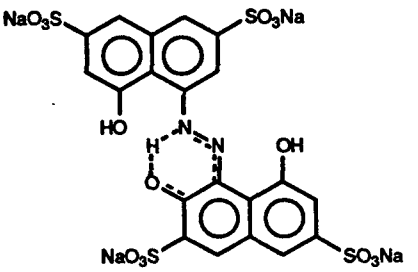

(IV)

Selective chemical cleavage reaction

To substantiate further the evidence from the previously described spectroscopic characterizations, selective chemical cleavage reaction was used as an additional route to aid the identification of the structure of the ligand. One of the well-known characteristics of an azo compound is the ease in which its -N=N- linkage can be reductively cleaved to yield products which both possess an amine functional group. Thus, the characterization of the structure of these products will provide further evidence regarding the molecular nature of calcichrome. The selective cleavage of the azo linkage was performed with tin(II) chloride as the reducing agent. The progression of the reaction was followed by color change. After reduction, separation via thin-layer chromatography indicated that the product consisted only of two major components. Unfortunately, both components slowly oxidized upon continued exposure to air, as was evident from a marked change in their optical properties. This is a well-known property of many phenols and aminophenols [23]. However, by protecting each component against air oxidation by adding tin(II) chloride to the eluent collection vials and by

conducting the separation in a short column (~5 cm), the degradation was effectively decreased. Because of the short column, the two products are not completely separated, which resulted in the observed differences in the relative intensities of two sets of ^{1}H-NMR bands. The spectrum consisted of four large peaks (all doublets) and three smaller peaks between 6.6 and 8.2 ppm (one singlet and two doublets). The more intense set of bands corresponds to four protons on the first eluent V; whereas the less intense set represents three protons on the second eluent VI. The peak splittings of the doublets (1.2-1.8 Hz) match that typically found for the meta coupling constants (J_{13}) of naphthyl protons [17,24]. These results support our conclusions regarding the structure of calcichrome as indicated by the following proposed reaction:

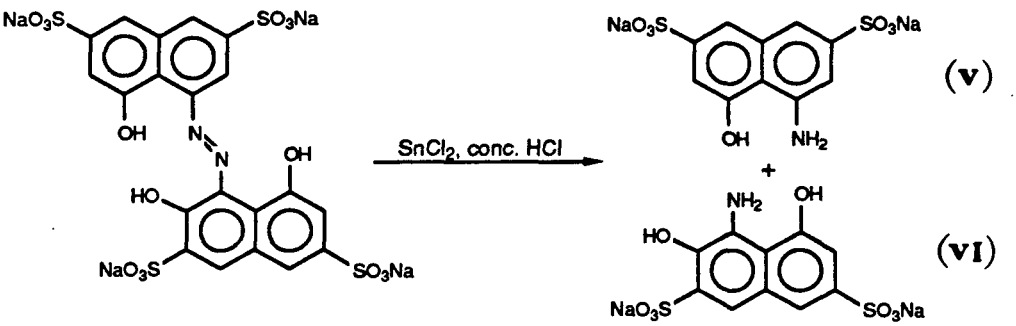

(1)

Water of crystallization

The water of crystallization for calcichrome was determined by measuring the free induction decay (FID) of the fixed and mobile protons with solid state ^{1}H-NMR. An on-resonance time decay after a single pulse excitation for this sample is shown in Figure 4. The details of the excitation and detection scheme have been described earlier. As is apparent, the FID curve indicates that there are two different relaxation processes. The first is characterized

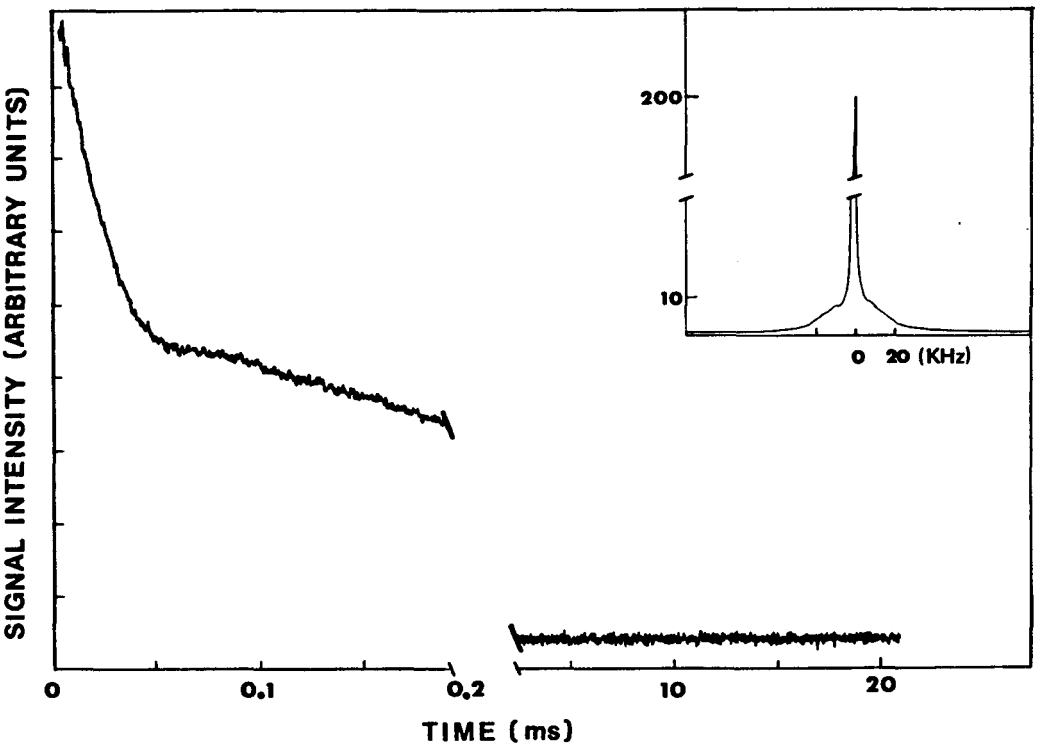

Figure 4. ^{1}H Free induction decay of calcichrome and the corresponding spectrum (inset)

by a relaxation time, t_2, of ~12μs and is due to the decay of the bound (rigid) protons. The second process, however, proceeds much more slowly (t_2 ~0.5 ms) and represents the relaxation of mobile protons in unbound water (moisture). The existence of two relaxation processes is further exemplified by the Fourier transformation of the FID response shown in the inset of Figure 4. The inset exhibits two lines: a broad feature with a full width at half height ($\Delta\nu_{1/2}$) of ~30 KHz and a narrow feature with a $\Delta\nu_{1/2}$ of ~600 Hz. The broad feature represents the decay of rigid protons, whereas the narrow feature is due to the decay of mobile protons.

To determine the number of crystalline water molecules per molecule of calcichrome, the following method was used. First, the total number of protons (rigid and mobile) in the sample, N_{1H}, was determined by comparison of the initial intensity (extrapolated to time zero) of the FID with that of a reference sample (H_2O doped with $FeCl_3$). This approach was also used to determine the number of rigid and mobile protons. The value of N_{1H} is related to the number of calcichrome molecules in the sample and is given by:

$$N_{1H} = N(n_r + 2n) \qquad (2)$$

where N is the number of calcichrome molecules in the sample, n_r is the number of rigid protons per molecule of calcichrome, and n is the total number of water molecules per calcichrome. The latter parameter includes both bound and mobile water molecules. The value for N can also be calculated from the following expression:

$$N = W_S N_A/(M_W + 18n) \qquad (3)$$

where W_S is the total weight of the solid sample, N_A is Avagadro's number, and M_W is the molecular weight of the ligand (neglecting any water of hydration). If equation 3 is substituted into equation 2 and rearranged to solve for n, the following expression results:

$$n = (W_S N_A n_r - H_{1H} M_W)/(18N_{1H} - 2W_S N_A) \qquad (4)$$

For calcichrome, n was found to equal 9.0±0.2.

Subsequently, the number of crystalline water molecules (n_c) per molecule of calcichrome can be calculated from the following expression:

$$n_c = (nR - n_r/2)/(1 + R) \quad (5)$$

where R is the ratio of rigid to mobile protons as determined from FID. With these values, we found $n_c = 2.9 \pm 0.2$. Therefore, each solid-phase calcichrome molecule carries three water molecules of crystallization, yielding a molecular formula for its sodium salt of $C_{20}H_{10}N_2Na_4O_{15}S_4.3H_2O$ (molecular weight = 792.5) This formula agrees with that reported by Stead [12].

Acid-base titrations

Potentiometric and photometric acid-base titrations were performed to determine the molecular weight and number and strength of the ionizable protons (in aqueous solution) of calcichrome. Results from a back-titration of excess HCl with 0.1 M NaOH in 0.2 M KCl clearly indicated that there were two titratable protons. Photometric titrations in 0.12 M KCl yielded pK_a values of 7.19±0.05 and 11.63±0.05 at 25°C. These results are in agreement with those reported in the first paper on this topic by Ishii and Einaga [6].

The potentiometric titration data can also be used to determine the molecular weight of calcichrome. Based on the number of moles of hydroxide consumed between the neutralization of the two titratable protons, the molecular weight for calcichrome is 759 g mol^{-1}. For structures I, II, and III, the molecular weights are 1122.8, 1122.8, and 738.5 g mol^{-1}, respectively. The titration data support our conclusion regarding the structure of calcichrome.

Composition and formation constant of the Ca(II)-calcichrome complex

The stoichiometric composition of the complex formed by the chelation of Ca(II) with calcichrome was determined via the continuous variation method. Solutions with equivalent concentrations of Ca(II) and ligand were prepared in such a way that the total volume of each mixture remained constant. All solutions were maintained at a pH of 12.1 with sodium hydroxide. The previously determined molecular weight of calcichrome was used to calculate the solution concentrations. Absorbance measurements were made at wavelengths of 525 and.510 nm and were plotted as a function of the mole fraction of Ca(II). The.maximum occurs at a mole fraction of 0.49, showing that Ca(II) complexes with calcichrome in a 1:1 stoichiometric ratio. This ratio was further confirmed by a spectrophotometric titration (vida infra).

To evaluate the formation constant, K_f, for the binding of Ca(II) with calcichrome, a form of the Ketelaar equation [25] was used:

$$1/(A-A_o) = 1/\Delta\varepsilon K_f' C_o C_m + 1/\Delta\varepsilon C_o \qquad (6)$$

where A is the absorbance of the metal complex, A_o is the absorbance of the initial concentration of calcichrome, K_f' is the conditional formation constant of the complex, C_o is the initial concentration of calcichrome, $\Delta\varepsilon$ is the difference in the molar absorptivities of the free ligand and the metal complex, and C_m is the concentration of Ca(II). Thus, a plot of $(A-A_o)^{-1}$ vs. C_m^{-1} allows the calculation of K_f'. Our experiments were performed at a pH of 12.3 at three different wavelengths. At a pH of 12.3, the dianion (HL^{6-}) is the dominant form of the ligand. The complexation reaction is then

$$Ca^{2+} + HL^{6-} = CaHL^{4-} \qquad (7)$$

and the equilibrium is expressed as:

$$K_f = [CaHL^{4-}]/[Ca^{2+}][HL^{6-}] \qquad (8)$$

Using conventional terminology to account for the dependence of K_f on pH, the expression for K_f' is:

$$K_f' = [CaHL^{4-}]/[Ca^{2+}][C_T] \qquad (9)$$

where $C_T = [H_3L^{4-}] + [H_2L^{5-}] + [HL^{6-}] + [L^{7-}]$, $K_f' = \alpha_2 K_f$, and $\alpha_2 = (K_{a1}K_{a2})/([H^+]^2 + K_{a1}[H^+] + K_{a1}K_{a2})$. From a least-squares analysis, K_f' equals $(6.93 \pm 0.24) \times 10^3$. At pH of 12.3, α_2 equals 0.86, yielding a value of K_f of 8.0×10^3. At pH values less than 11.5, where the dominant form of the ligand is H_2L^{5-} or H_3L^{4-}, K_f' dramatically decreases. This is consistent with the complexation scheme in equation 7.

Additional evidence for the 1:1 binding stoichiometry between Ca(II) and calcichrome was provided by a spectrophotometric titration of calcichrome with Ca(II) in 0.1 M KCl at pH 12.3. The presence of only one set of isosbestic points (425 and 556 nm) supports the earlier conclusion that the Ca(II)-calcichrome complex forms at a 1:1 stoichiometric ratio. Values of the molar absorptivity at the absorption maximum for both the complex and free form of the ligand are 1.37×10^4 L mol^{-1} cm^{-1} (at 522 nm) and 1.44×10^4 L mol^{-1} cm^{-1} (at 599 nm), respectively.

REFERENCES

1. German Patent 92 012, August 12, 1896.
2. Lukin, A. M.; Zavarikhima, G. B.; Sysoev, N. S. U.S.S.R. Patent 110 966, March 3, 1957; Chem. Abstr. **1958**, 52, 13546.
3. Close, R. A.; West, T. S. Talanta **1960**, 5, 221.
4. Herrero-Lancina, M.; West, T. S. Anal. Chem. **1963**, 35, 2131.
5. Pakalns, P.; Florence, T. M. Anal. Chim. Acta **1964**, 30, 353.
6. (a) Ishii, H.; Einaga, H. Bull. Chem. Soc. Jpn. **1966**, 39, 1154.
   (b) Ishii, H.; Einaga, H. Bull. Chem. Soc. Jpn. **1966**, 39, 1721.
   (c) Ishii, H.; Einaga, H. Bull. Chem. Soc. Jpn. **1967**, 40, 1531.
7. Tan, C.-L. Hua Hsueh Tung Pao **1966**, 368.
8. (a) Ishii, H.; Einaga, H. Bunseki Kagaku **1966**, 15, 577.
   (b) Ishii, H.; Einaga, H. Bunseki Kagaku **1966**, 15, 821.
   (c) Ishii, H.; Einaga, H. Bunseki Kagaku **1967**, 16, 322.
   (d) Ishii, H.; Einaga, H. Bunseki Kagaku **1967**, 16, 328.
   (e) Ishii, H.; Einaga, H. Bunseki Kagaku **1970**, 19, 371.
9. Einaga, H.; Ishii, H. Talanta **1981**, 28, 799.
10. Lukin, A. M.; Smirnova, K. A.; Zavarikhima, G. B. Zh. Analit. Khim. **1963**, 18, 444.
11. Mendes-Bezerra, A. E.; Stephen, W. I. Analyst **1969**, 94, 1117.
12. Stead, C. V. J. Chem. Soc. C **1970**, 693.
13. Gerstein, B. C.; Pruski, M. unpublished work, Department of Chemistry, Iowa State University.
14. Gerstein, B. C.; Chow, C.; Pembelton, R. G.; Wilson, R. C. J. Phys. Chem. **1977**, 81, 565.

15. Gerstein, B. C.; Dybowski, C. R. Transient Techniques in NMR of Solids: An Introduction to Theory and Practice; Academic Press: New York, 1985; Chapter 6.

16. Opella, S. J.; Frey, M. H. J. Am. Chem. Soc. **1979**, 101, 5854.

17. Memory, J. D.; Wilson, N. K. NMR of Aromatic Compounds; Wiley: New York, 1982; Chapter 4.

18. Hansen, P. E. Org. Magn. Reson. **1979**, 12, 109.

19. Ewing, D. F. Org. Magn. Reson. **1979**, 12, 499.

20. Bremsen, W.; Franke, B.; Wagner, H. Chemical Shift Ranges in Carbon-13 NMR Spectroscopy; Verlag Chemie: Weinheim, 1982.

21. Socrates, G. Infrared Characteristic Group Frequencies; Wiley: New York, 1980; p 63.

22. Bellamy, L. J. The Infrared Spectra of Complex Molecules, 2nd Ed.; Chapman and Hall: London, 1980.

23. Noller, C. R. Chemistry of Organic Compounds; W. B. Saunders: Philadelphia, 1966; Chapters 26, 30.

24. Leyden, D. E.; Cox, R. H. Analytical Applications of NMR; Wiley: New York, 1977; p 186.

25. Rose, N. J.; Drago, R. S. J. Am. Chem. Soc. **1959**, 81, 6138.